General Disclaimer

One or more of the Following Statements may affect this Document

- This document has been reproduced from the best copy furnished by the organizational source. It is being released in the interest of making available as much information as possible.

- This document may contain data, which exceeds the sheet parameters. It was furnished in this condition by the organizational source and is the best copy available.

- This document may contain tone-on-tone or color graphs, charts and/or pictures, which have been reproduced in black and white.

- This document is paginated as submitted by the original source.

- Portions of this document are not fully legible due to the historical nature of some of the material. However, it is the best reproduction available from the original submission.

FLUID DYNAMIC ASPECTS OF JET NOISE GENERATION

NEW YORK UNIVERSITY
DIVISION OF APPLIED SCIENCE
AEROSPACE AND ENERGETICS LABORATORY
MERRICK AND STEWART AVENUES
WESTBURY, L.I.,N.Y. 11590 NEW YORK

FINAL REPORT

September 1, 1972 through January 31, 1976

NASA GRANT NGR-33-016-177

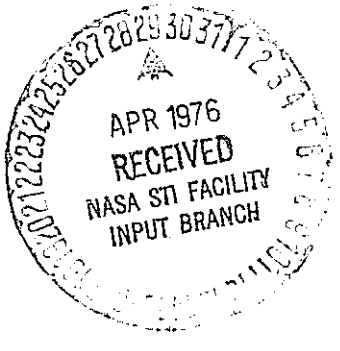

PREFACE

The work reported herein was prepared by Dr. Vincent Barra, Associate Research Scientist, New York University Aerospace and Energetics Laboratory and Dr. Sergio Panunzio, Senior Research Scientist, New York University Aerospace and Energetics Laboratory under NASA Grant NGR-33-016-177, during the period from September 1, 1972 through January 31, 1976.

TABLE OF CONTENTS

NOMENCLATURE

A, A'	Sinusoidal signal amplitudes
D	Nozzle exit diameter
F, $\bar{F}$	Functions of time
f	Fundamental frequency of the periodic signals
IA	Input attentuation of the analyzer
i	Integer between 0 and 99
K	Total number of (100 point) samples or summations
k,ℓ,m	Integers between 1 and K
M	Mean flow Mach number
M_j	Jet Mach number
N,n	Stationary random functions of time
P	Mean static pressure
p	Fluctuating static pressure
R_{FF}	Average auto-correlation of the function F(t)
$R_{FS'}$	Average cross-correlation between F(t) and S'(t)
R_N	Auto-correlation of N(t)
S	Periodic signal
S'	Sinusoidal reference signal
SPFL	Static pressure fluctuation level as defined in Equation 2
T	Period of the harmonic signals
T_o	Mean stagnation temperature of the flow
T_R	Total running time of the flow
t	Time
t'	Averaging time

NOMENCLATURE (cont'd)

t_d, τ	Delay times
Δt	Sampling increment
$\vec{x} = (x,y,z)$	
x	Streamwise coordinate
y	Vertical transverse coordinate
z	Horizontal transverse coordinate (= 0 in all cases)
α	Integer defined in Section IV
φ	Relative phase
ρ_m	Normalized correlation defined by Equation 14
ρ	Summation defined by Equation 16
σ_N^2	Variance of N(t)

Subscripts

e	Nozzle exit
rms	Root-mean-square amplitude

LIST OF FIGURES

FIGURE

FIGURE

FIGURE

FIGURE

I. INTRODUCTION

A substantial amount of work has been carried out in the field of jet noise in an effort to understand noise generation and propagation, and also to decrease the noise produced from the exhaust jet by changing the configuration of the engine nozzle. Much of the research has been characterized by an attempt to introduce local modifications in the flow field that do not require major modifications to the engine design. Therefore, schemes usually considered are limited to changes localized downstream of the converging section of the nozzle (Refs. 1-4).

The results of these investigations indicate that large reductions in noise levels at some distance from the engine can be obtained, e.g., Mangiarotty and Cuadra (Ref. 3). However, such reductions are consistently coupled with substantial decreases in thrust. A typical example of such results is presented in Fig. 1, where the amount of suppression is related to losses in thrust. Nagamatsu, Sheer and Gill (Ref. 4) have obtained large noise reductions (20dB) by splitting a supersonic jet into 191 smaller shrouded jets. The thrust loss was, however, 25%. Such losses are not easily acceptable, and they may be unnecessary, if the fluid dynamic changes required for decreasing the noise are incorporated initially in a good aerodynamic nozzle design.

The insight necessary for establishing rational suppressor design criteria has been sought by many research efforts aimed at determining the location of noise sources within jet flows, their relative importance to the overall radiated field, and the mechanisms by which noise generation occurs. Information of this type has been obtained

from detailed measurements of the level and spectral composition of the radiated sound in the far-field (as, for example, in Refs. 5-6), by the use of directional microphones to isolate the contribution to the radiated sound of small regions of the flow (Ref. 7), and by cross-correlation between the radiated acoustic field and either the velocity fluctuations (Ref. 8) or the pressure fluctuations (Refs. 9-11) in the source field.

In addition, detailed studies of the level and spectral distribution of the pressure fluctuations within small model jet flows have been made by Nagamatsu and several associates (Refs. 12-14). Part of the present investigation was directed toward a similar survey of the static pressure fluctuations within the cold supersonic jet flow exhausting from a relatively large 7 inch exit diameter convergent-divergent nozzle. The nozzle is designed to yield shock-free (balanced) flow with a jet Mach number $M_j = 2$. Both the flow in this perfectly expanded case, and an overexpanded flow with $M_j = 1.8$ were surveyed.

An important aspect of the problem of jet noise which could lead to a better understanding of noise generating mechanisms is the propagation of pressure disturbances in the presence of flow. Research in this area has included a study by Chih-ming and Kovasznay (Ref. 15) of periodic wave propagation across a two-dimensional layer of turbulence, and analytical investigations by Slutsky and Tamagno (Ref. 16) and Gottlieb (Ref. 17) of the field due to an harmonic source radiating from a two-dimensional region of flow, across a velocity discontinuity, into a medium at rest. Although the last reference also includes results for the reverse case of a source radiating into a region of

flow from one at rest, the use of an improper boundary condition at the interface is believed to invalidate the results for both cases. The problem of a source within a cylindrical flow region was treated by Slutsky (Ref. 18), and was extended by Liu and Maestrello (Ref. 19) to the case of a real axisymmetric flow with diverging boundaries. An experimental investigation of refraction (Ref. 20) has included measurements in the acoustic far-field of a pure-tone point source located inside a low speed jet flow.

Mixing induced disturbances at the periphery of an axisymmetric jet flow not only propagate into the surrounding medium but also toward the centerline of the flow. A recent analysis by Ferri, Ting and Werner (Ref. 21) has shown that the nonlinear propagation of a circumferential disturbance at the edge of a cylindrical supersonic flow toward the axis of the flow will exhibit effects such as focussing and distortion of wave profile. (Also included in this reference is a study, in the same vein as those described in the previous paragraph, of the propagation of an acoustic disturbance from the core of a supersonic jet through the shear layer, Fig. 2). An experimental verification of these phenomena requires the ability to first induce a known disturbance at the edge of a supersonic flow and then to observe the disturbance at it propagates into the flow. A major effort of the present investigation was the development of the experimental procedures and data processing necessary to accomplish this. (Although a method of detecting a weak acoustic signal in turbulent airflows has been investigated (Ref. 22), its scope, as will be discussed in Section IV, is rather limited).

The task of implementing the required facilities and instrumentation was divided into three phases:

a. construction of the facility providing two concentric jets of cold air; calibration of the jet's aerodynamic characteristics and measurement of noise generated in the far field and near field for evaluation of uniformity, intensity, spectrum composition.

b. construction of a signal generator providing a set of one to six signals of appropriate intensity, frequency and form; channeling of the signals to the desired injection points, establishment of the signal form at the injection points, time-delay control are studied in this phase.

c. assembling a data acquisition system consisting of pressure probes, a stand and scanning mechanism for the probes, a recording system, and a signal enhancement system for separation of the injected signal from the background noise of the jets.

Many of the results obtained from the application of these facilities and systems to the study of wave propagation, as well as to the survey of ambient static pressure fluctuations, have been presented in various articles published during the course of the investigation (Refs. 23-26).

II. EXPERIMENTAL FACILITIES AND PROCEDURES

A. Jet Facility

The facility utilized in the experimental program was designed with the objective of satisfying the following requirements:

a. That many nozzle configurations can be set up for experiment without introducing major changes in the facility

b. That the flow conditions through the primary and secondary nozzles can be controlled independently and that

c. The nozzle jets discharge in the open space outside the laboratory and their direction is such as to produce minimum reflections from the surrounding objects.

A steel cylinder, Fig. 3, (1½ ft. I.D. and 7 ft long) closed at the two ends by two flanges and designed for 1600 psi nominal pressure, is used as the settling chamber of the primary nozzle. One flange is blind while the other one has a central rectangular hole with 7 3/4" by 5 3/4" sides with rounded corners, bored into it. This flange was used to support the coaxial axisymmetric nozzles with circular cross sections (Fig. 4). The coaxial secondary nozzle has a separate annular settling chamber built around the nozzle itself. Cold air ($T_o \approx 500^\circ R$) was supplied to the settling chanber from a 1700 ft^3 bank at a maximum pressure of 2000 psi through three regulating valves.

The inner (primary) nozzle, with a throat diameter of 5.25" and an exit section of 7" diameter, provides a M = 2 supersonic jet, and requires 110 psia stagnation pressure to produce a jet with 14.7 psia exit static pressure, free of shock-expansion surfaces (mass flow 60 lbm/sec).

The outer (secondary) nozzle provides, in this configuration, an annular jet of 10" O.D. and 7" I.D. at M = 1 also balanced (Fig. 5), (P_o = 30 psia, P_e = 14.7 psia, 20 lbm/sec). The outer nozzle was designed initially for subsonic Mach numbers with a jet exit O.D. = 12" (also with a mass flow of 20 lbm/sec.) and tests of its characteristics, alone or together with the M = 2 inner jet, have been performed. This set of nozzles was implemented with a series of pressure taps and tested to verify the flow axial symmetry and the Mach numbers were obtained by using standard recording equipment.

A series of tests was conducted with various combinations of the jets mass flows, to measure the sound level in the far field at selected points; namely, at 46 ft., 92 ft. distance and about 600 ft. across the Harlem River, at various angles with the jets axis (Tables 1 and 2).

B. Signal Generators

Two acoustic signal generating systems were prepared for this investigation. The first consisted of a 100 watt Altec 290-E loudspeaker, with a 3 inch exit diameter catenoidal horn, driven by a H-P 3310A function generator (operating in the sine mode) through a Bogen 100 watt power amplifier. The sync output of the function generator acted as an external trigger for a General Radio pulse generator

(type 1340). The resulting pulse train, adjusted for proper amplitude, was recorded along with the transducer outputs and served to synchronize them with the loudspeaker generated signal.

The second (multi-source) generator is the pneumatic siren system shown in Fig. 6 and consists of a manifold receiving air from the high pressure line (2000 psig) reduced to 20-200 psig by a pressure control valve. The air flow from the manifold enters into six 5/8" I.D. nozzles and is alternately shut off and opened by a rotating valve. This rotating valve is formed by a disc attached to an electric motor with speed variable up to 10,000 rpm, and presents in front of the nozzles a row of 24 circular windows of 1/2" diam. From the other side of the rotating disc, six pipes of 5/8" I.D., placed in continuation of the six nozzles, bring the resulting pressure disturbances to the signal injection points. The six lines are symmetrically placed around the axis of the tunnel and have the same length (about 10 feet), except for a U-shaped segment that permits one to change the line length by about 1 foot, thereby introducing a delay-time in the signal arrival at the injection point of up to 1 msec. The synchronization pulse train in this case was again provided by the GR pulse generator being triggered now by a rotating contact-switch system aligned with the 24 windows of the rotating valve, Fig. 7.

C. Probes and Supporting Structure

Probes were supported in the flow by the structure shown in Fig. 8. A massive base can be moved down a 10 ft long track fixed to the ground and oriented along the x-axis, as well as normal to this streamwise direction. A motorized mechanism attached to the base allowed for a

13 inch vertical traverse of the flow at a speed of approximately 2 in/sec. Two pressure probes can be mounted, either singly or together (separated by 1.5 inches in the vertical y-direction), at the end of a knife-edged wing (Fig. 9) which was then fixed to the top of the traversing mechanism and extended into the flow. The wing also served to enclose the transducer cables.

Static pressure fluctuation measurements were made using two probes, both consisting of Kulite piezoresistive pressure transducers (Type CQS125-100) housed in the ends of a 6 inch long stainless steel tubes fitted with Bruel and Kjaer #UA0385 ogive nose cones, Fig. 9. One tube has a constant 1/4 inch O.D. and the other a 3/8 inch O.D. tapering to 1/4 inch. The transducer senses the pressure in a cavity (formed by the B & K nose cone) which is in contact with the outside pressure field through a wire mesh ring. A "blind" solid steel nose cone was constructed for use in determining how large a part of the transducer output signal was due to spurious, non-pressure noise such as that resulting from vibration of instrumentation cables. Specifications for the two transducers, identified as #1 and #7, as well as a typical circuit diagram are presented in Fig. 10. The resonance frequency of 130 kHz indicates a flat ($\pm$ 1 db) transducer frequency response of DC-40 kHz as shown in Fig. 11. The Helmholtz resonance of the probe cavity mentioned above should not significantly affect measurements within this range of frequencies. It is believed that this resonance frequency is much higher than the 20 kHz found in Ref. 27 for the cavity of a similar 1 inch diameter B & K nose cone. In fact, simple scaling considerations would indicate a frequency on the order of 80 kHz. The

sensitivities of the transducers were verified using a 1 kHz pressure field of known level (154 dB).

D. Instrumentation

A diagram of the instrumentation set-up for recording the transducer outputs and generating the acoustic signal with the Altec loudspeaker is shown in Fig. 12. The output voltage of transducer #1 was amplified and filtered by a Princeton Applied Research amplifier (Model 113) which has a maximum gain of 10^4. The RMS level of the amplifier output was monitored on a voltmeter. A Bruel and Kjaer Type 2606 measuring amplifier with a maximum gain of 96 db served the same purpose for the output of transducer #7, its meter indicating the RMS level of this output. Typical amplifier bandpasses used were 30-300,000 Hz on the PAR and 22.5-200,000 Hz on the B & K. The low frequency roll-offs were needed to eliminate the effect of 2 Hz mass flow fluctuations (created by valve oscillation) on the measurements. Both amplifier outputs were displayed on a 2 channel oscilloscope and recorded on a 7-channel Honeywell 5600 tape recorder.

Tape recordings were made primarily at 60 ips although a speed of 15 ips was also used. The transducer outputs were all simultaneously recorded both in FM double extended mode and Direct mode. The pulse train synchronized with the acoustic signal generator was recorded only in Direct mode. At 60 ips, the recorder bandwidth is DC-40 kHz for FM and 300-300,000 Hz for Direct. At 15 ips these become DC-10 kHz and 100-75,000 Hz, respectively. When the traversing mechanism was used, a marker signal locating the position of the probe along the y-axis in the flow was recorded in FM mode.

Basically, three experimental procedures were followed to acquire data. With one of the probes located at various fixed positions inside the jet, 15 to 20 second recordings were made of the transducer output at each position. The RMS level of the static pressure fluctuations represented by this output was determined from an on-line reading of the appropriate meter, while the recordings were later analyzed to obtain the spectral distribution of the fluctuations. Again with only one probe, the traversing mechanism was used to vertically scan the static pressure fluctuations across the jet. In this case the transducer output was recorded during the scan along with a signal marking the approximate position of the moving probe. In the last procedure, the set-up for which is shown in Fig. 13 for the loudspeaker, both probes (separated by 1.5 inches in the vertical direction) were placed in the field of the acoustic signal generator. The two transducer outputs were recorded both with and without jet flow. In the former case, 40 seconds of data was recorded to allow the subsequent processing to separate the acoustic signal from the jet pressure fluctuations.

The systems used to analyze the recordings are shown in Fig. 14. The jet traverse recordings were played through the RMS circuit of the B & K measuring amplifier and then displayed on the oscilloscope together with the marker signal, thus giving a trace of RMS level of static pressure fluctuations vs position traversed along the y-axis. In all other cases, RMS playback levels were monitored on a voltmeter. Spectral distributions of the recorded static pressure fluctuations at various points in the flow were obtained using a General Radio narrow band wave analyzer (Model 1900A) linked to a General Radio (Model 1521-B)

graphic level recorder. The signal recovery processing was accomplished by feeding the recorded transducer pick-ups in the field of the acoustic signal generator into one of the channels of a Saicor SAI-42 correlation and probability analyzer operating in the enhance (ensemble averaging) mode. In this mode, 100 values of the incoming signal are sampled (at a predefined increment), digitized and added to 100 memory bins each time a trigger pulse, of prescribed amplitude and duration, is sensed at the EXT SYNC terminal of the analyzer. These external triggers were provided by the pulse generator being itself triggered by the recorded synchronization pulse train. This procedure was followed because the pulse amplitude required by the analyzer is greater than that which can be recorded, and also due to the fact that some distortion occurs to the pulses in the recording/playback process. Thus, the pulse generator served, in a way, to transform the recorded pulse train into one having the required properties. At the end of the processing, the levels in the 100 bins of the analyzer were displayed across the oscilloscope screen and photographed.

An electronic simulation of this signal recovery processing was carried out using the system shown in Fig. 15. A General Radio (Type 1390B) random noise generator served to simulate the jet static pressure fluctuations while the sinusoidal output of the function generator represented the acoustic trace signal. The two were summed and filtered by the PAR 113 operated in its differential amplifier mode. The resulting sum was handled as if it were the amplified output of a transducer in the flow with the exception that recording was bypassed in some of the simulation studies. The meter could be used to monitor

the RMS levels of the noise and signal, separately or combined.

E. Modifications

At the beginning of the third year of the experimental program it became necessary to relocate the Jet Noise Facility from the Bronx, N.Y. to Westbury, L.I.,N.Y. Although the general configuration of the facility was kept unchanged, some advantages were derived from the new emplacement and some improvements were introduced as dictated by previous experience. They can be summarized as follows:

a) The concrete platform and the streamwise rails of the probe support structure was extended in length to 20' from the jet exit. The mechanism of moving and locking the probe support to the rails was improved to permit better control and faster operation as well as to explore the jet up to 28 D (Fig. 16)

b) The air bank volume available is twice as large as the one used previously permitting twice the number of test runs between the same limits of pressure and keeping the same test time and mass flow.

c) The valve control panel and the data recording instrumentation were placed close to each other and in a position from which a better visual control of the jet is possible and that permits the two operators to communicate easily.

The following additions and modifications were also made to the pneumatic signal generating system:

a) Fabrication of an injection ring placed at the exit of the primary nozzle that permits radial injection of 6 simultaneous signals (at variable phases) through 6 slots ½" wide and 3.5" long in the circumferential direction evenly distributed along the circumference (Fig. 17).

b) Fabrication of a manifold to distribute the high pressure air to the six port of the pneumatic siren.

c) Modification of the siren to reduce the gaps in front and aft of the spinning disc to eliminate unwanted resonances occurring in these gaps (Fig. 18).

III. STATIC PRESSURE FLUCTUATION MEASUREMENTS

A. General Remarks

Prior to dealing with the primary objective of this investigation, which was to develop and implement a procedure for externally injecting and then tracing an acoustic signal through jet flows, a survey was made of fluctuating static pressure levels in the primary flow. This survey was useful in two respects. It first of all provided a good idea of the sort of background noise levels which would have to be contended with in detecting the induced signal, and secondly, the data revealed the existence of several interesting phenomena related to the problem of supersonic jet noise generation. Although such measurements are common in the literature, as for example in Refs. 10-14, 28, it is also common to find these studies employing flows exhausting from nozzles with exit diameters on the order of 1 or 2 inches. Considering the probes ordinarily used, this leads to a ratio of jet diameter to probe diameter in the range 4-10. For the present investigation this ratio is 28, thus substantially decreasing the errors in measurement due to changes in the pressure field induced by the introduction of the probe in the flow. The effects of the probe wing support shown in Fig. 9 should be small due to the limited upstream influence in the supersonic flow regimes of the jet; and was minimized still further by making most of the measurements of this survey using only the upper, more slender probe (housing transducer #1), thus eliminating the bulky structure required to support the lower probe.

The validity of using the B & K ogive nose cones, described in Section II and shown in Fig. 9 , to accurately represent the static pressure fluctuations in subsonic and transonic flow has recently been verified (Ref. 11) with the use of an intersecting laser technique which does not require that obstructions be placed in the flow. It was also found that in supersonic flow there is a complex structure of weak shocks attached to the nose cone which would tend to give extraneously high pressure fluctuation measurements. But of three nose cones tested, the B & K was found to yield the most consistent results. It should be added that any vibration of the probes would tend to aggravate these problems of induced pressure disturbances, although such effects would be primarily confined to relatively low frequencies.

In general, the measured pressure fluctuations at a point $\vec{x}$ in the flow can be separated into several terms:

$$p_{meas}(\vec{x},t) = p(\vec{x},t) + p_{probe}(\vec{x},t) + p_{vib}(\vec{x},t) + p_{elec}(t) \qquad (1)$$

where $p(\vec{x},t)$ is the true jet static pressure fluctuation (i.e., the excursion from the mean static pressure, $P(\vec{x})$); $p_{probe}(\vec{x},t)$ is the pressure disturbance induced by the presence of the probe and support as discussed above; and $p_{vib}(\vec{x},t)$, $p_{elec}(t)$ are pressure equivalents of electrical noise induced by vibration of the transducer and cables, and inherent in the measuring electronics, respectively. By a procedure to be described, the overall RMS level of the third term above was found to be typically about 22 dB below that of the sum of all the terms. The noise floor of transducer #1 and its amplifier was 125 dB (in equivalent

pressure level re. 0.0002 μBar), while for transducer #7 it was 122 dB. This put the fourth term at least 35 dB below any of the measured levels. Thus, the disturbance created by the presence of the probe, particularly in the supersonic regions of the jet, is likely to be the most significant source of error in the measurements. (An estimate, either experimental or analytical, of the magnitude of this error is beyond the scope of the present study although some attempts have been made by previous investigators (e.g., Refs. 9 and 11). All of the above components of the measured pressure fluctuations are assumed to be stationary random functions of time.

It should be noted that error considerations of this kind are not of critical importance for the signal tracing aspects of this investigation. In that case, the measured pressure fluctuations will consist of the induced acoustic signal, as sensed by the transducer, plus a random component attributable to the various sources described in the previous paragraph. The individual contributions to this random noise background are significant only in the sense that they increase the total RMS level thus lowering the effectiveness of the signal recovery processing.

In what follows, the static pressure fluctuation level (SPFL) at a point $\vec{x}$ in the flow is calculated according to the formula,

$$SPFL(\vec{x}) = 20 \log_{10} \frac{p_{rms}(\vec{x})}{p_o} \quad dB \tag{2}$$

where

$$p_{rms}(\vec{x}) = \sqrt{\frac{1}{t'} \int_o^{t'} p^2_{meas}(\vec{x},t)\, dt}$$

and $p_o = 0.0002$ μBar $= 2.9 \times 10^{-9}$ psi.

A distinction is made from ordinary sound pressure level (SPL) since besides acoustic disturbances the static pressure fluctuations in a flow also include aerodynamic disturbances convected along streamlines.

The flow from the primary nozzle was studies in two running conditions. For the first, the chamber pressure was maintained at 80 psia, yielding a mass flow of 40 lbm/sec and a nozzle exit static pressure of 10 psia. The shadowgraph in Fig. 19 exhibits the initial shock structure associated with this overexpanded jet. The second was the design condition: a chamber pressure of approximately 110 psia (mass flow of 60 lbm/sec) yielding a balanced jet free of shock-expansion surfaces. For both flow conditions the exit Mach number $M_e = 2$, being determined by the nozzle geometry. Defining the jet Mach number, M_j, as the Mach number that would result from an isentropic expansion of a given chamber (total) pressure to atmospheric pressure, it is clear that $M_j = 2$ for the balanced jet, while $M_j = 1.8$ for the overexpanded jet.

All the static pressure fluctuation (and acoustic signal tracing) measurements for this study were made in the plane $z = 0$ (Fig. 3).

B. Static Pressure Fluctuation Levels in the Overexpanded Jet

A somewhat simplified illustration of the jet flow exhausting from the primary nozzle with an overexpanded exit static pressure of 10 psia is presented in Fig.20a. The lengths of the supersonic core and supersonic mixing zone were determined from equations empirically derived by Nagamatsu and Horvay (Ref. 29) which express these lengths in terms of the jet Mach number (in this case, $M_j = 1.8$). The position of the sonic line along the jet centerline was approximately verified by a

series of pitot and static pressure probe measurements. It was also assumed that the jet spreads initially at a total angle of 12^{o}.

The variation of overall SPFL along the centerline of this jet is shown in Fig. 21. Due to the supersonic exit Mach number, a point on the centerline does not "see" the nozzle lip or any part of the subsequent mixing layer until it is at least about one nozzle diameter (D) downstream of the exit. Consequently, the levels measured at $x/D \leq .5$ give a good indication of the pressure fluctuations existing in the flow, before it exhausts into the atmosphere, due to upstream turbulence created in the valves and settling chamber and to radiation from the nozzle boundary layer. The high levels ($\sim$ 165 dB) obtained in this region are not surprising since there was no attempt made to quiet the flow entering the nozzle by the use of screens or flow straightners. Such a procedure becomes necessary when the details of the far-field radiated sound due to the jet alone are sought (as in the case, for example, in Ref. 6 where upstream disturbances were lowered to negligible levels). Since the jet is overexpanded the supersonic core will contain a cell structure of shocks and expansions which is partially shown in Fig. 20a. Where the conical shocks of this structure converge on the centerline, a small Mach disc is formed, the first of which can be seen in the shadowgraph of Fig. 19. Very marked increases in pressure fluctuation level were found near both of the first two of these discontinuties, that is, at $x/D \cong .5$ and $x/D \cong 2$. The level was also found to vary erratically ($\pm$ 3 dB) during the course of a measurement at each of these positions. Such phenomena could have been the result of some interaction

between the weak shocks attached to the probe and the Mach discs, especially when the probe is vibrating, or due to the convection of the high level upstream disturbances through the jet shock structure. If the latter is the more important effect, as is believed to be the case at least for the overall increase in level, these regions could be significant sources of radiated noise. The remaining measurements made along the centerline indicate an increase in level up to a maximum at about 9 diameters downstream of the exit (i.e., the end of the supersonic core), and a fall-off afterwards. Similar results were obtained by Nagamatsu and Sheer (Ref. 14) for an $M_j = 1.4$ flow from a 1 inch exit diameter convergent nozzle. Using a specially designed 1/8 inch probe, they found a peak static pressure fluctuation level on the jet axis also at the end of the supersonic core (i.e., at approximately 7 diameters).

Spectral densities of the static pressure fluctuations at selected points along the jet centerline are presented in Figs. 22-28. The initial distribution ($x/D = 1$, Fig. 22) shows that there is a significant amount of low frequency (50-300 Hz) energy at the outset of the flow. This could be due to both long wavelength disturbances originating in the settling chamber and to low frequency mass flow fluctuations. The pressure fluctuations at this position were analyzed for high frequency content and show that, beyond 30 kHz, complex resonance phenomena begin to occur. The strong peak at 70 kHz, for example, recurs in every spectrum analyzed at this frequency and is thought to be the Helmholtz resonance of the nose cone cavity. A comparison of this first spectral

distribution with the one at x/D = 2 (Fig. 23) shows an unusual increase in energy at almost all frequencies of between 5 to 10 dB. Recalling that this is the approximate position of the second Mach disc in the flow, it is possible that such a discontinuity serves to locally amplify upstream disturbances. The steeper fall-off in energy above 4 kHz (10 dB/octave as compared to the previous 7 dB/octave) would seem to indicate that this amplification loses its effectiveness at the higher frequencies or perhaps is extremely localized spatially. The two peaks at 1200 and 1700 Hz are unique to this position (x/D = 2) among those at which measurements were made.

Except for the spectrum at x/D = 2.6 (Fig. 24) which is basically similar to that at x/D = 2 (other than actually containing less total energy), those remaining along the centerline show a regular increase in energy within the range 50-2000 Hz up to the end of the supersonic core (x/D = 8.6, Fig. 26), and then downward shifts in this same range for the two beyond this point (Figs. 27 & 28). At least two sources are believed to contribute to the growth of energy within this range of frequencies. First there are the disturbances (largely below 300 Hz) originating upstream of the nozzle which seem to be transmitted and reinforced by the shock cell structure of the supersonic core, and second there are the pressure fluctuations on the centerline induced by the jet mixing whose contribution to frequencies below 2000 Hz should increase with distance downstream since the length scale of mixing increases. (It is difficult to determine from the spectra whether the shock structure also serves to amplify these mixing induced fluctuations.) The importance of the

supersonic core to the first effect can be seen in the one spectral distribution at a considerable distance downstream of the core (x/D = 15.7, Fig. 28). Compared to the distribution near the core tip (Fig. 26) there is a sharp drop, as high as 12 dB at 70 Hz, in the energy of frequencies between 50 and 300 Hz, while for frequencies above 500 Hz the drop is less pronounced (3 or 4 dB). This would indicate that the very low frequency disturbances propagating through the core region of the jet cannot be sustained, or are dissipated, once mixing begins to occur. The general subsidence of fluctuations over all frequencies is accounted for by the decreasing mean flow velocity in this now fully turbulent region of the jet.

Above 2000 Hz all the latter spectra show a fall-off of energy at an almost constant rate of 8 or 9 dB/octave with minor shifts in level as the measuring position is varied.

The spectra of the static pressure fluctuations measured within the supersonic core of the overexpanded jet (Figs. 22-25) all contain a strong peak at a frequency which varies between 800 and 900 Hz. It is thought that this is a manifestation of the phenomenon known as supersonic screech, that is, the coupling of some discrete upstream disturbance with the shock structure of the jet through a feedback loop. The spectral density of the radiated sound field at a distance of 10 feet from the nozzle exit and an angle of 45° from the centerline is included in Fig. 29 to lend support to this conclusion. Measured with a separate acoustic microphone and amplifier, the radiated sound clearly shows a screech frequency (or shock tone) at about 800 Hz. The reasons for the slight differences in the

frequency at which the peak occurs were not established.

To determine the degree to which spurious electrical noise induced by the vibration sensitivity of the transducer and cables affected these results, a series of measurements were made at x/D = 2.6, the spectral analyses of which are shown in Fig. 30. The uppermost curve is the spectral distribution of the static pressure fluctuations measured at this point by the probe fitted with the usual B & K nose cone. Its similarity to one obtained previously at this position (Fig. 24) is an indication of the reproducibility of the results. The two lower distributions are of transducer output signals obtained with the B & K nose cone replaced by one which seals-off the transducer from the jet pressure fluctuations (see Fig.9). As indicated, some pressure disturbances (particularly at frequencies below 500 Hz) were reaching the transducer until the threads by which this "blind" nose cone was attached to the probe were sealed with a silicone compound. With this accomplished, it could be seen from the lowermost curve that, over a wide range of frequencies, the spectral distribution of the electrical noise induced by vibration was at least 20 dB below that of the static pressure fluctuations at this position. It is possible that, even with the precautions taken, some pressure disturbances were still being transmitted through the "blind" nose cone to the transducer, in which case the estimate above is conservative. The overall measured levels in the two cases were 144 dB and 166 dB. The conclusions reached here are valid for other measurements in the flow since the general vibration level was not noticed to change appreciably with position.

The variation of overall SPFL with vertical distance from the centerline (y/D), at selected downstream stations, is presented in Figs. 31a & b. The initial profiles show peak fluctuations occuring in the jet mixing region. There are rapid decreases in level outside the flow, while the interior is characterized by regions of constant level around the centerline. The sharp rise in fluctuations near the centerline at x/D = 2 has been discussed previously in relation to the flow discontinuity which exists at this position. Here it can be seen that the effect is very local in terms of the transverse direction to the flow. The tendency for the mixing region peaks to first move in toward the centerline and then to diverge outward is an indication of the initial contraction of the flow streamlines resulting from the overexpanded nozzle exit pressure of 10 psia. Although there is a general trend in these initial profiles for the level to rise for all y/D as the downstream distance increases, this occurs at an accelerated rate in the core of the jet until at x/D = 8.6 the most intense static pressure fluctuations along the cross-section are found near the centerline. Beyond this point, near the end of the supersonic core, the flow becomes fully turbulent and the jet centerline is also the center of mixing. The last two profiles show more even distributions of level across the flow and a decreasing trend with distance downstream.

A recent investigation (Ref.30) of a small $M_e \cong 2$ jet has included profiles of RMS hot-wire voltage fluctuations in the flow. The similarity in the shape and development of these profiles to those measured here would perhaps call for an examination of the relationship between the two measured properties of the jets.

C. Static Pressure Fluctuation Levels in the Balanced Jet

The changes that occur in the jet flow field when the nozzle exit static pressure is raised from 10 psia to the level of the ambient atmospheric pressure are depicted in Fig. 20b. Besides the disappearance of any finite flow discontinuities in the supersonic regions of the jet, the entire flow structure is elongated in the streamwise x-direction. Again, the extend of the various regions of flow were determined according to the results of Ref. 29. The measurements made in the overexpanded jet were basically repeated for this now shock-free, balanced jet and are presented in Figs. 32-40.

The first, that of the variation of overall SPFL along the centerline of the jet (Fig. 32), shows that the initial level of static pressure fluctuations (mainly originating upstream of the nozzle exit) is approximately the same as before ($\sim$ 165 dB). Missing, though, are the strong peaks in level near the exit which were previously associated with the shock structure of the overexpanded jet. After a similar increase with distance downstream, a maximum level of about 171 dB is reached between x/D = 9 and 12. Although this again corresponds to the approximate position of the supersonic core tip (i.e., x/D = 10), the maximum level is now 6 dB lower than that obtained, at x/D = 8.6, along the centerline of the overexpanded jet (Fig. 21). Thus even with the 33% lower mass flow, the static pressure fluctuations along the centerline of the overexpanded jet are generally higher than those for the balanced jet. This is directly relatable to the shock structure present in one flow and not in the other. It is interesting to note that at x/D $\cong$ 15, where

the effects of the shock structure are not as important, the levels in the two jets are about the same ($\sim$ 170 dB).

There are some striking differences in the spectra obtained for the two flows. The original low frequency (50-300 Hz) content in the static pressure fluctuations is still present as can be seen in Fig. 33 . But now, in the shock-free flow, the energy within this band of frequencies does not grow appreciably with distance downstream. For example, at 50 Hz there is a 4 dB variation among all the measured positions while, previously, a growth in level of 20 dB occurred, at this frequency, from x/D = 1 to x/D = 8.6. With this very low frequency effect absent, the contribution of the jet mixing to the static pressure fluctuations on the centerline can be more clearly identified. Before the rapid fall-off in energy at high frequencies, a "shoulder" can be seen to exist in all the spectral distributions. Besides growing in level consistently with each position further downstream, this "shoulder" is centered about monotonically decreasing frequency for each such position. At x/D = 1 (Fig.33) it is located around 1500 Hz with a level of approximately 120 dB, while at x/D = 15 (Fig. 39) its center frequency is more like 350 Hz and its level has almost reached 140 dB. It has already been mentioned that, as the mixing region of the jet increases in size, the pressure disturbances created would reasonably be expected to contain energy at correspondingly decreasing frequencies. The shifting frequency above is a clear demonstration of this effect. The strong peak between 800 and 900 Hz that appeared in the spectra for the over-expanded jet is also now missing. This is more support for the previous conclusion that the peak is

associated with a shock-related phenomenon (screech). For high frequencies, the spectral distributions behave similarly for the two flows. Except for the first (Fig. 33) which falls-off above 4 kHz at 7 dB/octave, all the distributions in the balanced jet (Figs. 34-39) show a decrease in energy above 3 kHz at a constant rate of 8 or 9 dB/octave.

The profiles of overall SPFL at various cross sections of the balanced jet (Figs. 40a & b) also show significant changes. The first three profiles are bascially the same with the only change being that the peaks in level occurring in the mixing layer of the jet are located in line with the nozzle lip since the flow now exists more or less parallel to the centerline. The sharp rise in level at $x/D = 2$ near the centerline, previously associated with the Mach disc present at that position, no longer exists. Although the profiles again show a pattern of increasing levels with distance downstream, the shift of the peak to the centerline does not occur. What is seen instead is a broadening of the peaks as the mixing region grows in size. Even after the flow is believed to have become fully turbulent (i.e., $x/D > 10$), the highest levels of static pressure fluctuations occur at some distance off-center. The remarkable growth of the very low frequency energy along the centerline of the over-expanded jet, which does not take place here, is thought to be responsible for the special significance the centerline has to the profiles in that flow. As the turbulence becomes fully developed and the mean flow velocity drops, the profiles in both flows (i.e., at $x/D \cong 15$) become rather flat and show a trend toward decreasing levels.

Due to the limited number of measurements in this survey of static pressure fluctuations in the two flows, the results are intended to show only general trends. A detailed investigation of the phenomena observed here would require a more extensive series of measurements.

IV. ACOUSTIC SIGNAL TRACING IN SUPERSONIC JET FLOWS

A. Basis for Signal Recovery Processing

In general, an understanding of interactions between perturbations generated by turbulence produced at a given point of a flow and pressure fluctuations induced at a different point is still lacking. The usual approach to such investigations is based on acoustic theory. However, this approach is not sufficiently accurate in the investigation of interactions taking place inside jet flows. Any fluctuation produced at a given point fixed with respect to the nozzle exit, propagates like a sonic boom produced by a supersonic airplane. The amplitude of this effect when considered in terms of variable speed of sound, decreases with distance from the source as indicated by acoustic theory, however, the wave shape ultimately steepens to form an N-wave of finite length. It is especially interesting in this connection that on the basis of linear theory, waves radiated from out of phase eddy disturbances would tend to cancel at the jet axis. On the basis of nonlinear theory, however, it is seen that the waves do not cancel on the axis or anywhere else. Instead there is a tendency to generate strong shocks near the jet axis which can interact strongly with existing jet shocks, and there is always an increase in the relative strength of the high frequency spectral content of the sound generating mechanism and corresponding radiation. For example, two waves of same time history but opposite sign are pictured in Fig. 41, originating at different points A and B on the periphery of a jet (41a). The initial time histories are idealized as cycles of a simple sine wave (41b). These waves steepen, and if the jet

is big enough will appear as diagrammed in Fig. 41c. When these waves interact on the axis point 3, they would be sensed by a microphone as a sawtooth of double the frequency of the original components. In any event, the phase structure has so shifted that the original phase cancellation can no longer occur. This phenomenon explains some of the longitudinal waves found experimentally in supersonic jets. The investigation of all these interactions are of extreme importance for the understanding of the interaction between turbulent cells produced by shear flow at different regions of the jets.

An experimental study of the propagation of pressure waves in the interior of a jet flow requires a means of measuring certain properties of a trace signal which has become a relatively small component of the pressure fluctuations at a point in the flow. The properties of interest for a periodic trace signal would be its overall amplitude, the amplitude and phase of a significant number of its harmonic components (so as to yield an estimate of the time signature), and its phase (or time delay) relative to a reference. Measurement of these signal parameters would be required for the determination of wavefront orientations when studying refractions, and for detecting the presence of focussing and nonlinear steepening phenomena (as discussed above and theorized in Ref. 21). These last two manifestations are of course related since pressure amplitude is a governing factor in the nonlinear steepening of compression waves. Strictly speaking a single temporal disturbance of reasonable form and duration could yield the information required to investigate these effects, but as a practical matter, the separation or recovery of the trace signal from the high level random pressure fluctuations present in the jet can

only be realized if the signal is periodic.

Leaving the actual physical situation for the moment, the problem can be stated as follows. Given a function of time,

$$F(t) = S(t) + N(t) \ , \tag{3}$$

which is the sum of a periodic, deterministic signal (S) with period T, and stationary random noise (N), how does one extract a useful representation of the signal (i.e., determine any of its unknown parameters) if the RMS amplitude of N(t) is much greater than that of S(t)? The problem is, in a general sense, one of filtering, that is, the removal of as much of the obscuring noise as possible from F(t). This procedure could be characterized as a transformation , such that

$$\bar{F}(t) = T\left[F(t)\right] = S(t) + n(t) \tag{4}$$

where again n(t) is stationary random noise. The effectiveness of such a procedure would be typified by the improvement in signal-to-noise ratio (SNR) from S_{rms}/N_{rms} to S_{rms}/n_{rms}. More generally, instead of the signal S(t) with some noise, the transformation could be such as to yield directly some required property of S(t) with an error, e.g., the amplitude of one of its frequency components.

With this in mind, some of the possible approaches to the problem are frequency filtering, auto and cross correlation, or ensemble averaging. The first method involves filtering out all frequencies in the spectrum of F(t) except those in a narrow band which includes either the fundamental frequency, $f = {}^{1}/T$, of the signal or any of its harmonics. If the spectrum of N(t) is spread over a sufficiently wide range of frequencies,

this filtering would considerably increase the signal-to-noise ratio thus allowing a more accurate measurement of the amplitudes of the spectral components of S(t). The theory of filtering, as well as certain aspects of correlation techniques, are dealt with thoroughly in Ref. 31 for application to problems in radio engineering. Of course, a very large literature exists in the field.

The use of correlation methods is practical when S(t) is a sinusoidal signal Acos $2\pi ft$. By calculating the average auto-correlation of the function F(t)

$$R_{FF}(\tau) = \frac{1}{t'} \int_{o}^{t'} F(t)\, F(t-\tau)\, dt \tag{5}$$

for $t', \tau \to \infty$; or the average cross-correlation of F(t) with some reference signal, $S'(t) = A' \cos(2\pi ft + \varphi)$,

$$R_{FS'}(\tau) = \frac{1}{t'} \int_{o}^{t'} F(t)\, S'(t-\tau)\, dt \tag{6}$$

for $t' \to \infty$, it is shown in Ref. 22 that

$$R_{FF}(\tau) \to \frac{1}{2} A^2 \cos 2\pi ft \tag{7}$$

and

$$R_{FS'}(\tau) \to \frac{1}{2} AA' \cos(2\pi ft + \varphi) \tag{8}$$

where φ is a relative phase. These results are obtained under the condition that the noise, N(t), has a zero mean and is uncorrelated with the signals S(t) and S'(t). In most circumstances, these conditions are readily satisfied. Thus the auto-correlation procedure leads to an estimate of the sinusoidal signal amplitude A, while cross-correlation yields both A and the

phase, ω, of the unknown signal relative to some chosen reference. The shortcomings are that, besides not providing any phase information, the auto-correlation processing requires a long delay time τ, and that both techniques are not readily applicable to periodic signals of arbitrary harmonic composition. For an initial signal-to-noise ratio of -20 dB, Smith and Lambert (Ref. 22) using a 1000 Hz signal and an analog correlator obtained improvements in SNR of 20 dB for auto-correlation and 40 dB for cross-correlation. Typical improvements using frequency filtering are on the order of 30 dB.

Ensemble averaging, as it is applied in this investigation, involves the sampling of one-hundred equally spaced values of the function F(t) a certain number of times, K. The resulting sequence of values,

$$F_i^{(k)} \equiv F(t_k + i\Delta t) \quad i = 0, 1, \ldots, 99 \qquad k = 1,2,\ldots K \tag{9}$$

is summed according to

$$\bar{F}_i = \frac{1}{K}\sum_{k=1}^{K} F_i^{(k)} = \frac{1}{K}\sum_{k=1}^{K} = S_i^{(k)} + \frac{1}{K}\sum_{k=1}^{K} N_i^{(k)} \quad i=0,1,\ldots 99 \tag{10}$$

In the above, Δt is the sample increment and t_k is the time when sampling of the k-th set of 100 values of F(t) is begun. The success of this method depends on choosing the t_k's such that they are synchronous with the periodicity, T, of the signal S(t), that is,

$$t_k = t_d + \alpha\,(k-1)T \qquad k = 1,2,\ldots,K \tag{11}$$

where t_d is a relative time delay which can be related to a phase,

φ, by $\varphi = 2\pi t_d/T$; and α is the smallest integer for which $t_{k+1} - t_k = \alpha T > 99\ \Delta t$. Ordinarily, Δt is chosen such that $99\Delta t$ is nearly a full period T, in which case $\alpha = 1$ and each successive cycle of S(t) is sampled. In this way, it can be seen that the sequence of sampled values $S_i^{(k)} = S(t_k + i\Delta t) = S(t_d + i\Delta t) \equiv S_i$ for all k. It follows that,

$$\bar{F}_i = S_i + \frac{1}{K}\sum_{k=1}^{K} N_i^{(k)} = S_i + n_i \quad i = 0,1,\ldots,99 \tag{12}$$

where $\bar{F}_i$ is now a 100 point approximation of S(t).

Assuming that N(t) is stationary random noise, uncorrelated with S(t) and with zero mean, an estimate can be made of how the error (or noise), n_i, in this representation of S(t) will vary with the total number of summations, K. Noting that the expected value of $\bar{F}_i$ is S_i, it is possible to show that the variance of $\bar{F}_i$ can be written as,

$$\text{var}[\bar{F}_i] = \frac{\sigma_N^2}{K}\left[1 + 2\sum_{m=1}^{K-1}\left(1 - \frac{m}{K}\right)\rho_m\right] \tag{13}$$

where σ_N^2 is the variance of N(t) ($\sigma_N = N_{rms}$), and ρ_m is the normalized correlation between $N_i^{(k)}$ and $N_i^{(k+m)}$, that is, if the auto-correlation of N(t) is $R_N(\tau)$,

$$\rho_m = \frac{R_N(m\alpha T)}{\sigma_N^2} \tag{14}$$

The noise in the final 100 point representation of S(t) will have an RMS level given by $n_{rms} = \sqrt{\text{var}[F_i]}$ and can be seen to be (for large K) less than the original N_{rms} by a factor $\sqrt{1 + \rho(k)}\ /\sqrt{K}$, that is,

$$\frac{n_{rms}}{N_{rms}} = \frac{\sqrt{1 + \rho(K)}}{\sqrt{K}} < 1 \tag{15}$$

where

$$\rho(K) \equiv 2 \sum_{m=1}^{K-1} \left(1 - \frac{m}{K}\right) \rho_m \qquad (16)$$

Since for a given K this factor is a minimum when $\rho(K) = 0$ (it is unlikely that $\rho(K) < 0$)), large positive correlations, ρ_m, between successive samples of N(t) tend to adversely affect the outcome of this procedure.

In conclusion, the improvement in SNR achieved by this method of signal enhancement will be

$$20 \log \frac{\sqrt{K}}{\sqrt{1 + \rho(K)}} = 10 \log \frac{K}{1 + \rho(K)} \quad \text{dB}$$

For a sufficiently large number of summations K, an accurate estimate can thus be obtained of the signal amplitude, time signature ($\bar{F}_i$, i = 0,...,99) and relative phase (φ).

When S(t) is a sinusoid, it would be possible to increase the effectiveness of this technique by combining it with the frequency filtering discussed earlier. That is, by first filtering the spectrum of F(t) outside a band which includes the frequency of the signal, the <u>total</u> SNR improvement after subsequent ensemble averaging would be significantly higher than that obtained by the use of this method alone. In the general case, however, of a signal with harmonic components, the relative phase shifts induced between the components by electronic filters would make the results unacceptable for subsequent ensemble averaging. The wider filter bandwidth required to pass all the harmonics would also diminish the advantages of filtering. For these reasons, the use of filtering in conjunction with ensemble averaging was not considered

further in this investigation.

B. Electronic Simulation Results

To investigate the parameters involved in the procedure just described and to calibrate the processing system to be used, a simulation study was conducted with the set-up shown in Fig. 15. The random noise, N(t) was simulated first by electronically generated "pink" noise, and then also by filtered "white" noise (bandpass: 1000-3000Hz). The signal, S(t), provided by the function generator was a sinusoid with a period $T = 180$ μsec ($f \cong 5500$ Hz). The signal and noise were summed by the differential amplifier and then fed into the digital analyzer operating in its enhance (or ensemble averaging) mode. Under these controlled conditions, it was possible to measure and vary the input signal-to-noise ratio. The sample increment, Δt, used in all cases was 2 μsec. Initiation of sampling at the times $t_k = t_d + 2(k-1)T$ ($k = 1,2,\ldots,K$) was accomplished by a sequence of pulses, synchronized with the sinusoidal output of the function generator, acting as triggers for the analyzer. The factor of 2 in the expression for t_k is to take into account the fact that the sampling of each 100 points took 200 μsec, thus requiring that the separation between successive t_k's be two periods, 2T. That is slightly more than one cycle of the signal was sampled for each k and only every other pulse triggered the analyzer. The delay time $t_d = 0$ since no delay developed in the signal between the output of the function generator and the input to the analyzer.

The signal definition at the output of the analyzer has been shown to depend on the number of summations performed and on the auto-correlation

of the noise. Two other factors affecting the outcome are the input attenuation (IA) of the analyzer and whether the analyzer processes the data in full or clip mode. In full mode there is a proportional relationship between the analog voltage, $S(t) + N(t)$, being sampled and the digitized data stored and then summed; whereas the clip mode operates such that all sampled positive voltages are digitized as + 1 and negative voltages as -1. The discussion and conclusions reached in the preceding section obviously apply to the full mode of operation. The use of clip rather than full mode processing results in significantly higher improvements in SNR. Implicit in the use of this mode, however, is the condition that the input SNR be somewhat less than 1. In the limiting case of $N(t) \equiv 0$ (SNR $\gg$ 1), it can be seen that this mode will take an input sinusoidal signal and process it into a square wave. Such distortion does not occur if the input has a significant random component. This leads to the conclusion that, in the case of signal recovery from a background of high level noise, clip is the favorable mode of operating, while the full mode is useful for improving the definition of slightly noisy signals or for displaying clean signals in a format comparable to other processed data.

Calibration curves for these two modes of operation are shown in Figs. 42-44. The signal amplitude at the conclusion of processing in the full mode (Output S_{rms}) can be seen from Fig. 42 to be directly proportional to the signal amplitude being processed (Input S_{rms}) and the number of summations (K), while inversely proportional to the input attenuation (IA). The situation in the clip mode is quite different (Fig.43). Although still depending directly on the number of summations (since the

output in both the full and clip modes is the result of a straight sum and not an average), the output signal amplitude now varies in direct proportion to the signal-to-ratio of the data being processed (Input S_{rms}/N_{rms}). For large signal-to-noise ratios, this linear relationship breaks down and it can be seen that there is a limit to the output signal amplitude which can be obtained for a given number of summations. As indicated by the arrow, for $S_{rms}/N_{rms} > .8$, the distortion referred to in the previous paragraph begins to occur to the output signal. On the other hand, there is a limit (for a given K) on how low a SNR can be processed to yield a signal free enough of noise to be reasonably identified. This subjective limit is indicated on the two curves of Fig. 43 by vertical lines. The limit is lowered by a factor of two (from $S_{rms}/N_{rms} = .003$ to .0015) when the number of summations is quadrupled. Although final SNR's were not systematically measured, indications are that the improvement in SNR with clip mode processing increases approximately as the $\sqrt{K}$ and is independent of the spectral distribution, and thus the auto-correlation of the background noise (i.e., $\rho(K) \rightarrow 0$ in the expressions derived previously). The curve in Fig. 44 indicate that the output signal amplitude in the clip mode is independent of the input attenuation setting of the analyzer if it is chosen within a proper range.

A sequence of output signals obtained from the clip mode simulation processing are shown in Fig.45 . The variation of output signal amplitude and definition (i.e., final SNR) with input SNR is clearly demonstrated. The limit of reasonable definition mentioned above can be seen to be somewhere between the fifth and sixth trace.

In the physical problem under consideration, the random noise, N(t), to be dealt with (at some point $\vec{x}$ in the jet flow) is the $p_{meas}(\vec{x},t)$ discussed and surveyed in Section III. These high level random pressure fluctuations act to critically obscure the presence of a periodic acoustic signal $S(\vec{x},t)$ at that point, whose source is an artificially generated periodic disturbance at the edge of the flow. To make use of the results obtained in the electronic simulation just described, it must be assumed that the jet pressure fluctuations and the acoustic trace signal at each point $\vec{x}$ combine in an additive manner, that is, such that the transducer senses $S(\vec{x},t) + p_{meas}(\vec{x},t)$. Also required is that $p_{meas}(\vec{x},t)$ be stationary, have zero mean, and be fully uncorrelated with $S(\vec{x},t)$. Under these conditions, the transducer output voltage can be recorded, along with a pulse train synchronized with the signal source disturbance, and processed using the clip mode, ensemble averaging technique to recover a useful representation of the unknown signal, $S(\vec{x},t)$. The success of this processing has been seen to depend on the initial signal-to-noise ratio, $S_{rms}(\vec{x})/p_{rms}(\vec{x})$, and the number of summations performed, K. The definition of the final signal representation could thus be improved by increasing the amplitude of the signal source, by decreasing the level of jet pressure fluctuations, or by maximizing K. The only reasonable way to accomplish the second is by lowering the level of disturbances originating upstream of the nozzle. The maximum number of summations possible in the processing is equal to the number of cycles of the signal that are recorded, i.e.,

$$K_{max} = fT_R \tag{17}$$

where f is the signal frequency and T_R is the total duration of each measurement in the flow. The choice of frequency is restricted by the response limits of the signal generator and, more importantly, by any physical requirements of the propagation study. The running time of the jet flow is determined solely by the available air supply.

Once a measurement in the flow was processed, the signal amplitude at the output of the analyzer was used, in conjunction with the results of Fig. , to obtain the signal-to-noise ratio $S_{rms}(\vec{x})/p_{rms}(\vec{x})$. The acoustic signal amplitude at the point $\vec{x}$ in the flow, $S_{rms}(\vec{x})$, was then determined by multiplication of this ratio by $p_{rms}(\vec{x})$ as measured during processing (i.e., since the signal level in all cases was very small it could be assumed that $p_{rms}(\vec{x}) \equiv [p_{meas}(\vec{x},t)]_{rms} \cong [S(\vec{x},t) + p_{meas}(\vec{x},t)]_{rms}$. The time signature of the signal as well as its phase relative to the source disturbance can be estimated directly from the analyzer output representation.

As a reference, a recording of the acoustic signal at each point $\vec{x}$ in still air (i.e., without the jet flow) was also processed. Since an intense noise background does not exist in this case, the processing was done in the full mode of operation.

C. Results of Signal Tracing

1. Loudspeaker Signal

In the first experimental application of the signal recovery procedures, an attempt was made to map the field created by a single Altec loudspeaker within the primary jet in the two running conditions described in Section III. The mouth of the loudspeaker horn was placed at

the edge of the flow near the nozzle exit, i.e., 4 in. below the jet centerline and 2 in. downstream of the nozzle exit as shown in Fig. In order to maximize the possible number of summations in the signal recovery processing, a relatively high loudspeaker signal frequency of 5500 Hz ($T \cong 180$ μsec) was chosen along with a total running time for each measurement in the flow of 40 sec. This allowed for $K_{max} = 220{,}000$ possible summations, and a corresponding maximum possible improvement in signal-to-noise ratio of approximately 53 dB. The output amplitude of the loudspeaker was also optimized to a level of about 150 dB at the center of the horn exit plane. As described in Section II, the loudspeaker was powered in a sinusoidal mode. The mapping of the loudspeaker signal field consisted of an attempt to observe, through signal recovery processing, the acoustic signal present at several positions along the centerline of the jet ($Y/D = 0$) and along a parallel line 1.5 inches below ($Y/D = -.2$), for downstream distances ranging only as far as 19 inches ($x/D = 2.7$). Due to the high levels of background pressure fluctuations and the limited signal source strength, successful recovery was restricted to this initial section of the jet.

Signal traces resulting from the processing of measurements at these positions in the balanced jet are presented in Figs. 46-51. (The spikes which appear on some of the traces just to the left of center are due to an effect in the electronics and should be ignored.) At each position (identified according to the labels assigned in Fig.52), two traces are shown; the upper is of the acoustic signal as it exists at that point in still air, while the lower shows, when the recovery processing succeeds, the signal arriving at that point in the presence of the supersonic flow.

Due to the sample increment used in the processing (Δt = 2 μsec), each of these 100 point traces is of 200 μsec of the signal, that is, of slightly more than one cycle. Next to each trace is an indication of the sound pressure level of the signal it represents. The variation of signal level in still air and within the flow is summarized in Fig. 52.

The acoustic signal field in still air can be seen to be very complex. There is a significant amount of distortion occurring to the original sinusoidal disturbance as it propagates both directly and after reflection from nearby surfaces to each measuring position. The distortion itself can be related to the high level of the initial disturbance, while the spatial complexity of the field is due to the high frequency of the signal and the proximity of the signal generator to a number of scattering bodies (Fig. 13). One consequence of the high frequency, and the resulting wavelength in still air of about 2.5 inches, is that signals originating from opposite edges of the source disturbance (the 3 in diameter exit of the loudspeaker horn) arrive at some positions with significant phase shifts. The variation of signal level (Fig. 52) shows that, in the vicinity of the loudspeaker where measurements were made, the acoustic field is very directional with most of the energy concentrated close to the axis of the horn.

Appreciable changes occur to the field in the presence of the balanced supersonic flow. Although a strong directionality pattern still exists (Fig. 52), it is now centered about a ray making an angle of approximately 60° with the axis of the horn. Since the Mach angle in the flow is 30° (M = 2), this is a demonstration that, once the initial disturbance crosses the thin mixing layer present in this early stage of the jet, its region of

influence is determined (due to the supersonic convection) by the characteristic lines in the flow (two of which are shown). As a result, little if any of the disturbance would be able to reach points upstream of the characteristic which emanates from the nozzle lip. This is clearly the case since no signal is recovered at the first four positions along the centerline and the first two along y/D = - .2 (Figs. 46-47). (When the processing does not yield anything which can be reasonably identified as a signal, an estimate is made of the minimum signal level which could have been recovered from the known noise level at each point. This estimate is indicated in Fig.52 by horizontal dashes. The signal level at these positions is then somewhere below this mark.) The maximum signal levels attained within the flow are lower than those in still air possible due to the fact that not all of the source energy is transmitted across the flow boundary, that is, some is reflected back toward the source. A series of measurements along both sides of the flow boundary would be required to investigate the mechanisms involved in the transmission of the disturbance through the shear layer at the boundary. As would be expected, the peak level along y/D = - .2 is slightly higher than that along the centerline in still air, but within the flow the reverse is true. This is perhaps an indication of a focussing phenomenon which could be enhanced and explored further using a circumferential distribution of source disturbances around the periphery of the jet. An attempt was made to determine whether the signal level downstream of x/D = 2.7 along the centerline increased due to an interior reflection of the disturbance from the opposite edge of the flow (i.e., at $y/D \cong + .5$). Although there were some signs of such an effect, the signals recovered in this region were generally too weak to allow a definite

conclusion to be reached.

The traces obtained in the presence of the flow, particularly where the signal levels are high (Figs. 48-49), clearly show that the source disturbance remains sinusoidal as it propagates through the jet. The complex pattern of distortion occurring to the signal profiles in still air does not exist in the flow, at least as far as can be seen from the "cleanly" recovered signals. This could be due to the lowering of the initial disturbance level by the reflection at the flow boundary combined with the absence of any scattered fields within the flow. On the other hand, this effect together with the absence of significant phase differences between signals arriving at various points within the flow (i.e., 6a,6b,7a,7b), might involve phenomena requiring further investigation.

The measurements at two positions in the flow (6a and 5b) were repeated and are presented as 6a' and 5b' in Fig. 53 . Except for slight differences in the still air signals (due to errors in positioning the probe in the spatially intricate field), the results show the basic reproducibility of the measurements and subsequent processing.

In Figs. 54-60 are presented the results of a sequence of measurements tracing the acoustic signal within the overexpanded jet (P_e = 10 psia). Other than the absence of data for positions 8a and 8b, they consist of the same set of measurements made in the balanced jet. The interpretation of the results here, however, is more difficult for two reasons. The region of the jet through which the signal is being traced is no longer one of constant mean flow velocity, but rather consists of the previously described shock-cell structure. Furthermore, at the time these measurements in the overexpanded jet were made, the signal being recovered at

each point in the flow was the sum of the usual acoustic signal plus a non-pressure (electrical) signal being induced (electromagnetically) in the recording instrumentation by the signal generating system. The two main sources of this spurious signal were found to be the proximity of the loudspeaker power amplifier to the transducer amplifiers and the existence of a section of unshielded cable leading to the loudspeaker. The signals recovered at the first few positions in the flow (Fig. 54) were primarily due to these sources since the points are outside the zone of influence of the acoustic source. This conclusion was verified by repeating the measurements at two of these positions (1a and 1b) using the "blind" nose cone shown in Fig. 9 to seal-off the transducer from any acoustic signal. The signal levels obtained from processing these measurements were only slightly lower than those obtained with the transducer capable of sensing pressure fluctuations, thus indicating that although most of the signal is due to nonpressure sources, some acoustic signal can still perhaps reach these positions by upstream propagation through the subsonic mixing and boundary layers in the flow. The actual error caused by the electrical signal would depend on the phase it has relative to the acoustic signal at each point. (The sources of the electrical signal were largely eliminated prior to making measurements in the balanced flow.)

The signal traces obtained within the overexpanded jet, as well as the variation of signal level shown in Fig. 60, must therefore be interpreted with some caution. However, several of the basic phenomena observed for the signal in the balanced jet can still be seen to occur here. The signal traces recovered with some clarity (Figs. 55 and 56) again show that the disturbance remains sinusoidal as it now propagates through the various

flow regions comprising the initial cell structure of the overexpanded jet. There is also, as before, an absence of large differences in phase between many of the signals within the flow. Although the acoustic signal field is again convected downstream (Fig. 60), the shift is significantly less than it was in the balanced flow. There are two possible reasons for this. The most obvious is that the Mach number at which the field is convected drops from $M = 2$ to $M \cong 1.6$ across the first shock in the flow shown in Fig. 60 Less obvious is the fact that, due to this shock, the initial flow streamlines will be deflected toward the centerline of the jet causing the flow boundary to move away from the signal source disturbance. Since the convection would then begin closer to the lines along which measurements were made, it is reasonable that the convected distances are less. These two effects can be pictured more clearly in terms of the characteristics in the flow. The first can be seen as an increase in the angle of the characteristic lines with respect to the flow direction, and the second as an upward (vertical) shift of the points from which the characteristics emanate.

The failure to recover a signal at positions 3a and 10a (Figs. 55 & 58) in the overexpanded jet was due to the unusually high level of jet pressure fluctuations resulting from the presence, near these positions, of the first two Mach discs in the flow.

2. Multi-Source Siren Signal

It was clear from the beginning of this experimental program that a study of the propagation of mixing induced disturbances into the core of a supersonic jet could best be accomplished using a circumferential

distribution of signal sources. To this end the pneumatic siren system described in Section II was designed, constructed, and installed. The system consists of a rotating-value siren that generates from one to six signals (Fig. 6), lines (5/8" I.D. and approximately 17 ft long) for channelling the signals to the flow (Fig. 16), and a ring that injects each signal along a 60^{o} arc of the flow boundary near the nozzle exit (Fig. 17). The system was designed to allow independent control of the amplitude and phase of each of the six signals: the amplitude by six valves controlling the siren back-pressures and the phase by the variable length of the delivery lines. The frequency of all the signals was the same but variable through the speed of the rotating-valve (disc).

Early preliminary testing of the siren was conducted with only one signal line operating and with the disc at a speed of 2000 rpm, giving a signal frequency of 800 Hz. The signal was measured at a distance of 4" from the outlet of various lengths of 5/8" I.D. straight pipe emanating from the siren. As expected, for high back-pressures a significant amount of steepening occurs to the compression phase of the signal as it propagates along the pipe. For back-pressures higher than 30 psia and pipe lengths greater than 1 ft. the signal at the measuring position is sensed as a series of spikes instead of the more sinusoidal signal that results when the back-pressure is much lower. In order to regenerate a more acceptable signal, several resonator type devices were added to the end of the pipe. The best results were obtained with the configuration shown in Fig. 61. The signal measured after a length of 10 ft. of pipe is shown in Fig. 62a, and that which results after the addition of this resonator appears as Fig. 62b. The signal amplitudes in the two cases

were .14 psi zero-to-peak and 134 dB, respectively.

It was also discovered during these early studies of the siren that a significant amount of unwanted sound was being generating by leaks at the disc-air supply interface and by resonances excited at certain disc speeds in the cavities surrounding the disc. One possible solution to this problem was to provide a sound isolating enclosure for the siren. The solution chosen, was to make the modifications to the siren shown in Fig. 18,* also shown in this figure is a ball-bearing support which was added to the siren shaft to uncouple the siren disc from the electric motor.

Once the multi-source signal generating system was put in the final operating configuration shown in Fig. 16, tests were conducted to determine the effects of the siren disc speed (frequency), and the back-pressure and length of each of the signal lines on the signal amplitude, phase and shape. This had to be done for each of the six lines individually and in various combinations, including of course the case where all the lines operated simultaneously. The signal was measured in each case at the centerline of the injection ring shown in Fig. 17 (coinciding with the centerline of the jet nozzle), just downstream of the exit plane of the ring.

To obtain the relative phase of each signal, a reference or synchronization signal was required. This was first provided by the output of a

---

* i.e. to enclose the rotating disc between two fixed thick plates, leaving a gap of $\sim$ 1/16" between the disc and each plate

pressure transducer sensing the signal along one of the six lines near the downstream side of the siren. While this line was being used to provide the reference signal it had to be disconnected from the injection ring so as not to affect the signal measured from each of the other five lines. Because of this inconvenience and the fact that the transducers available did not quite have the necessary sensitivity for this application, a mechanical contact-switch device was developed. This system, shown in Fig. 7, consists of a disc attached to the siren motor shaft whose rim is made up of alternating conductive and non-conductive regions aligned with the 24 windows of the siren's rotating-valve. A contact switch riding on the rim of the disc opens and closes a bridge circuit yielding an alternating voltage (zero when closed, 3 volts when opened) which is then used to trigger an electronic pulse generator. The final result at the output of the pulse generator is a continuous train of pulses at the precise frequency of the siren signals and whose amplitude and duration can be adjusted to any required values. Besides serving as a reference with respect to which the relative phases of the six siren signals could be measured, the pulse train could also be used to set the siren disc speed (i.e., by measuring the pulse frequency with a counter) and to synchronize the signal recovery processing as described in Section II.

The signals measured with each of the six lines operated one at a time are shown in Figs. 63a and b. The signal frequency is approximately 670 Hz (disc speed 1575 rpm) and the siren back-pressures were set so as to yield a signal level of 120 $\pm$ 2 dB in each case. Although the length of each of the signal lines was approximately the same, it can

be seen that there are slight differences in phase between each of the signals. Also evident are significant differences in signal shape from one source to another. Both of these effects can be related either to irregularities in the physical construction of the individual signal lines, to differences in back-pressure required for each of the lines, or to slight variations in setting the siren disc speed for each measurement. The signal shape was found to be particularly sensitive to disc speed (frequency) - small changes in speed resulted in dramatic changes in the signal shape.

The effect of back-pressure on signal shape and phase is demonstrated by the traces of Figs. 64a and b. Again the frequency is about 670 Hz, but now the back-pressure in each line has been increased so that the peak-to-peak signal amplitude is approximately ten times that of the signals of Fig. 63. The considerable changes in signal shape that occur can be related to the nonlinear variation of the local speed of sound at the higher back-pressures which manifests itself as steepening of the compression phase of the signals as they propagate along the delivery lines. The changes in signal phase are more difficult to explain but are most likely related to the dependence of the speed of porpagation of the signals on back-pressure and to irregularities in the construction of the signal generating system which became significant, in terms of affecting the signal phase, at the higher back-pressures.

Before proceeding with the next step which was to operate two or more signal lines simultaneously, it was necessary to insure that the signal characteristics of any one line were not altered by the operation of any other line. This was accomplished by providing six ports on the injection

ring near the entrance to the triangular chambers of the ring (Fig. 17) through which the signal could be sensed by a pressure transducer. First it was verified that the signal measured at each of these ports was due predominantly to the signal arriving along each of the respective lines and not for example due also to signals travelling across the ring from other lines. Then the port signal for a given line was measured with that line operating alone and, successively, together with each of the other five lines. This procedure was repeated for each of the six ports and it was found that in each case the measured signal did not significantly change in going from single to multiple operation.

Once this was verified, it was possible to set-up the amplitude and phase of each of the six signal sources individually and to assume that the signal measured during simultaneous operation would be just the sum of the individual component sources. An example of the signal measured with all six sources activated is shown in Fig. 65a. The individual sources are set-up approximately as in Fig. 63, the frequency being 670 Hz. The overall signal amplitude is about 135 dB. This measurement was repeated several different times and the trace shown in Fig. 65b demonstrates the reproducibility of the result.

V. CONCLUSIONS

A facility has been constructed to provide two coaxial axisymmetric jets of unheated air. The inner primary flow exhausts from a 7" exit diameter convergent-divergent nozzle at M = 2, while the concentric secondary flow has a 10" outside diameter and is sonic at the exit. The large dimensions of the jets permit one to place probes inside the jet core without significantly disturbing the flow.

Static pressure fluctuations were measured within the primary flow in two running conditions. One yielded a perfectly expanded (balanced) flow with a jet Mach number $M_j = 2$, and the other an overexpanded flow with $M_j = 1.8$. The maximum level of static pressure fluctuations along the centerline of both flows was found to be near the end of their respective supersonic cores. However, even with the lower mass flow, the levels along the centerline of the overexpanded jet were generally higher than those for the balanced jet. This was particularly the case in the area of the Mach discs in the former flow where appreciable increases in level were detected. The spectral composition of these static pressure fluctuations tended to show that the higher levels along the centerline of the overexpanded jet could be related to the shock-cell structure present in that flow. Starting near the exit of the nozzle with a level and spectral distribution of upstream disturbances that was similar in both flows, the static pressure fluctuations in the balanced jet increased with distance downstream due to the addition of energy which could be traced to disturbances originating in the mixing layer, while in addition to this effect, the fluctuations in the overexpanded jet

included an amplification of disturbances propagating through the cell structure. This was particularly evident for the low frequency disturbances originating upstream of the nozzle (e.g., due to mass flow fluctuations and the large size of the settling chamber). Since this was the only probable source of disturbances with frequencies on the order of 100 Hz, the growth in energy of the static pressure fluctuations at these frequencies along the centerline of the overexpanded jet could best be accounted for in terms of the intensification of these disturbances by the shock structure in the core of this jet. Downstream of this structure (i.e., where the jet becomes fully turbulent), the level and spectrum of the fluctuations were again similar to those in the balanced flow. Another shock-related phenomenon (screech) was believed to be the cause of a strong peak in fluctuations between 800 and 900 Hz within the overexpanded jet.

The similarity between the two flows near the exit of the nozzle and then after the flows become fully turbulent was also evident in the profiles of the variation of static pressure fluctuation level with radial distance from the centerline. In the initial flows, these profiles showed a peak level occurring in the mixing layer, and a lower, more constant level about the centerline. Far downstream, the profiles in both jets indicated a more uniform distribution of level across the fully turbulent flows. In between these regions, one significant difference could be seen in the profiles for the two flows. While the peaks in the mixing layer broadened as the scale of mixing grew in the balanced jet, a shift in the peak level to the centerline occurred in the overexpanded jet. The intensification of disturbances in the core of this

jet was believed to be responsible for the shift.

The tracing of an acoustic signal through the jet flow required the development of two systems; one for externally injecting and then detecting the signal within the flow, and another that would allow for observation of the signal amidst the random pressure fluctuations of the flow. Two signal generating systems were utilized. An electro-acoustic loudspeaker was chosen because of its relatively high output over a wide frequency range, the control it allows over signal shape, and the ease with which it permits synchronization of the signal for subsequent processing. A mult -source pneumatic siren was also developed to provide a circumferential distribution of sources at the periphery of the flow. Size and high frequency response were the basic criteria used in selecting the transducers for sensing the signal (and jet pressure fluctuations), although obvious consideration had to be given to the requirement that the high levels of mean and fluctuating jet pressure were within the operating range of the transducers. If not for this requirement, transducers with higher sensitivities could have been chosen.

Of the possible procedures available for recovering or separating a periodic signal from a high level random noise background, it was concluded that ensemble averaging most directly yields all the required properties of the signal (i.e., amplitude, time history, and relative phase). An electronic simulation study of the processing involved in this procedure was made to determine how various parameters affected the outcome and to calibrate the instrumentation being used. The definition with which the signal is recovered by the processing was found to depend approximately on the square-root of the number of cycles of the signal available for

processing. Obviously, it would also directly depend on the initial signal-to-noise ratio of the data being processed. But since the output level of the signal generators was limited and the level of jet pressure fluctuations (noise) could not be easily lowered, an attempt was made to maximize the effectiveness of the processing by increasing the number of cycles of the signal sensed during a measurement in the flow, that is, by choosing a high signal frequency and running the flow for as long as possible.

With the loudspeaker, a combination of a signal frequency of 5500 Hz and a running time of 40 sec. permitted a maximum possible improvement in signal-to-noise ratio of about 53 dB. Even with this high degree of improvement in signal definition, the successful application of these procedures to the recovery of the loudspeaker generated signal within the primary jet flow was restricted to a limited region of the flow. The data that were acquired did suggest the existence of several effects. They clearly demonstrated the supersonic convection of the acoustic field and the resulting limited upstream influence of the signal source. Also indicated was a possible increase of signal strength as it propagated toward the centerline of the flow. Missing in the signal traces recovered within the flow, however, was the development of any distortion in the initial sinusoidal profile. Since this was seen to occur for the acoustic field in still air, it would be of interest to investigate why it doesn't within the flow. This would apply as well as to the absence of appreciable phase differences between signals arriving at various points in the flow.

During this investigation the multi-source pneumatic signal generator was made operational and its characteristics were studied. Since this is a useful tool for studying wave steepening and focussing in an axisymmetric flow, its use in investigating these and other propagation phenomena would be valuable. The basic techniques developed during this experimental program could be applied to investigate wave propagation both subsonic and supersonic flows.

REFERENCES

1. Dosanjh, D.S., Bassiouni, M.R., Bhutiani, P.K., and Ahuja, K.K., "Potential of Coaxial Multinozzle Configurations for Reduction of Noise from High Velocity Jets," Proceedings of the Interagency Symposium on University Research in Transportation Noise, Raleigh, North Carolina, Vol. 1, pp. 162-177, June 1974.

2. Nagamatsu, H.T., Sheer, R.E., Jr., and Gill, M.S., "Characteristics of Multitube Multishroud Supersonic Jet Noise Suppressor," AIAA Journal, Vol. 10, No. 3, pp. 307-313, 1972.

3. Mangiarotty, R.A. and Cuadra, D.E., "Acoustic and Thrust Characteristics of the Subsonic Jet Efflux from Model Scale Sound Suppressors-Part 1, Unheater Jets," Boeing Report No. 06-15071, 1968.

4. Nagamatsu, H.T., Sheer, R.E., Jr., and Gill, M.S., "Flow and Acoustic Characteristics of Subsonic and Supersonic Jets from Convergent Nozzle," AIAA Paper No. 70-802, 1970.

5. Eldred, K.M., et. al., "Far Field Noise Generation by Coaxial Flow Jet Exhausts, Volume 1 - Detailed Discussion," FAA Report No. RD-71-101,1, November 1971.

6. Mollo-Christensen, E., Kolpin, M.A., and Martucelli, J.R., "Experiments on Jet Flows and Jet Noise Far-Field Spectra and Directivity Patterns," J. Fluid Mech., Vol. 18, No. 2, pp. 285-301, 1964.

7. Laufer, J., Chu, W.T., Schlinker, R.H., and Kaplan, R.E., "Supersonic Jet Noise Investigations," Proc. Inter. Symp. Univ. Res. Transp. Noise, Raleigh, N.C., Vol. 1, pp. 59-73, June 1974.

8. Lee, H.K. and Ribner, H.S., "Direct Correlation of Noise and Flow of a Jet," J. Acoust. Soc. Amer., Vol. 52, No. 5, pp. 1280-1290, 1972.

9. Siddon, T.E., "Some Observations on Source Detection Methods with Application to Jet Noise," Proc. Inter. Symp. Univ. Res. Transp. Noise, Raleigh, N.C., Vol. 1, pp. 74-89, June 1974.

10. Scharton, T.D. and White, P.H., "Simple Pressure Source Model of Jet Noise," J. Acoust. Soc. Amer., Vol. 52, No. 1, pp. 399-412, 1972.

11. Scharton, T.D., White, P.H., Rentz, P.E., et. al., "Supersonic Jet Noise Investigations Using Jet Fluctuating Pressure Probes," Air Force Aero Propulsion Laboratory Report No. TR-72-35, June 1973.

12. Nagamatsu, H.T., Sheer, R.E., Jr., and Gill, M.S., "Flow and Acoustic Characteristics of Subsonic and Supersonic Jets from a Convergent Nozzle," General Electric Research and Development Center Report NO. 69-C-310, September 1969.

13. Nagamatsu, H.T., Sheer, R.E., Jr., and Bigelow, E.C., "Mean and Fluctuating Velocity Contours and Acoustic Characteristics of Subsonic and Supersonic Jets," AIAA Paper No. 72-157, January 1972.

14. Nagamatsu, H.T. and Sheer, R.E., Jr., "Subsonic and Supersonic Jets and Supersonic Suppressor Characteristics," AIAA Paper No. 73-999, October 1973.

15. Chih-ming, H. and Kovasznay, L.S.G., "Acoustic Wave Propagation Through a Two-Dimensional Turbulent Jet," Proc. Inter. Symp. Univ. Res. Transp. Noise, Stanford, California, Vol. 1, pp. 3-17, March 1973.

16. Slutsky, S. and Tamagno, J., "Sound Field Distribution About a Jet," General Applied Science Laboratories Technical Report No. 259, December 1961.

17. Gottlieb, P., "Sound Source Near a Velocity Discontinuity," J. Acoust. Soc. Amer., Vol. 32, pp. 1117-1122, September 1960.

18. Slutsky, S., "Acoustic Field of a Cylindrical Jet Due to a Distribution of Random Sources or Quadrapoles," General Applied Science Laboratories Technical Report No. 281, February 1962.

19. Liu, C.H. and Maestrello, L., "Propagation of Sound Through a Real Jet Flowfield," AIAA Paper No. 74-5, January 1974.

20. Kelsall, T., "Suppression of Refraction in Jet Noise," Proc. Inter. Symp. Univ. Res. Transp. Noise, Raleigh, N.C., Vol. 1, pp. 2-6, June 1974.

21. Ferri, A., Ting. L., and Werner, J., "Supersonic Jet Engine Noise Analysis," Proc. Inter. Symp. Univ. Res. Transp. Noise, Stanford, California, Vol. 1, pp.39-54, March 1973.

22. Smith, M.W. and Lambert, R.F., "Acoustical Signal Detection in Turbulent Airflows," J. Acoust. Soc. Amer., Vol. 32, No. 7, pp. 858-866, 1960.

23. Ferri, A., Slutsky, S., and Panunzio, S., "Fluid Dynamic Aspects of Jet Noise Generation," Proc. Inter. Symp. Univ. Res. Transp. Noise, Stanford, California, Vol. 1, pp. 55-63, March 1973.

24. Slutsky, S., Panunzio, S., and Barra, V., "Fluid Dynamic Aspects of Jet Noise Generation," Proc. Inter. Symp. Univ. Res. Transp. Noise, Raleigh, N.C., Vol. 1, pp. 178-183, June 1974.

25. Panunzio, S., Ferri, A., and Slutsky, S., "Fluid Dynamic Aspects of Jet Noise Generation," NYU Report No. AA-74-10, October 1974.

26. Barra, V., Slutsky, S., and Panunzio, S., "Ambient and Induced Pressure Fluctuations in Supersonic Jet Flows," AIAA Paper No. 75-482, March 1975.

27. Bruel & Kjaer Instruments Inc., "Product Manual," Copenhagen, Denmark, February 1967.

28. Benzakein, M.J. and Knott, P.R., "Supersonic Jet Exhaust Noise," Air Force Aero Propulsion Laboratory Report No. TR-72-52, August 1972.

29. Nagamatsu, H.T. and Horvay, G., "Supersonic Jet Noise," AIAA Paper No. 70-237, January 1970.

30. McLaughlin, D.K., Morrison, G.L., and Troutt, T.R., "Experiments on the Instability Waves in a Supersonic Jet and Their Acoustic Radiation," Proc. Inter. Symp. Univ. Res. Transp. Noise, Raleigh, N.C., Vol. 1, pp. 113-127, June 1974.

31. Wainstein, L.A. and Zubakov, V.D., Extraction of Signals from Noise, Dover Publications Inc., New York, 1962.

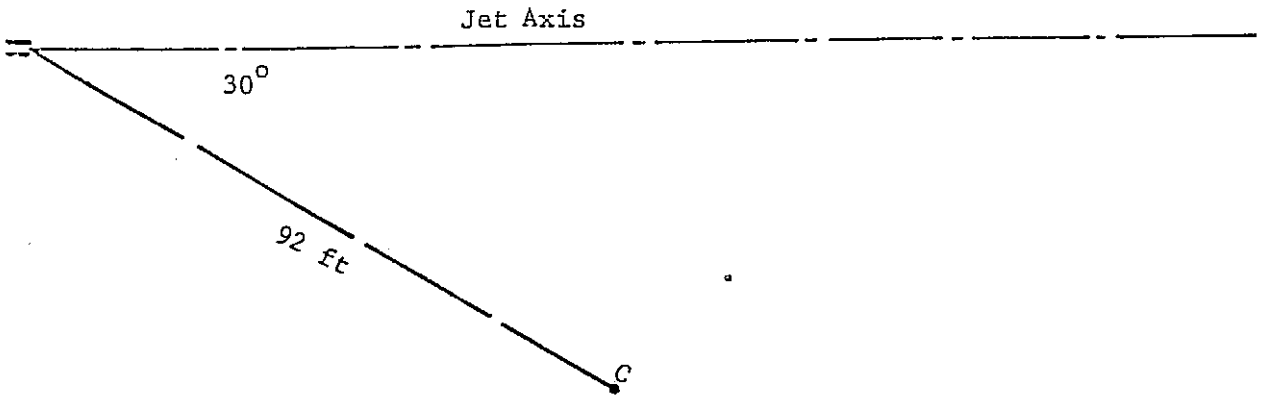

TABLE I

NOISE LEVELS DUE TO PRIMARY JET FOR VARIOUS RUNNING CONDITIONS (T_o = 490°R)

M_e	P_o	P_e		SPL AT POINT C
.95	36 psia	14.6 psia	19 lb/sec	109 dB
1.18	41 psia	17.2 psia	21 lb/sec	118 dB
1.99	79 psia	10.3 psia	41 lb/sec	122 dB
2.00	101 psia	12.9 psia	52 lb/sec	127 dB
2.00	107 psia	13.5 psia	55 lb/sec	128 dB

TABLE II

FARFIELD NOISE LEVELS DUE TO PRIMARY JET - ACROSS THE HARLEM RIVER ($T_o = 490^oR$)

DISTANCE FROM EXIT	ANGLE FROM CENTERLINE	P_o	SPL
600'	0^o	107 psia	95 dB
620'	15^o	108 psia	104 dB
850'	15^o	107 psia	101 dB
500'	30^o	107 psia	100 dB

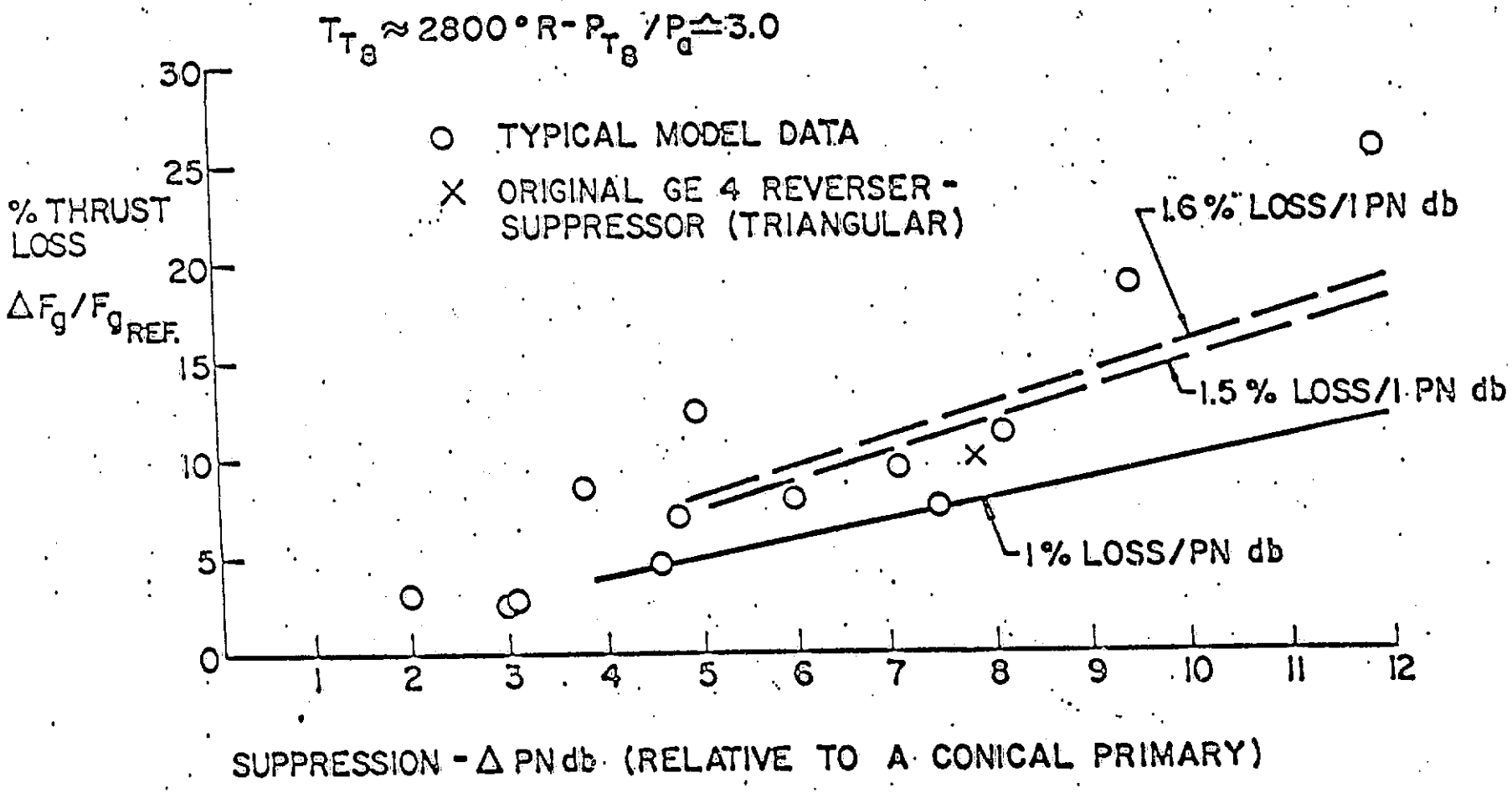

Fig. 1 Suppression - ΔPN db (relative to a conical primary) versus thrust loss

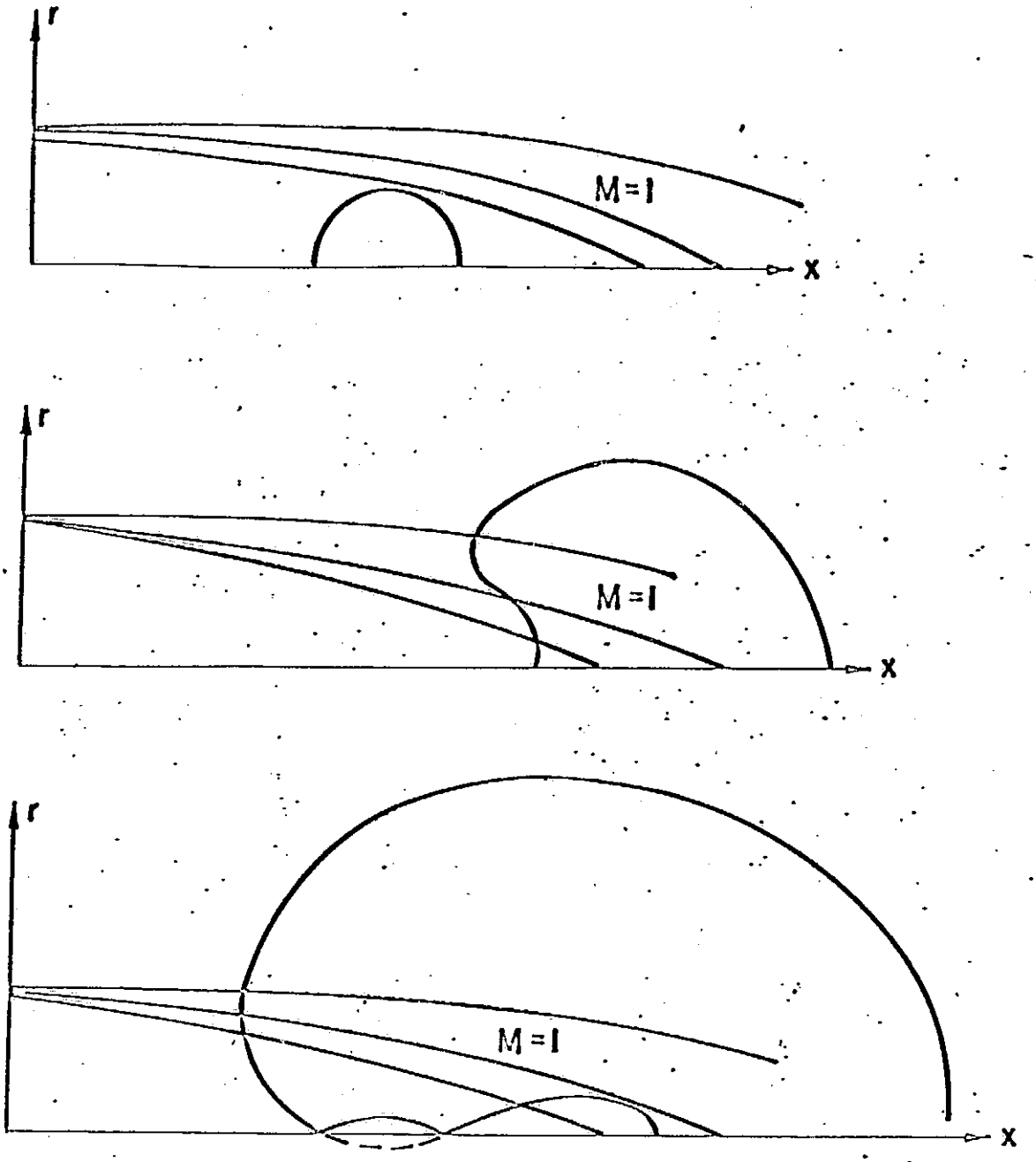

Fig. 2 Propagation of a pulse through the mixing zone

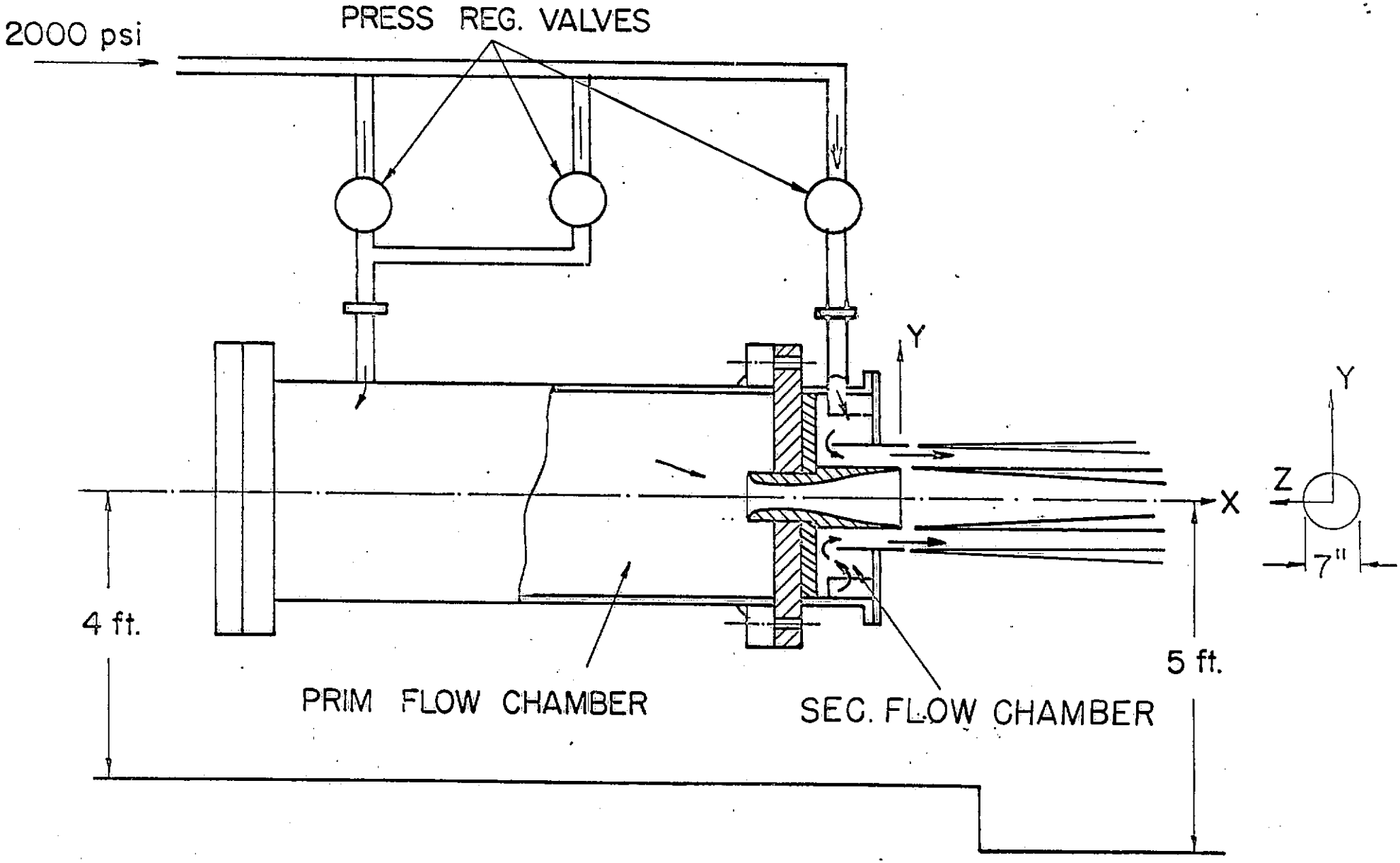

Fig. 3 Facility configuration

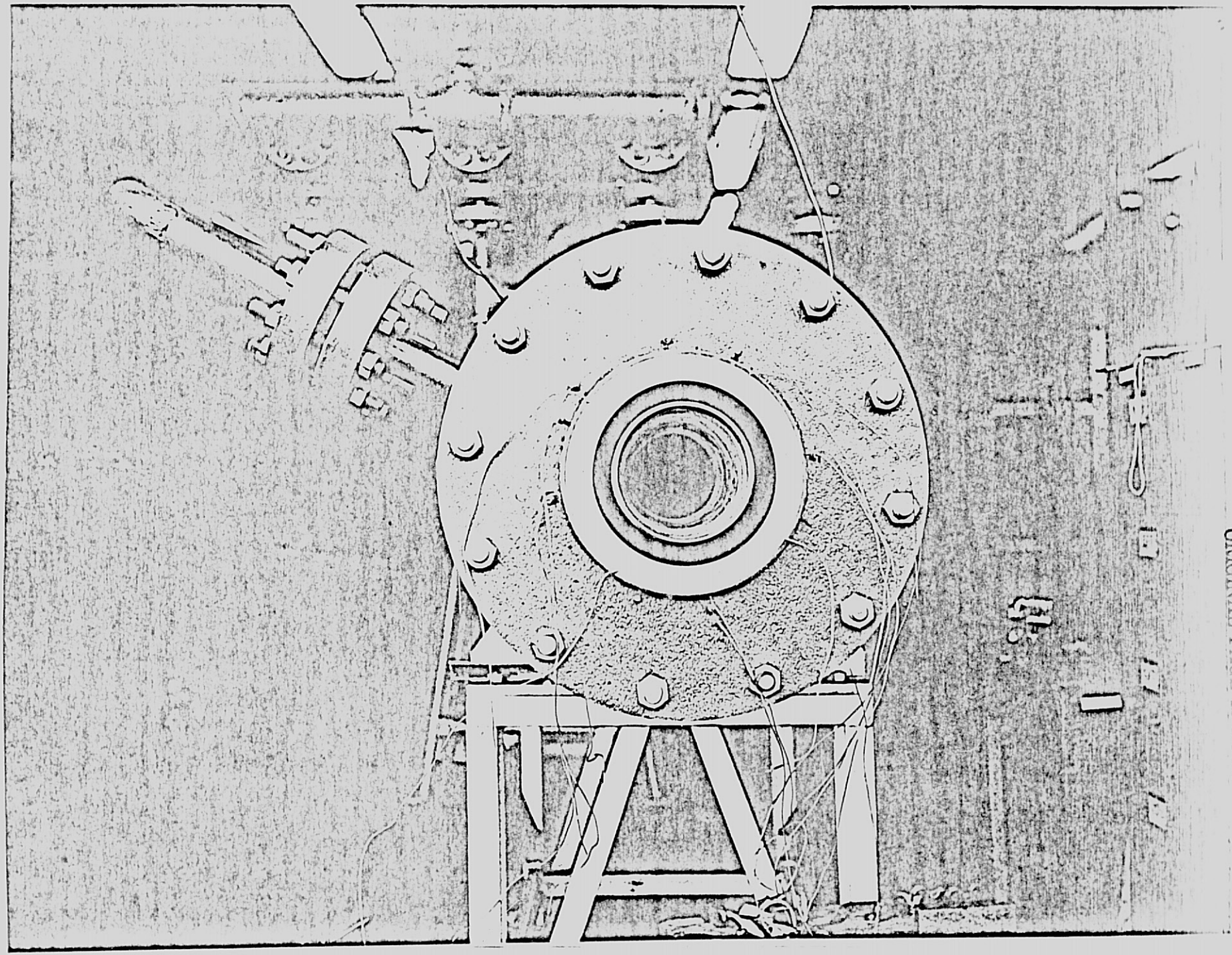

Fig. 4 Coaxial nozzles

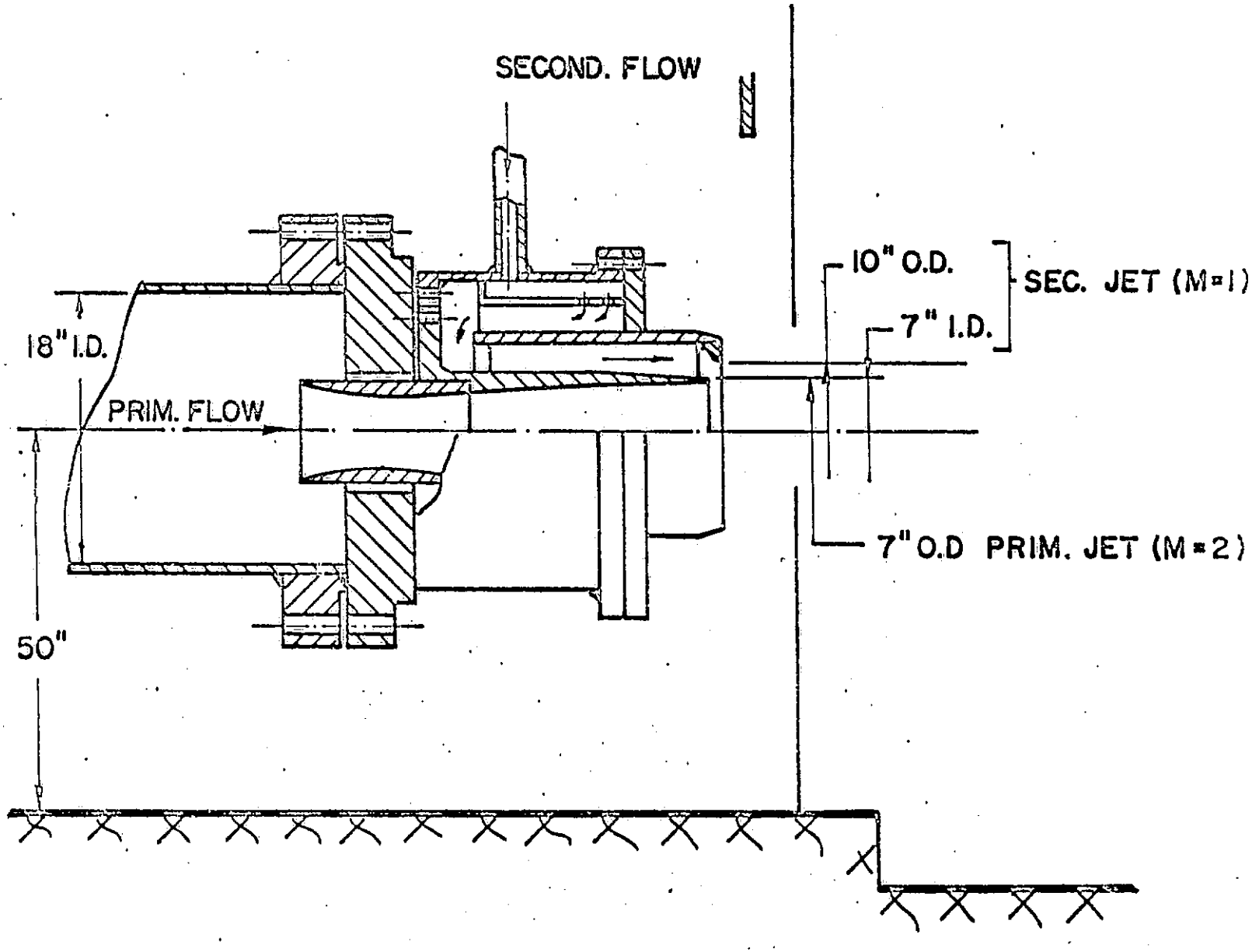

Fig. 5 Coaxial jets with modified outer (secondary) jet to M = 1

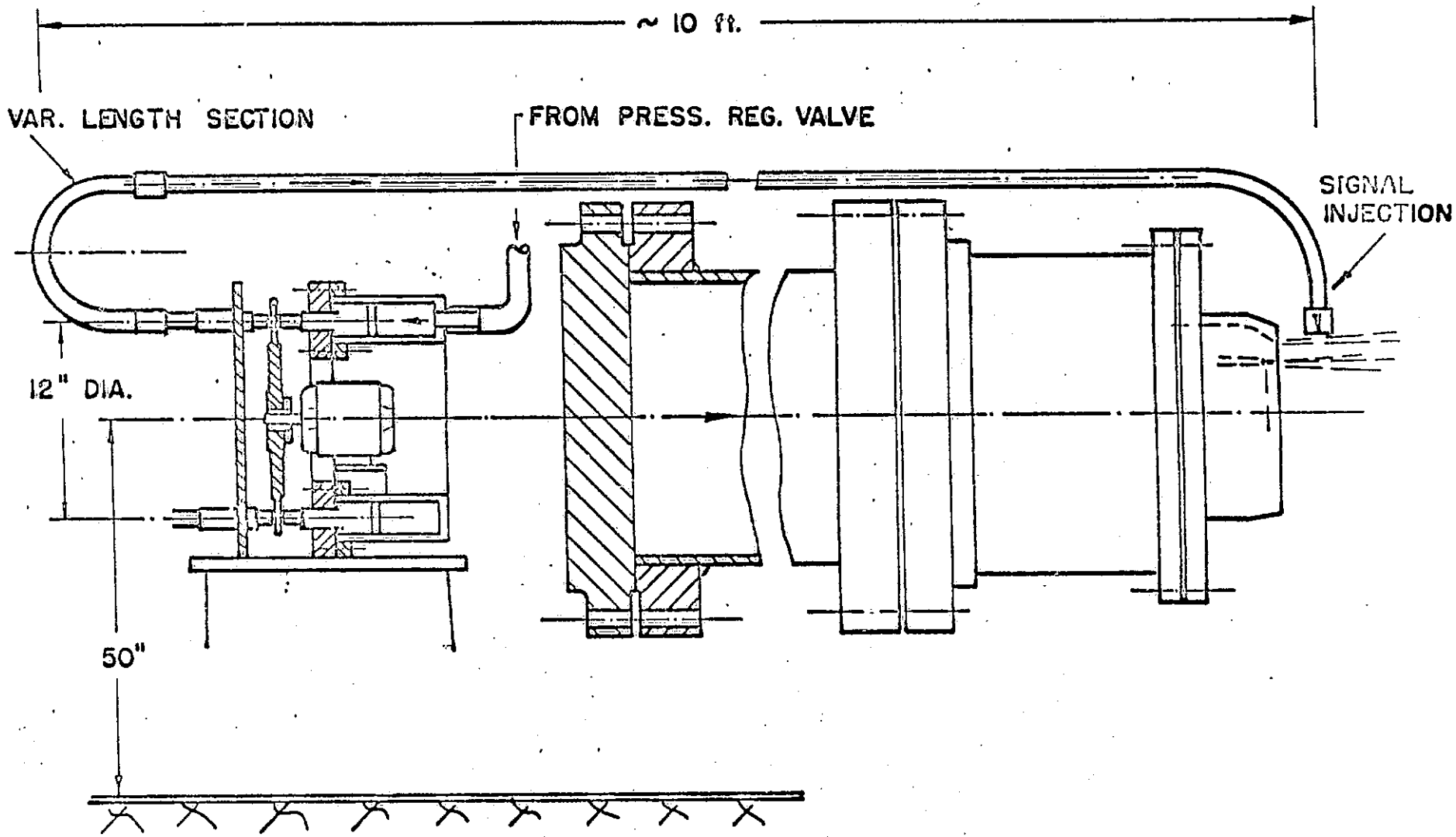

Fig. 6 Pneumatic signal generator (siren) and conduction to signal injection points

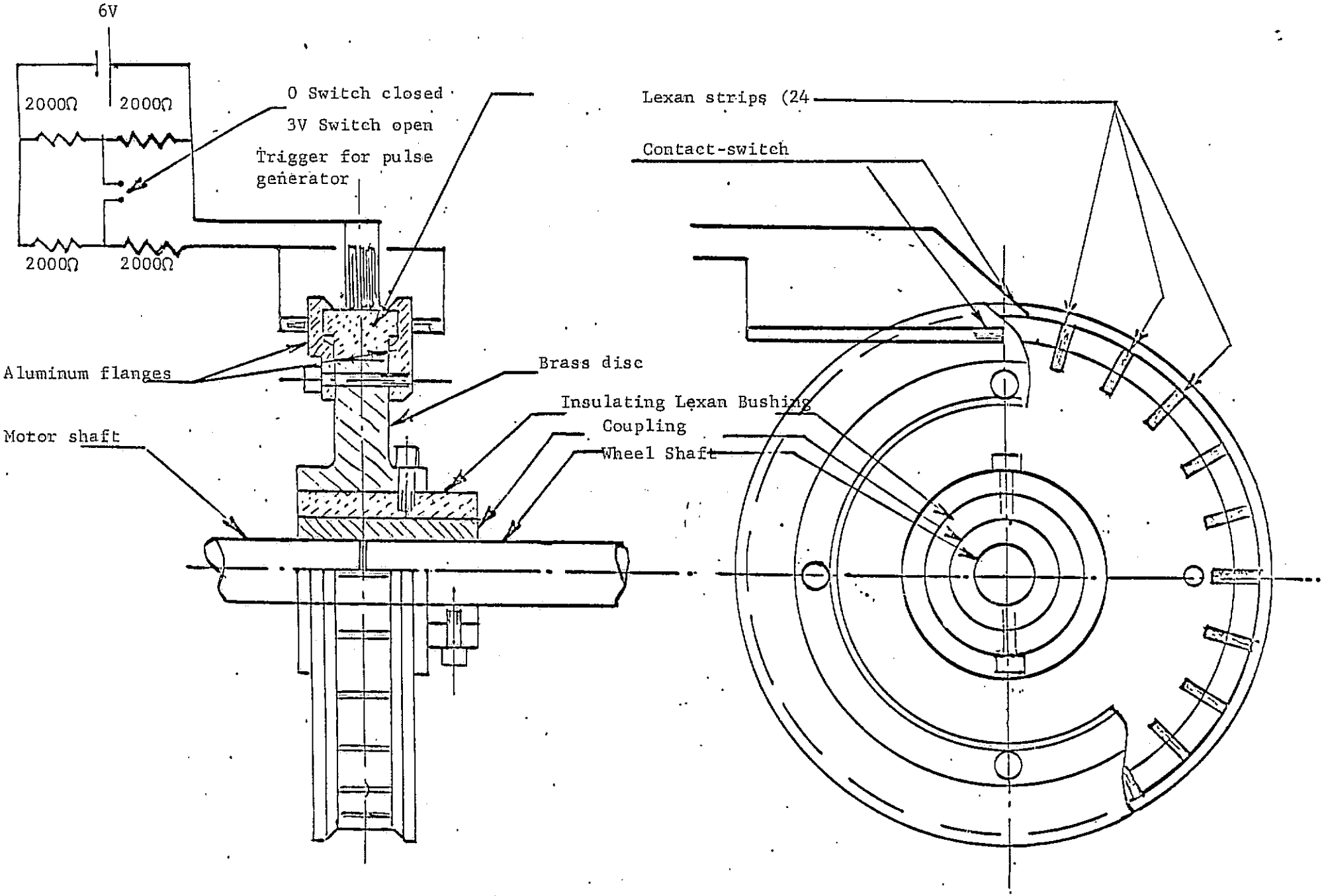

Fig. 7 Contact-switch system for synchronization of siren signal

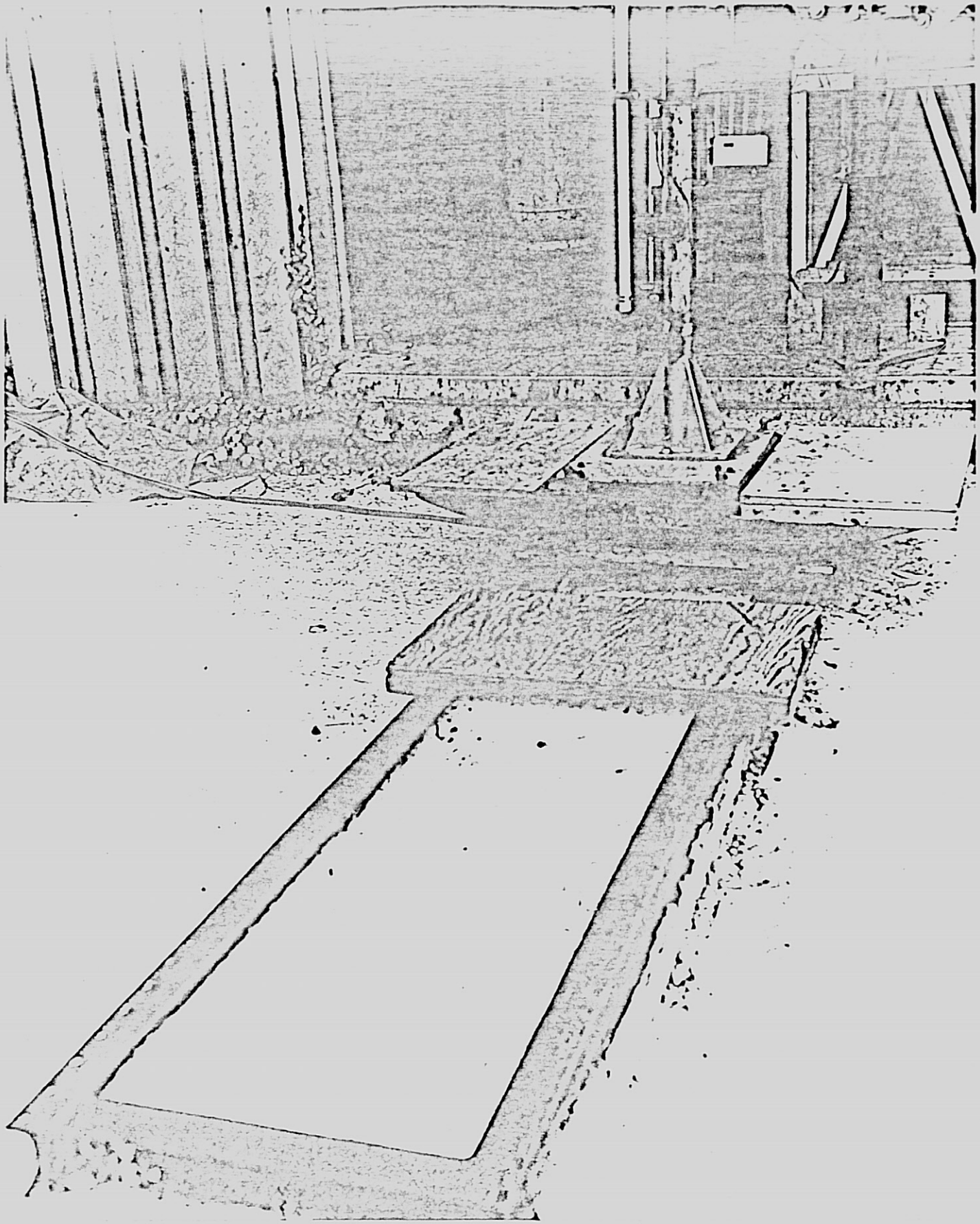

Fig. 8 Prope support structure

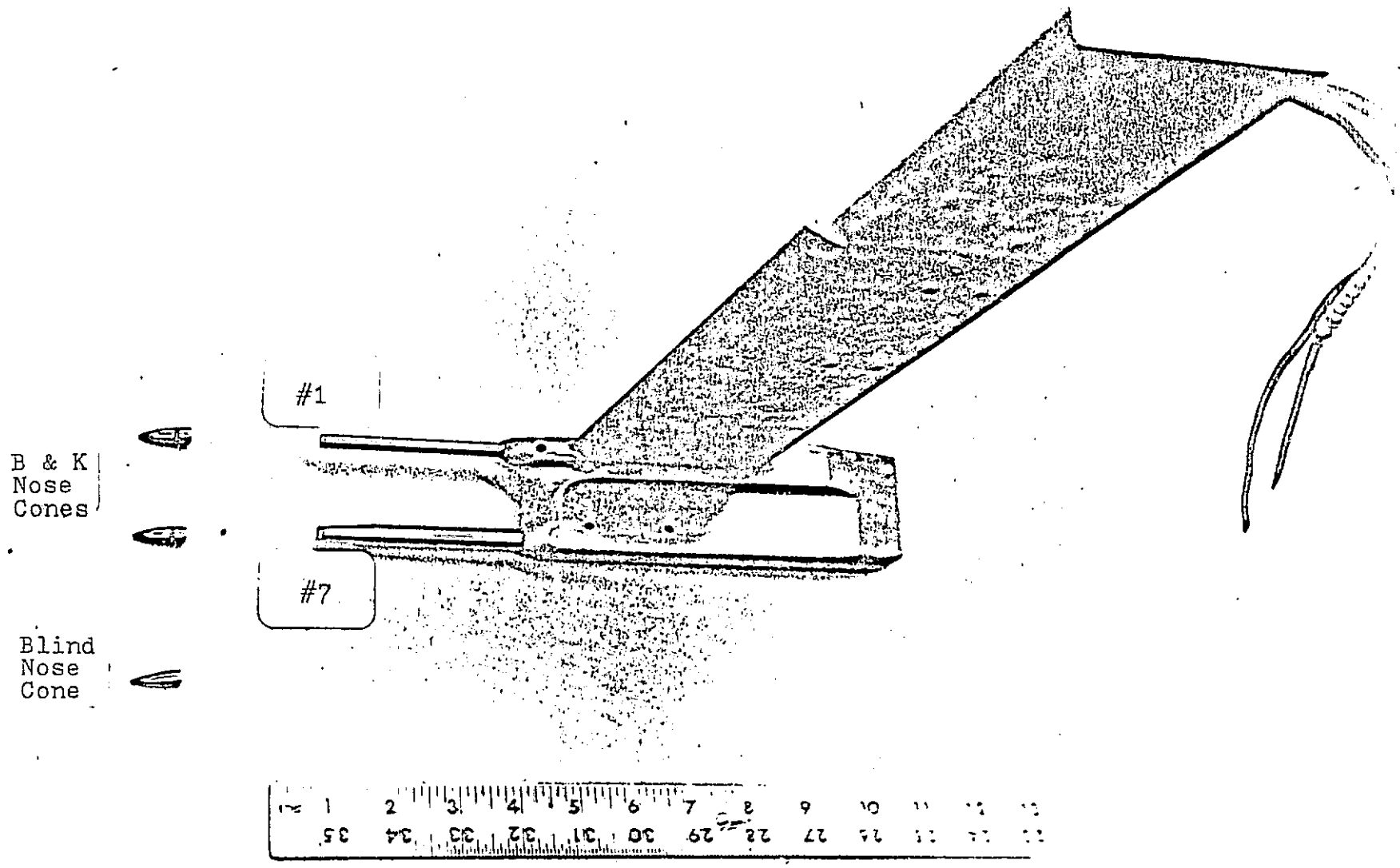

Fig. 9 Wing support with probes and nose cones

TRANSDUCER	NO. 1	NO. 7
TYPE	KULITE COS-125-100	KULITE COS-125-100
SERIAL NO.	2065-4-1	2065-5-7
RATED PRESSURE	100 psi	100 psi
SENSITIVITY	.293 mv/v/psi	.331 mv/v/psi
MAX. INPUT VOLTAGE	5 VDC	7.5 VDC
OUTPUT IMPEDANCE	304 Ω	326 Ω
OPERATING TEMP.	< 250° F	< 250° F
CHANGE OF SENS. WITH TEMP. (APPROX.)	± 2.5% /100° F	± 2.5% /100° F
NATURAL FREQ. (APPROX.)	130 kHz	130 kHz
ACCELERATION SENS. PERPENDICULAR TRANSVERVE	0.0002 % FS/g 0.00004 % FS/g	0.0002 % FS/g 0.00004 % FS/g

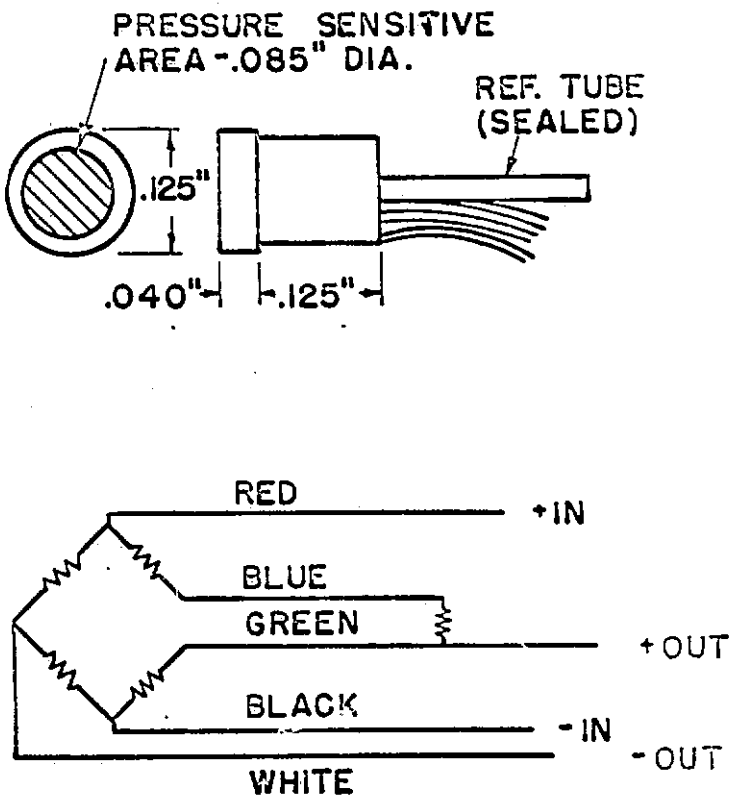

Fig. 10 Transducer specifications and circuitry

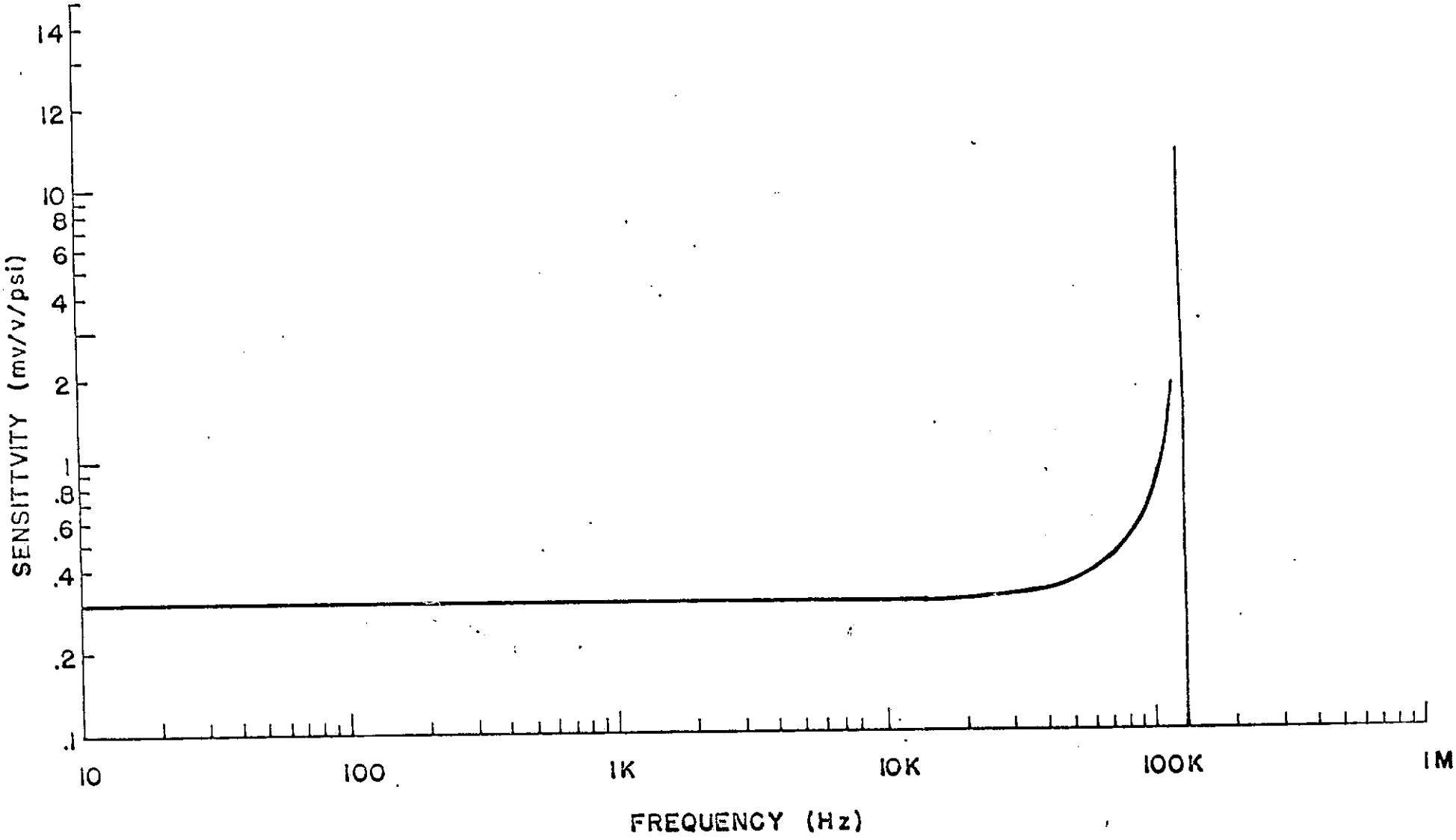

Fig. 11 Typical frequency response of Kulite CQS-125 pressure transducers

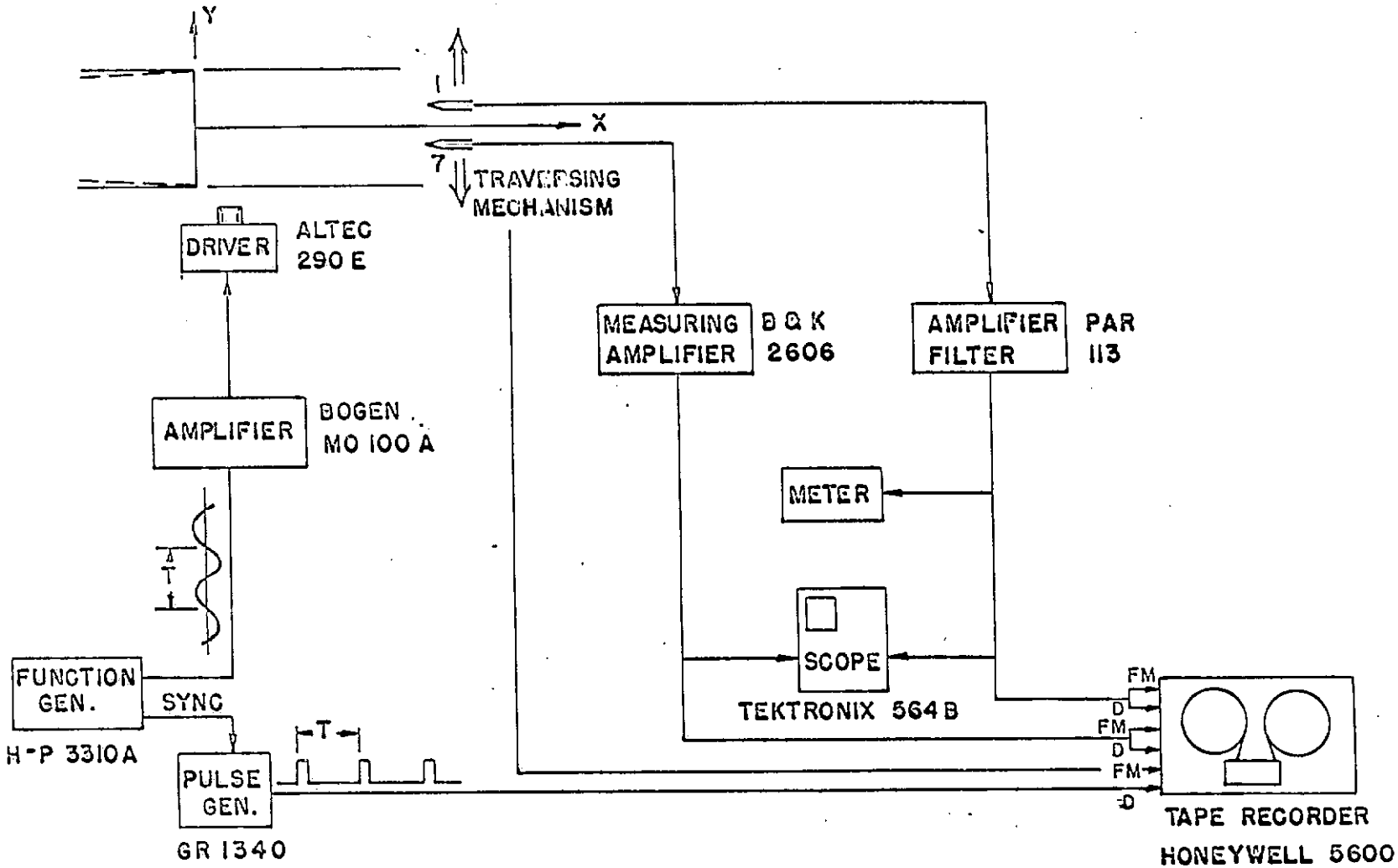

Fig. 12 Recording and loudspeaker signal generating systems

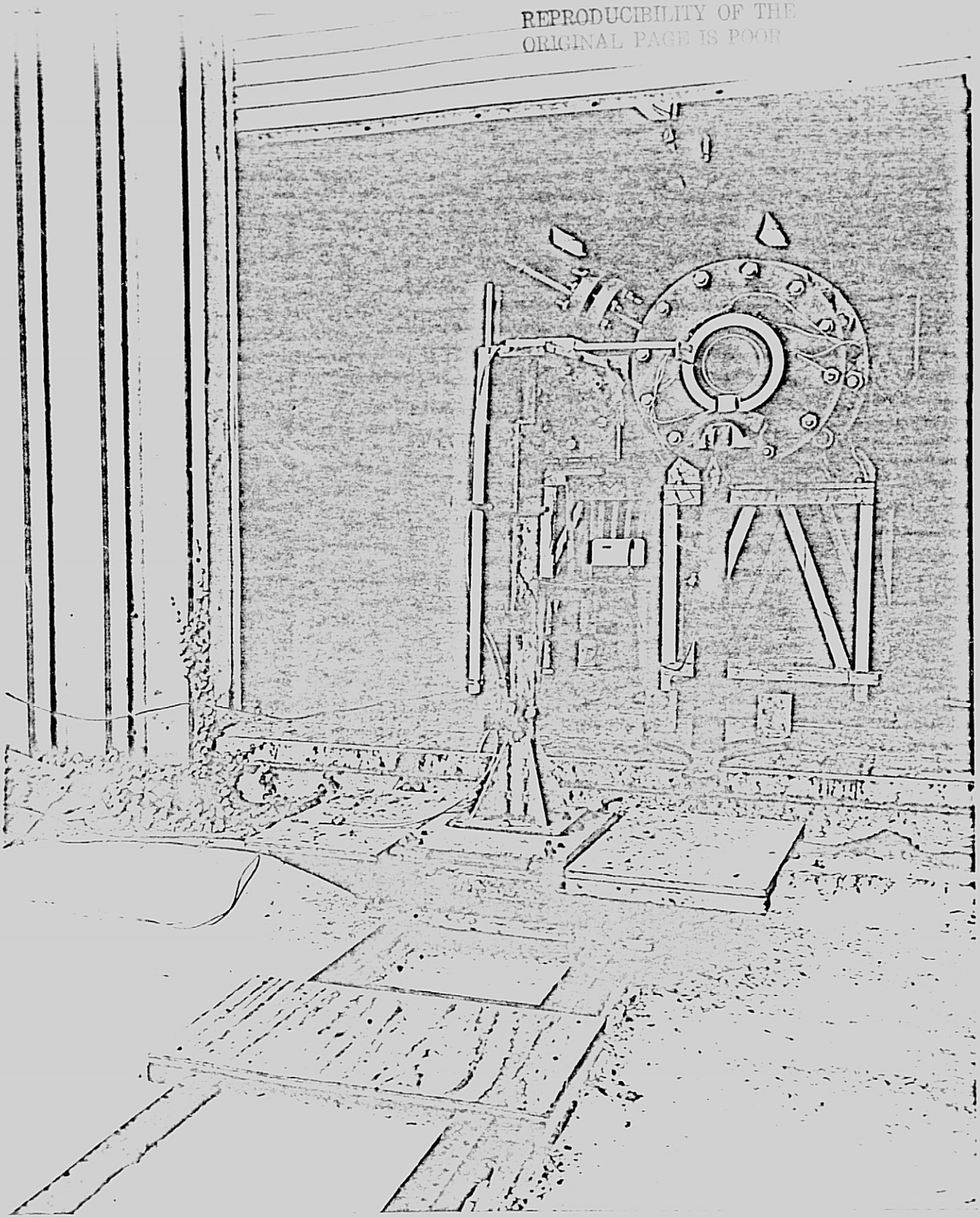

Fig. 13 Experimental set-up for acoustic signal tracing using the loudspeaker

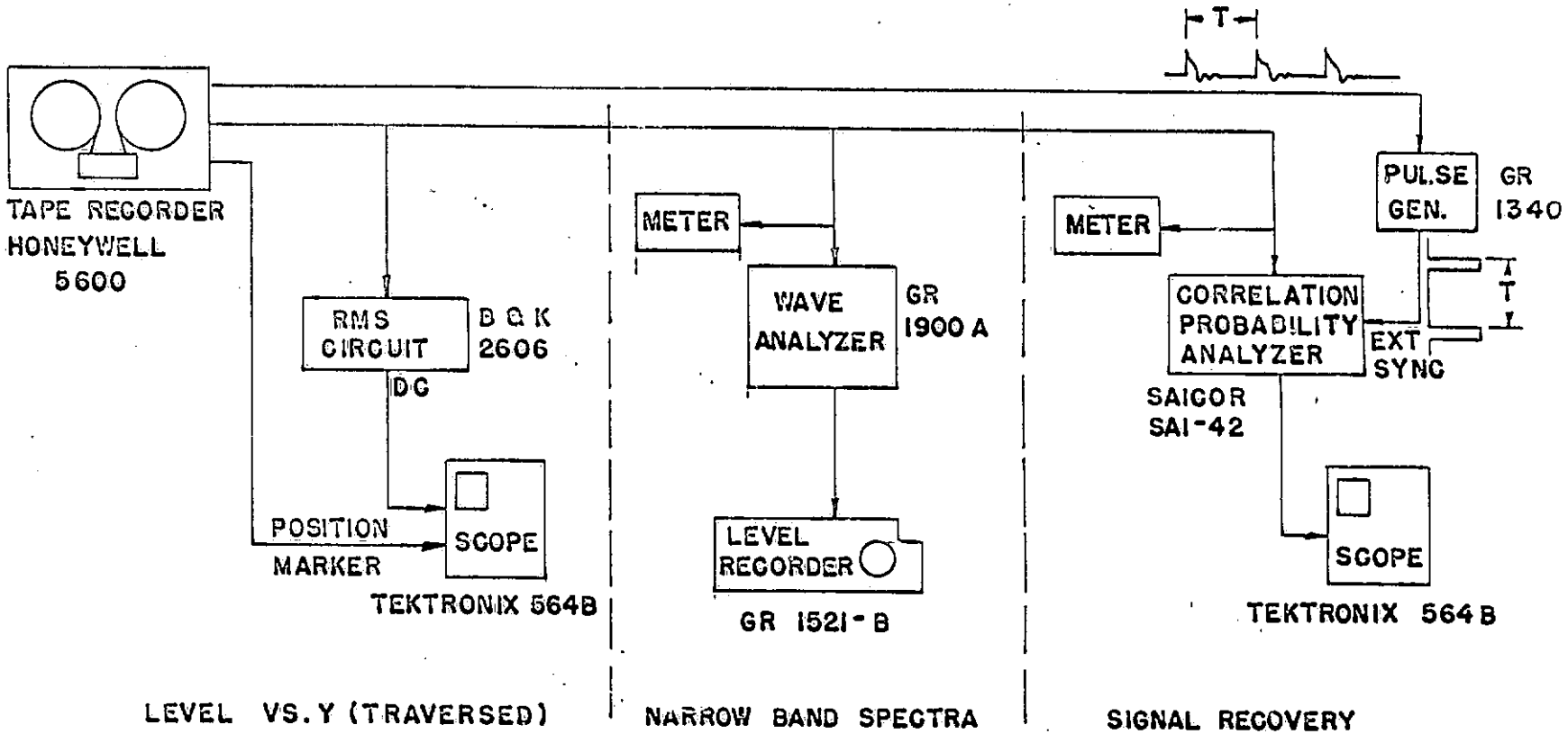

Fig. 14 Data analysis systems

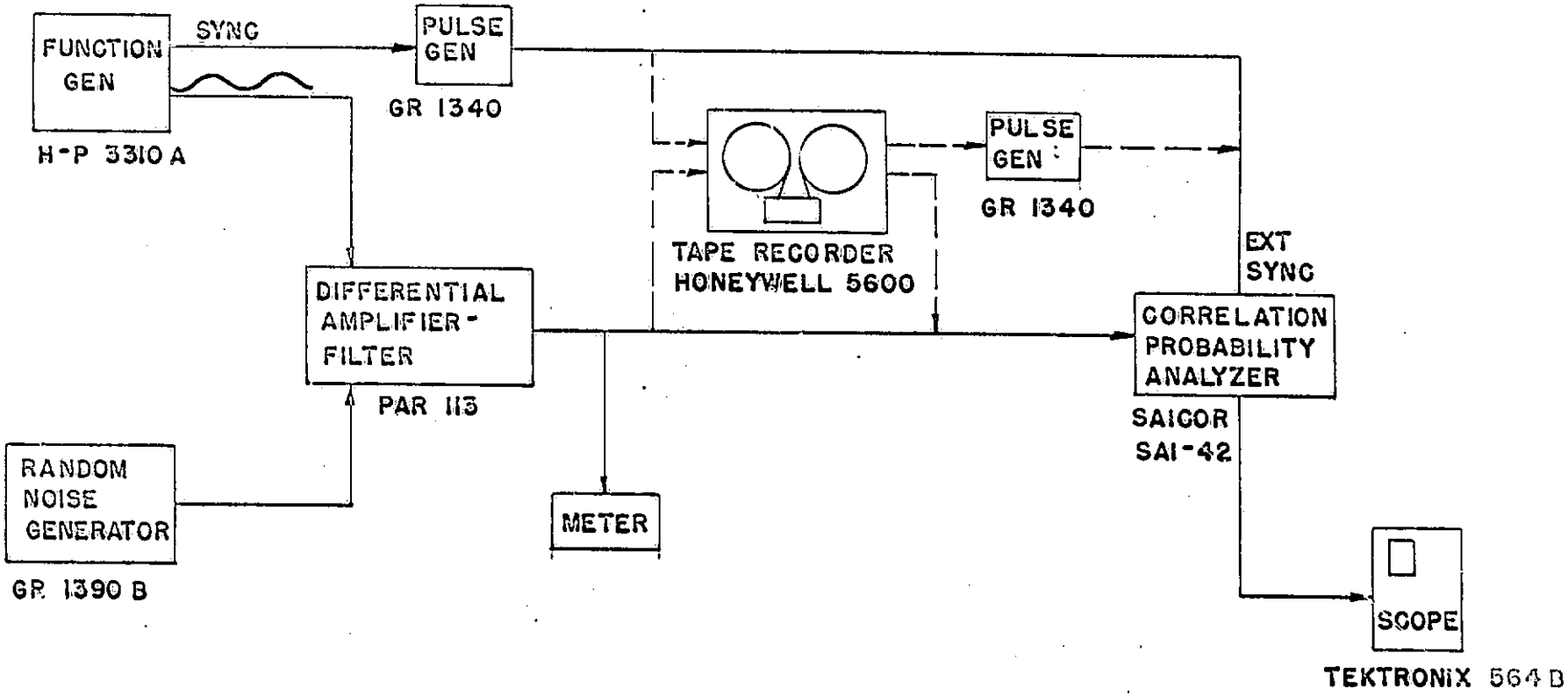

Fig. 15 Signal recovery simulation system

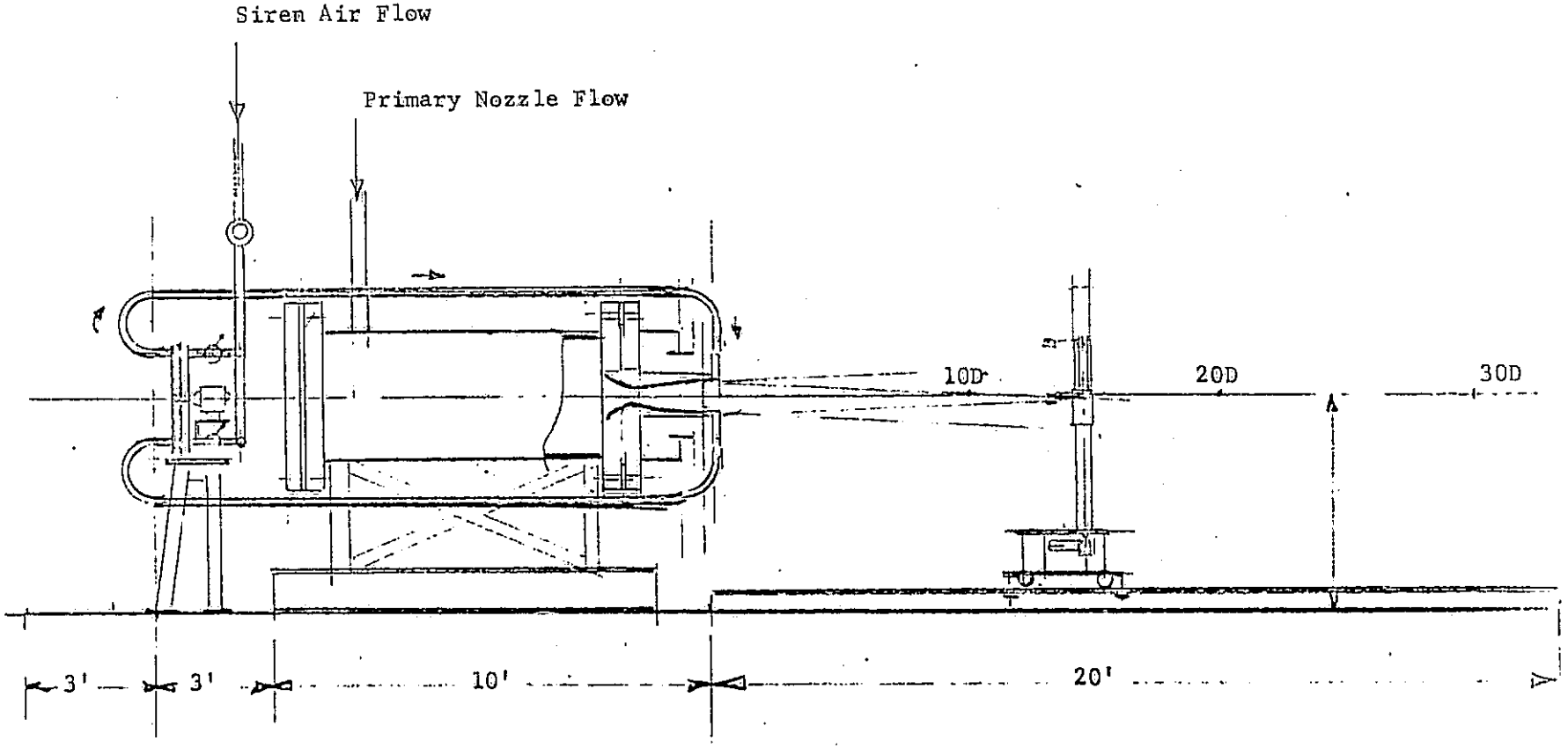

Fig. 16 Facility modifications

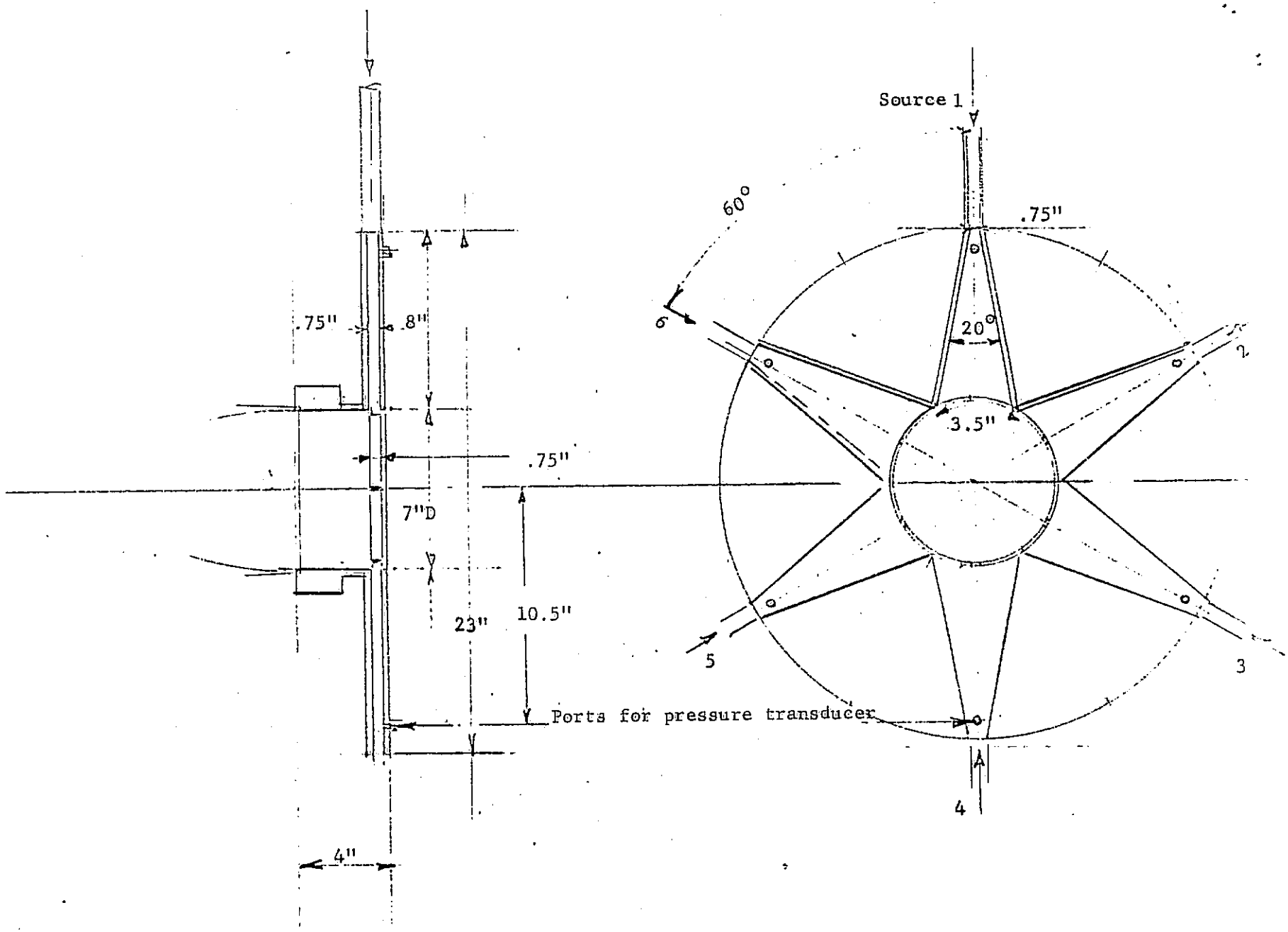

Fig. 17 Six-source injection ring

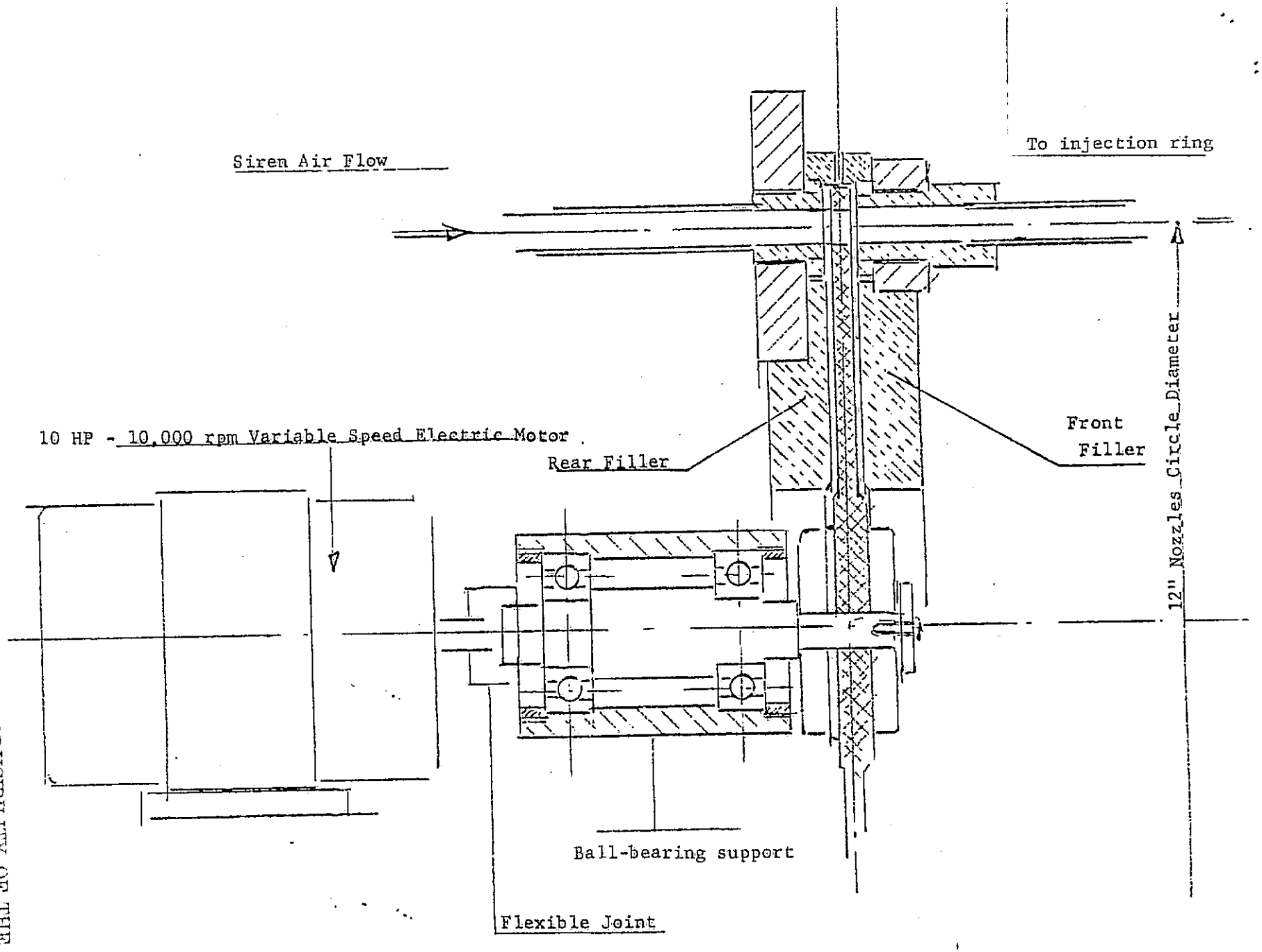

Fig. 18 Siren modifications

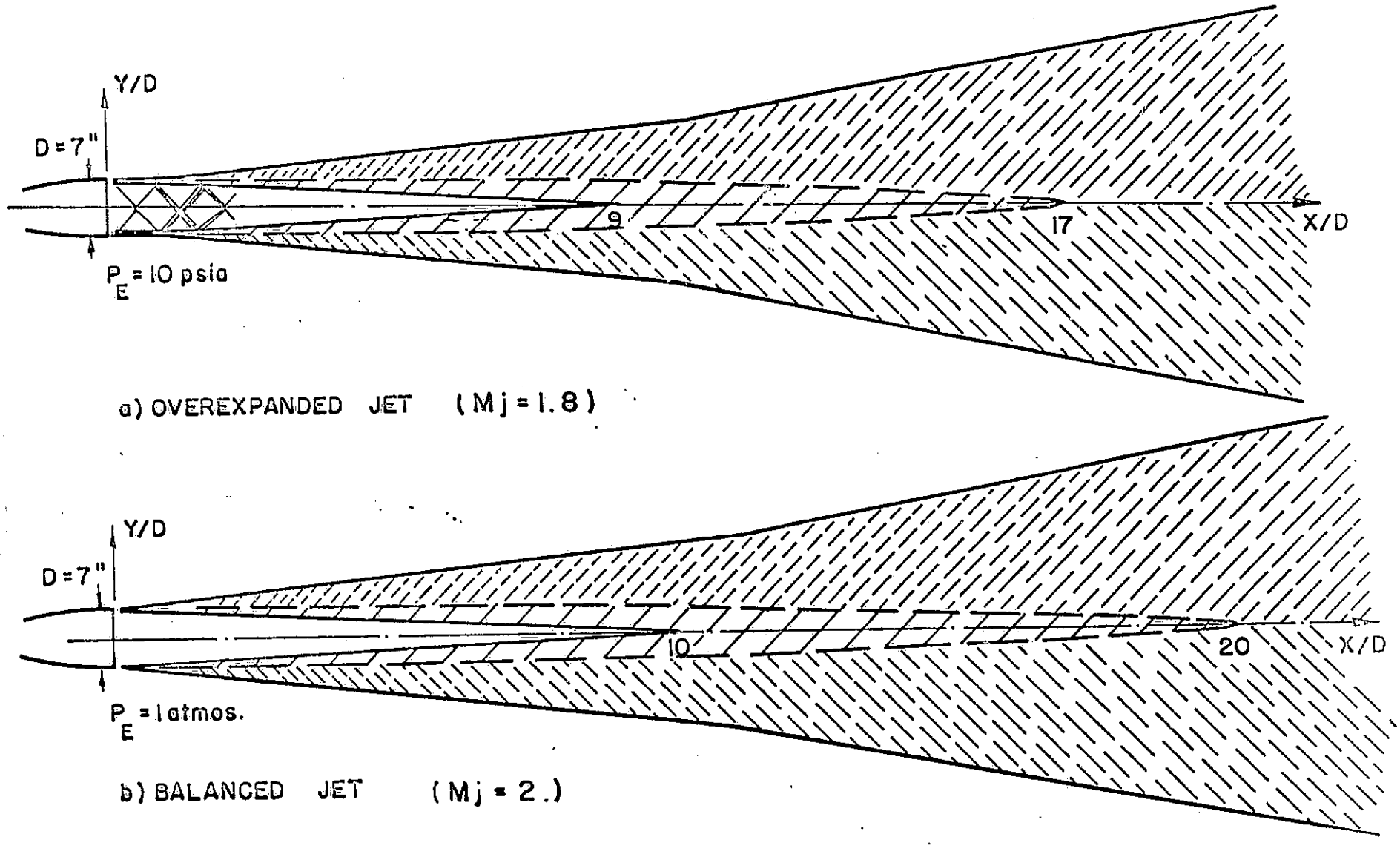

Fig. 20 Schematics of jet flow fields

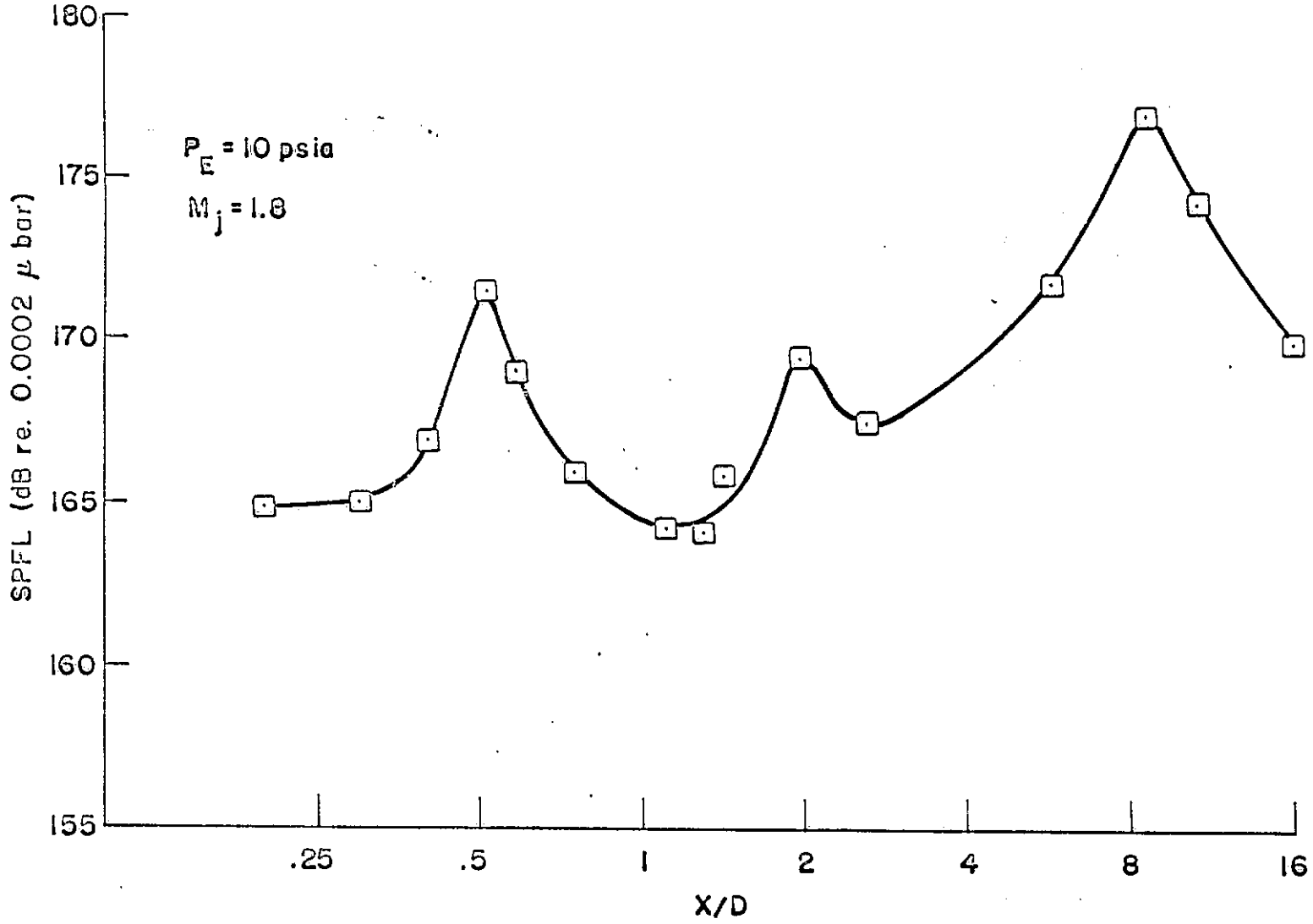

Fig. 21 Variation of static pressure fluctuation level along centerline of overexpanded jet

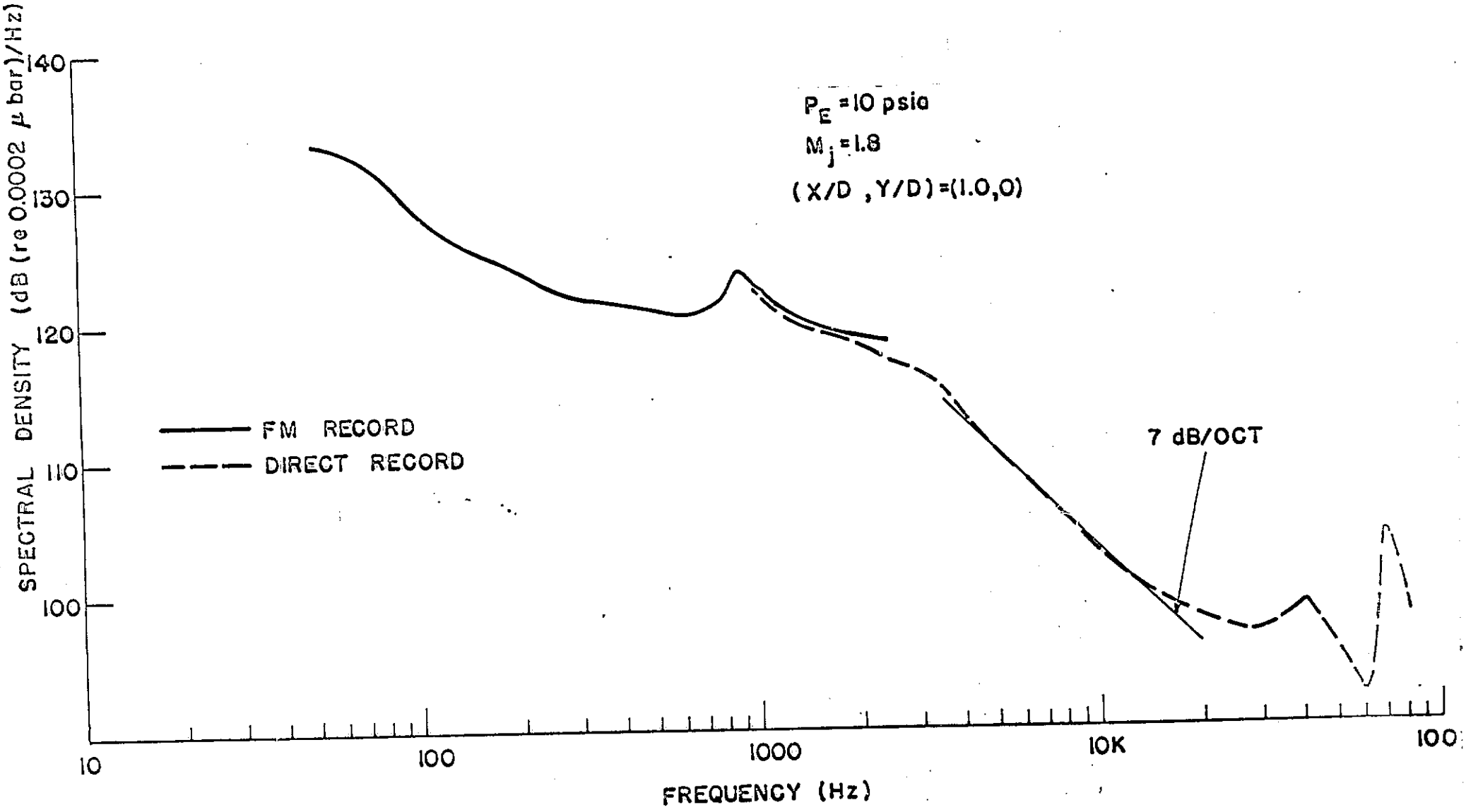

Fig. 22 Spectral distribution of the static pressure fluctuations at x/D = 1 along centerline of overexpanded jet

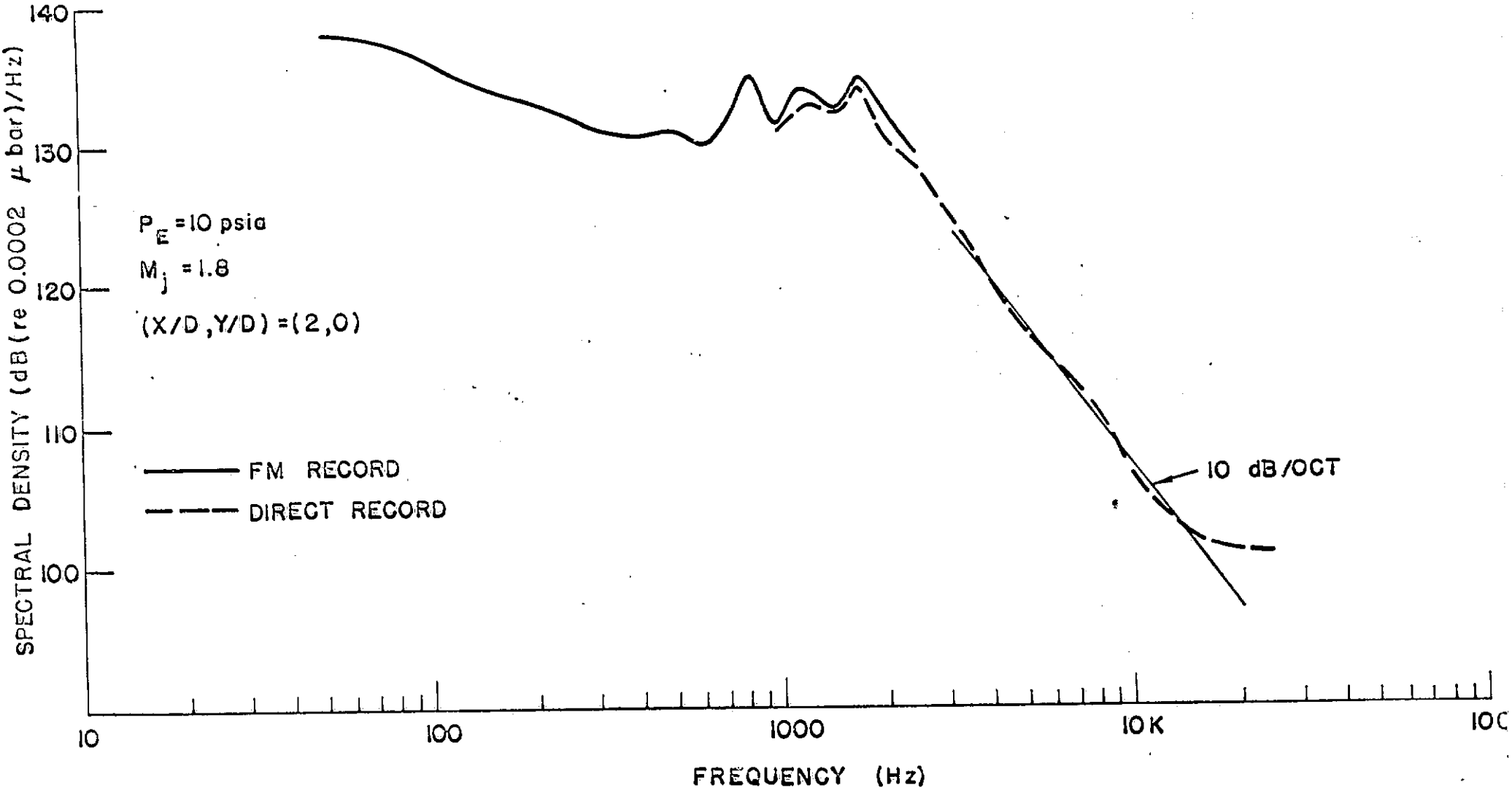

Fig. 23 Spectral distribution of the static pressure fluctuations at x/D = 2 along centerline of overexpanded jet

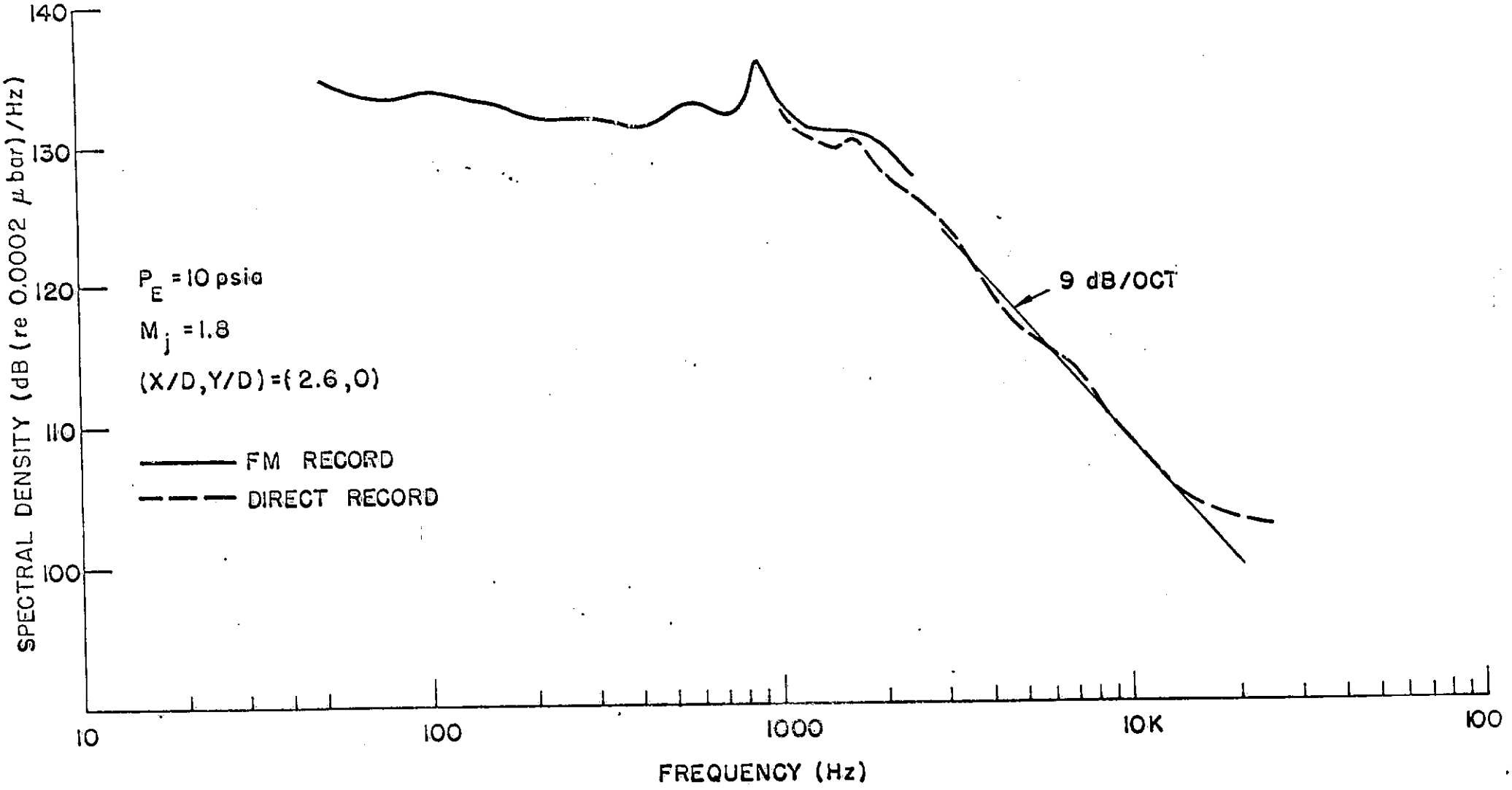

Fig. 24 Spectral distribution of the static pressure fluctuations at x/D = 2.6 along centerline of overexpanded jet

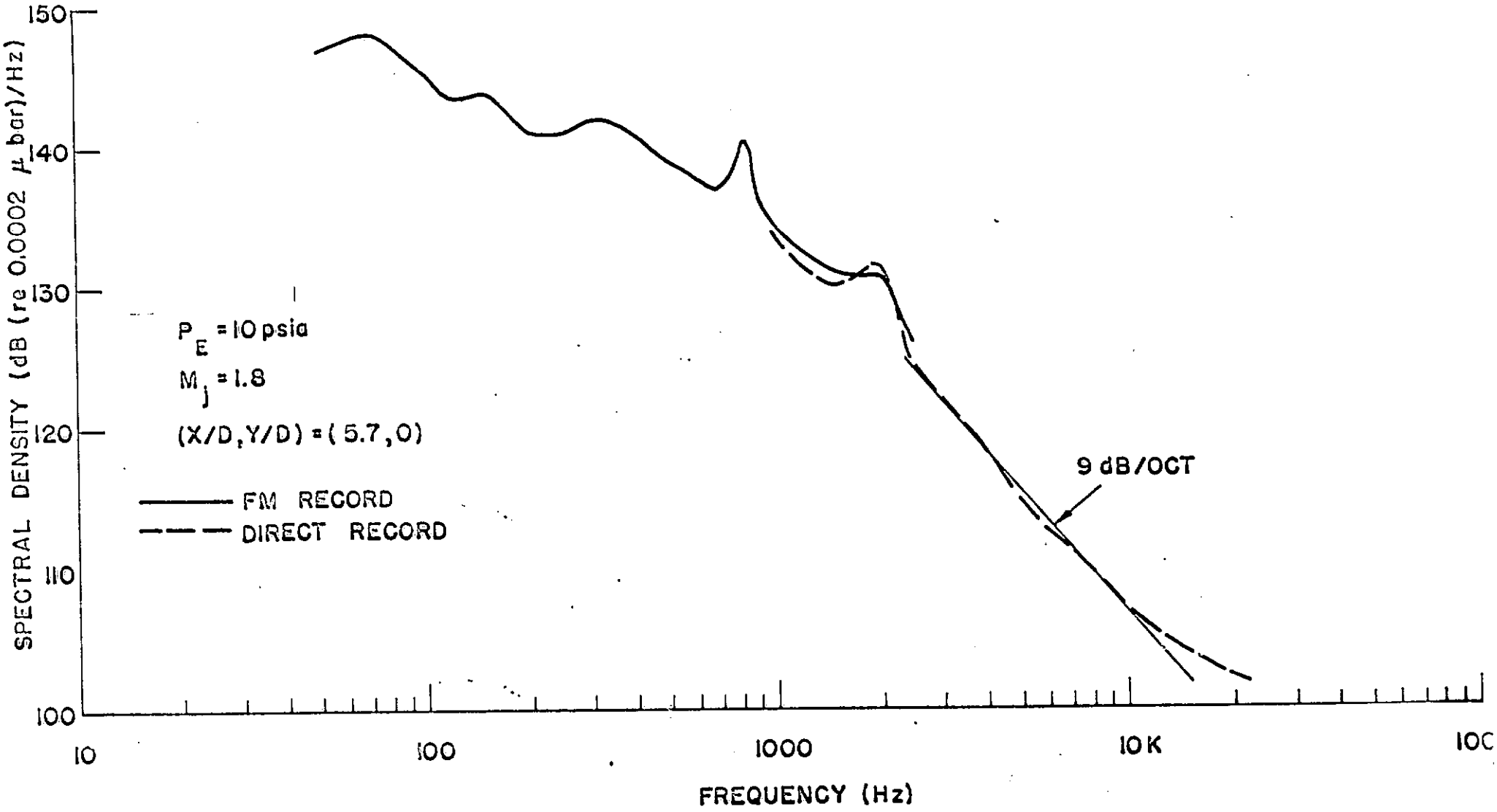

Fig. 25 Spectral distribution of the static pressure fluctuations at x/D = 5.7 along centerline of overexpanded jet

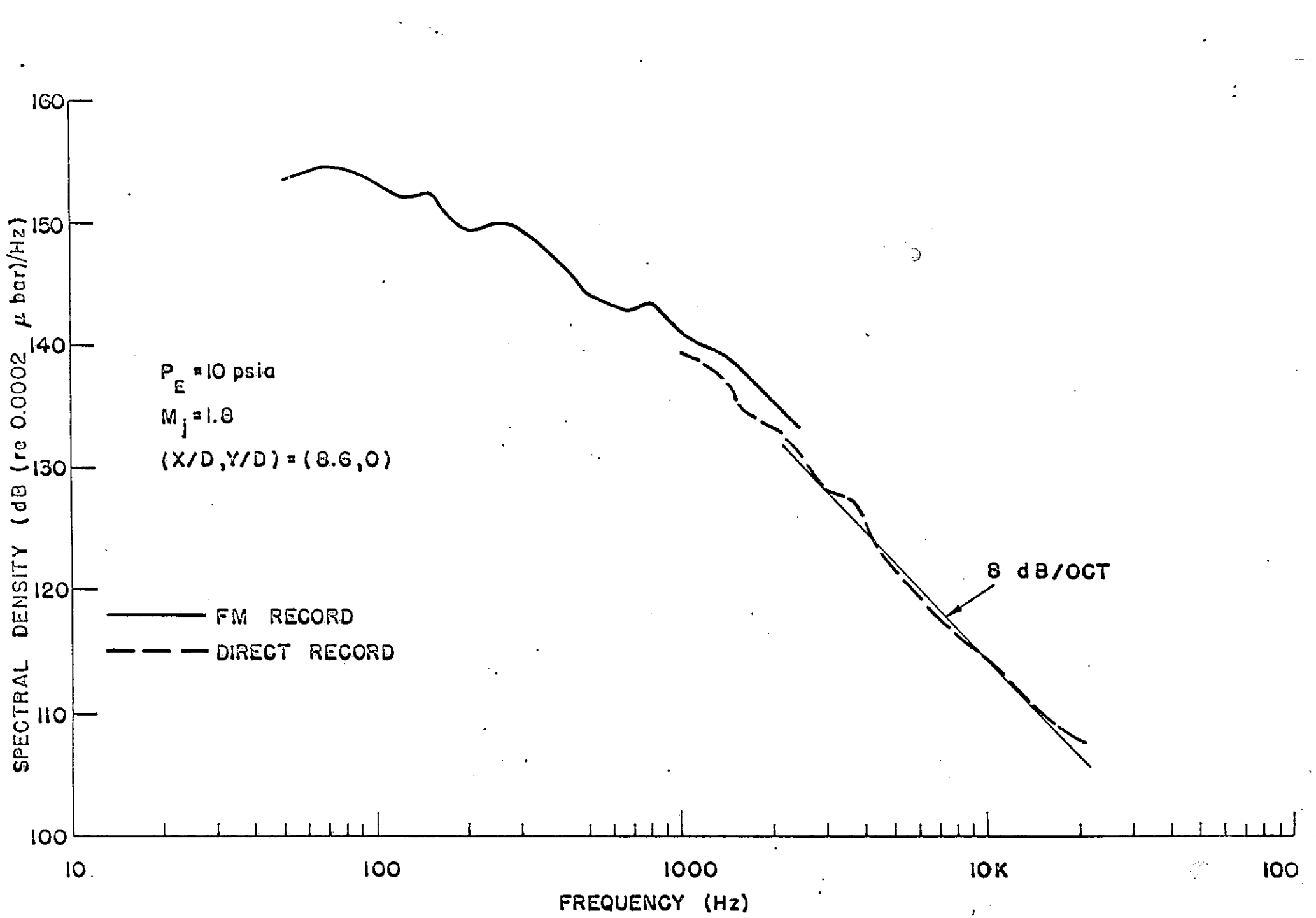

Fig. 26 Spectral distribution of the static pressure fluctuations at x/D = 8.6 along centerline of overexpanded jet

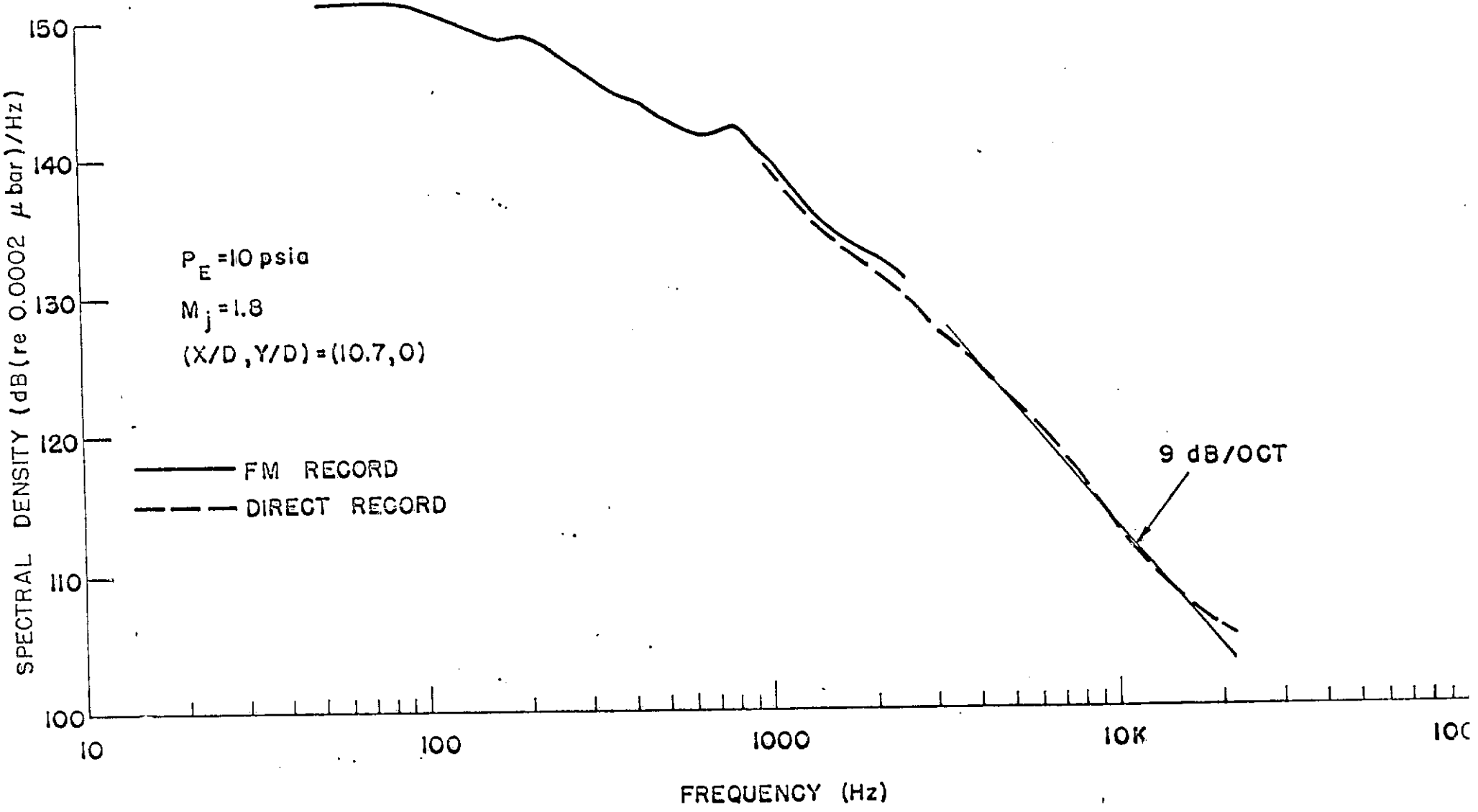

Fig. 27 Spectral distribution of the static pressure fluctuations at x/D = 10.7 along centerline of overexpanded jet

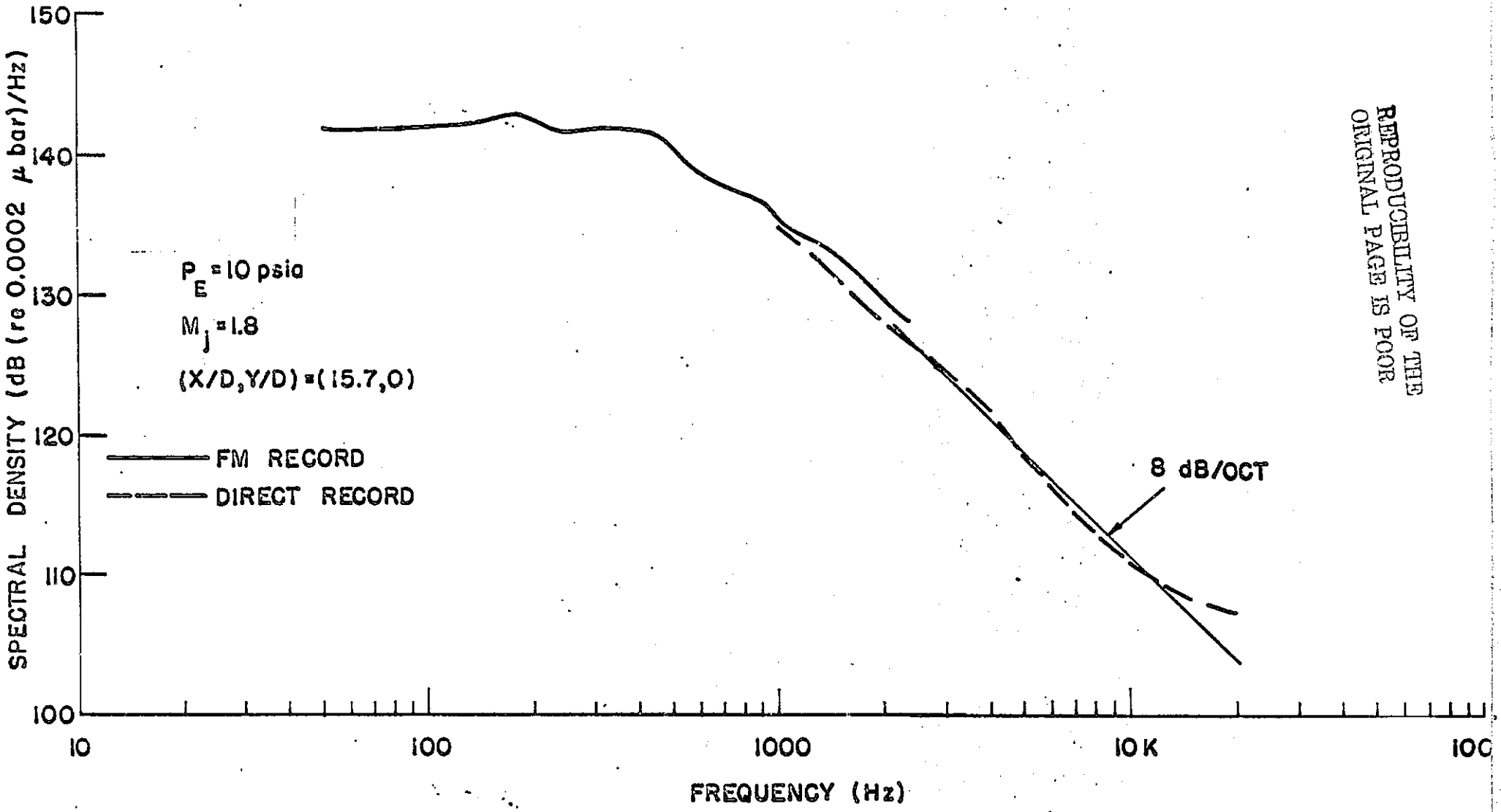

Fig. 28 Spectral distribution of the static pressure fluctuations at x/D = 15.7 along centerline of overexpanded jet

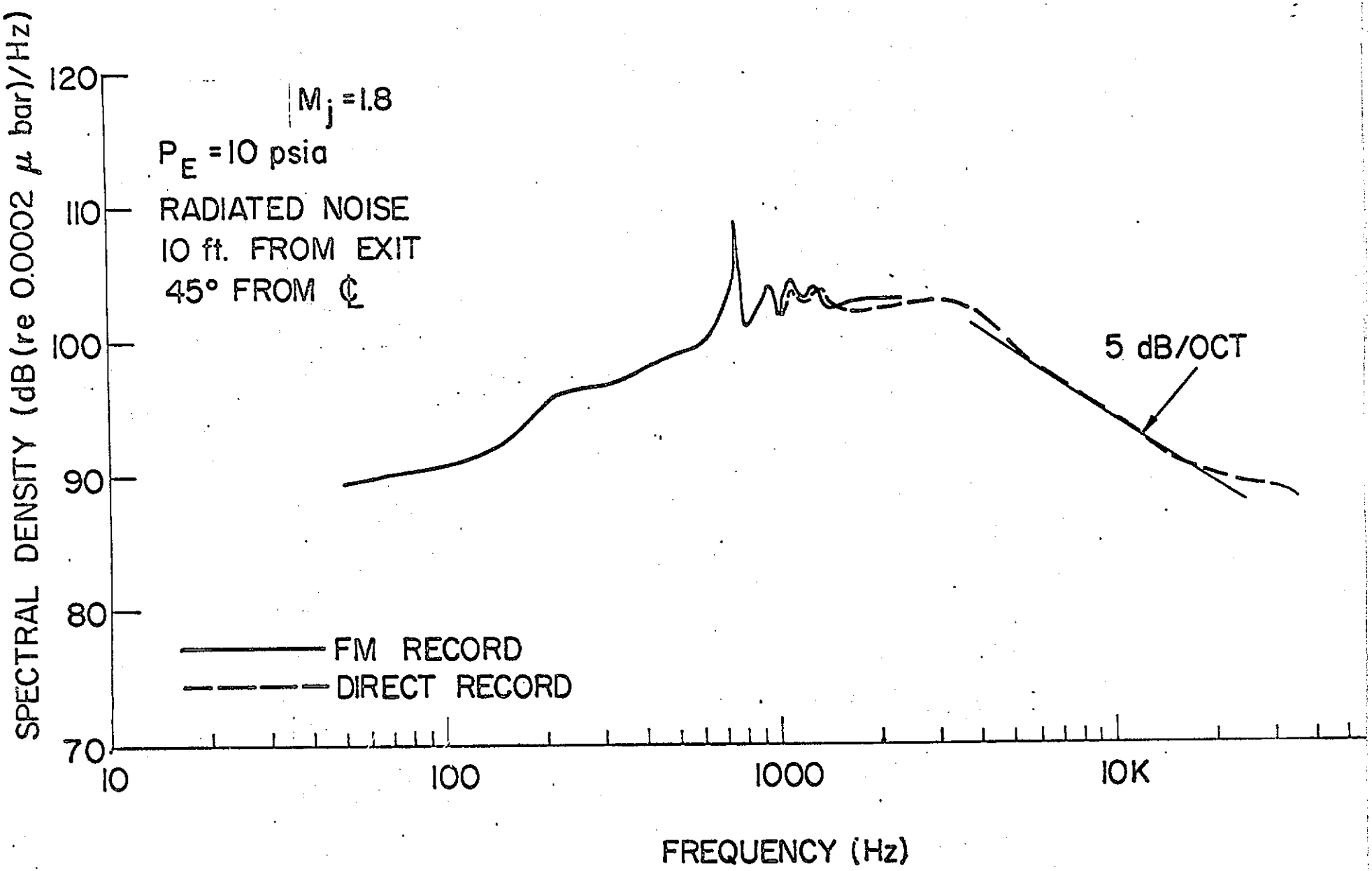

Fig. 29 Spectral distribution of the radiated sound of the overexpanded jet

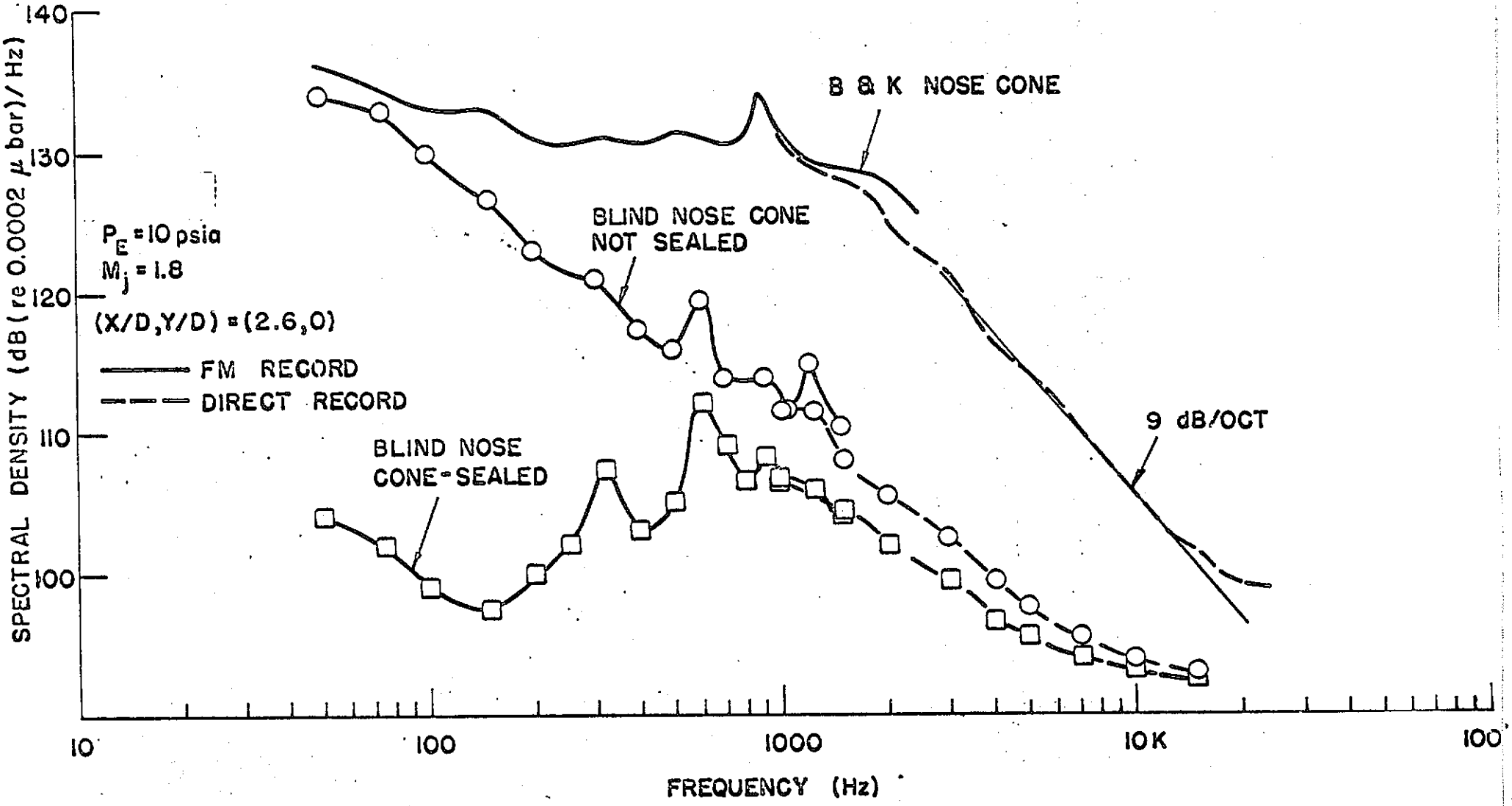

Fig. 30 Spectral distribution of vibration induced electrical noise.

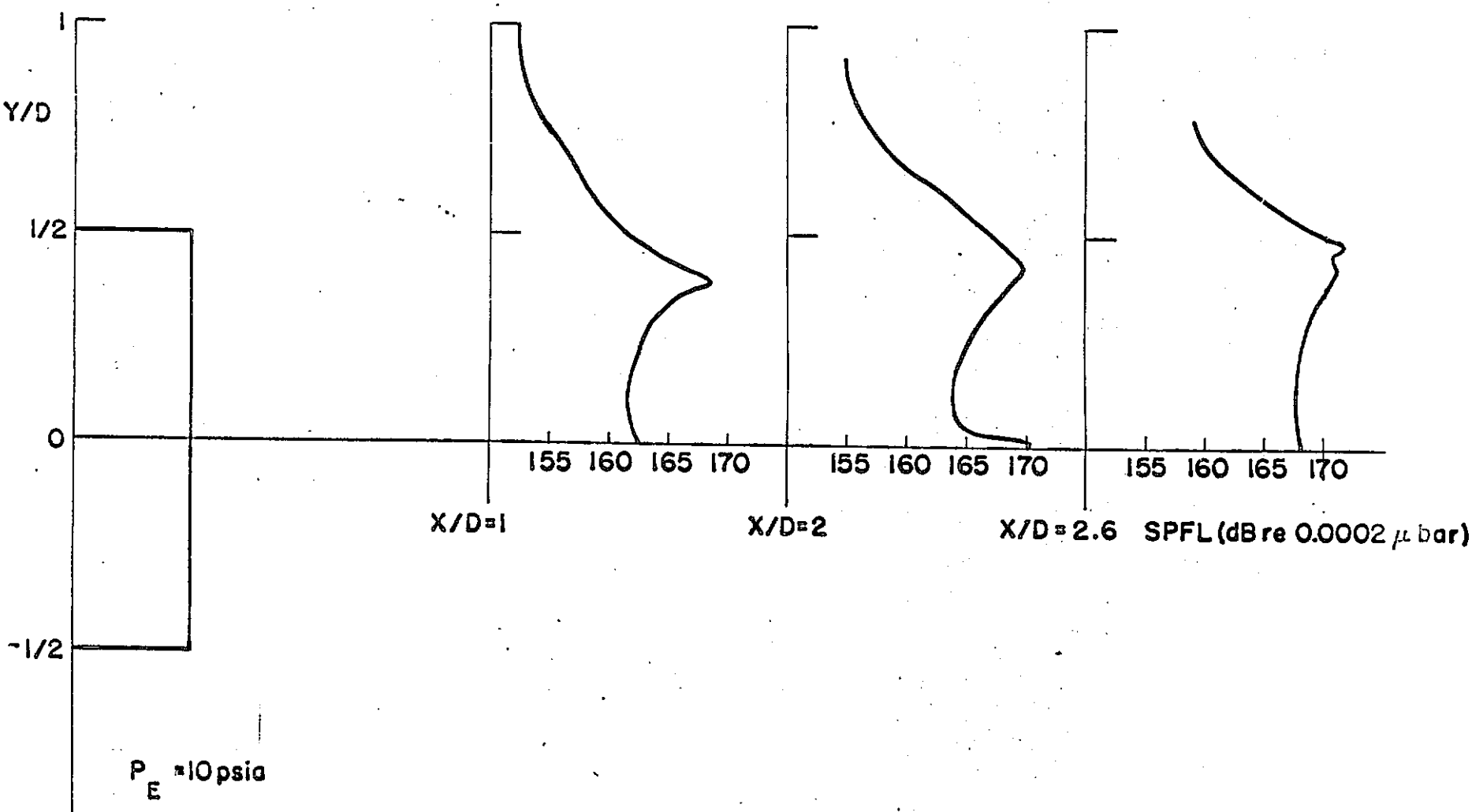

Fig. 31a Variation of static pressure fluctuation level with radial distance from centerline of overexpanded jet

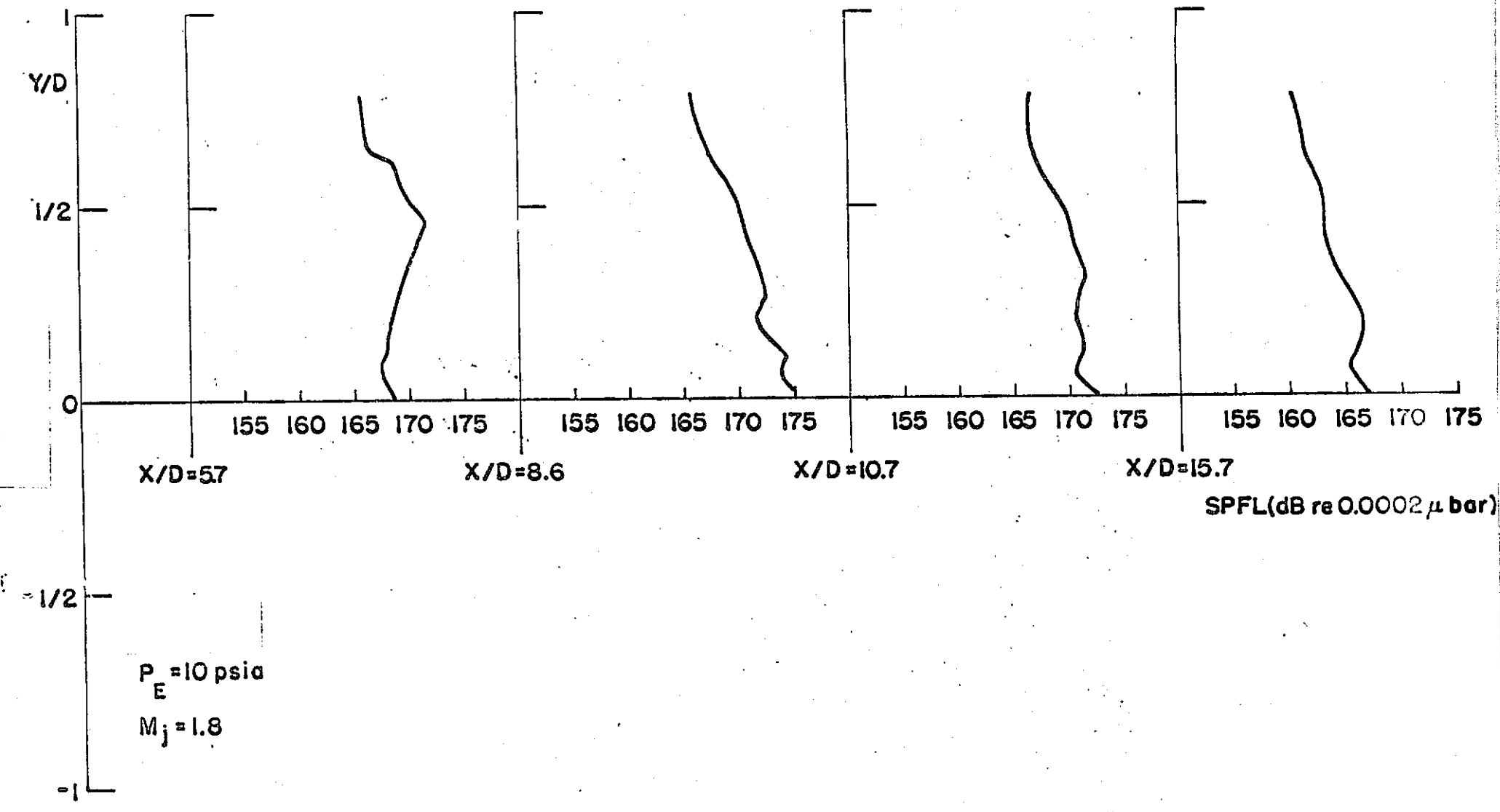

Fig. 31b Variation of static pressure fluctuation level with radial distance from centerline of overexpanded jet

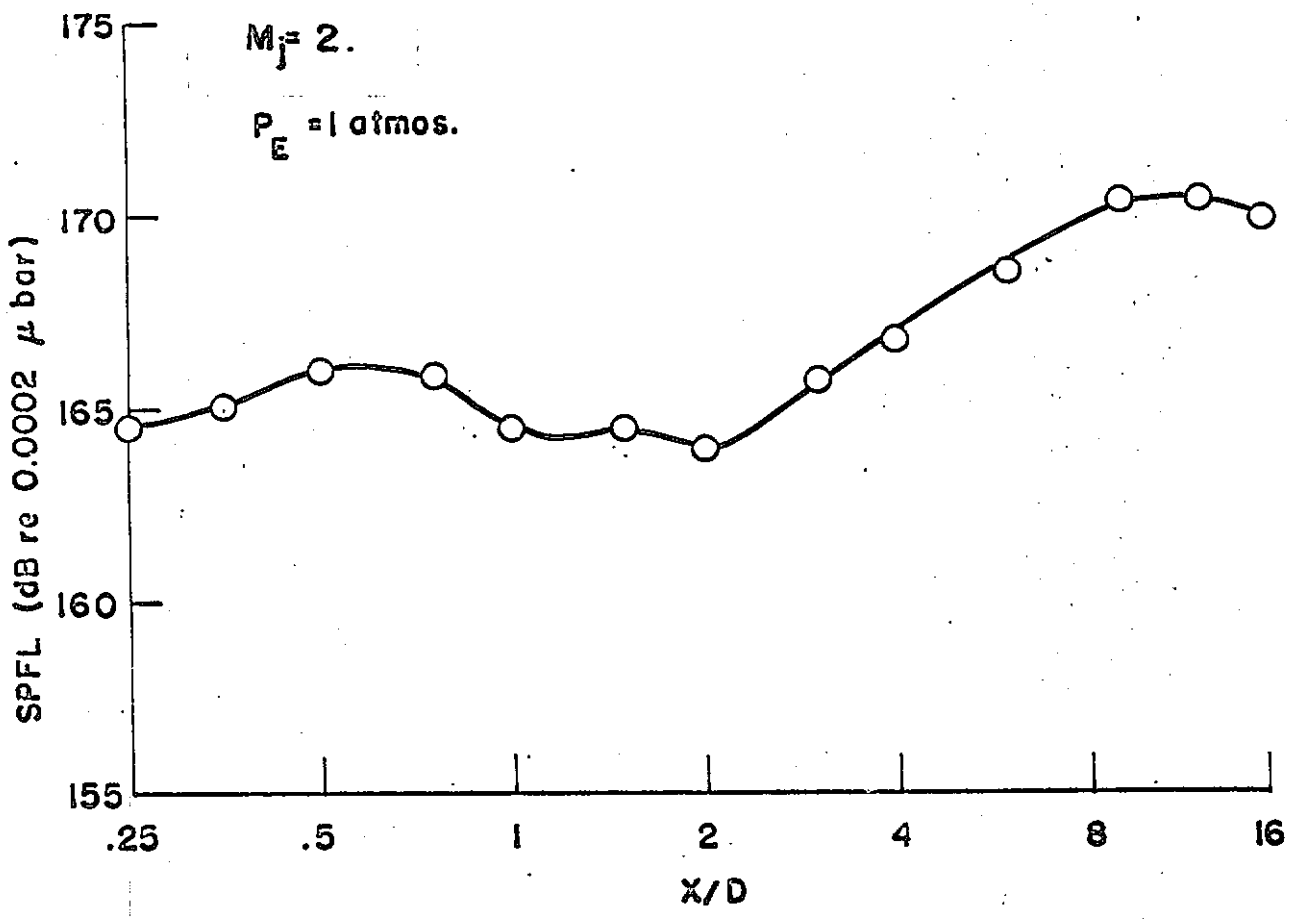

Fig. 32 Variation of static pressure fluctuation level along centerline of balanced jet

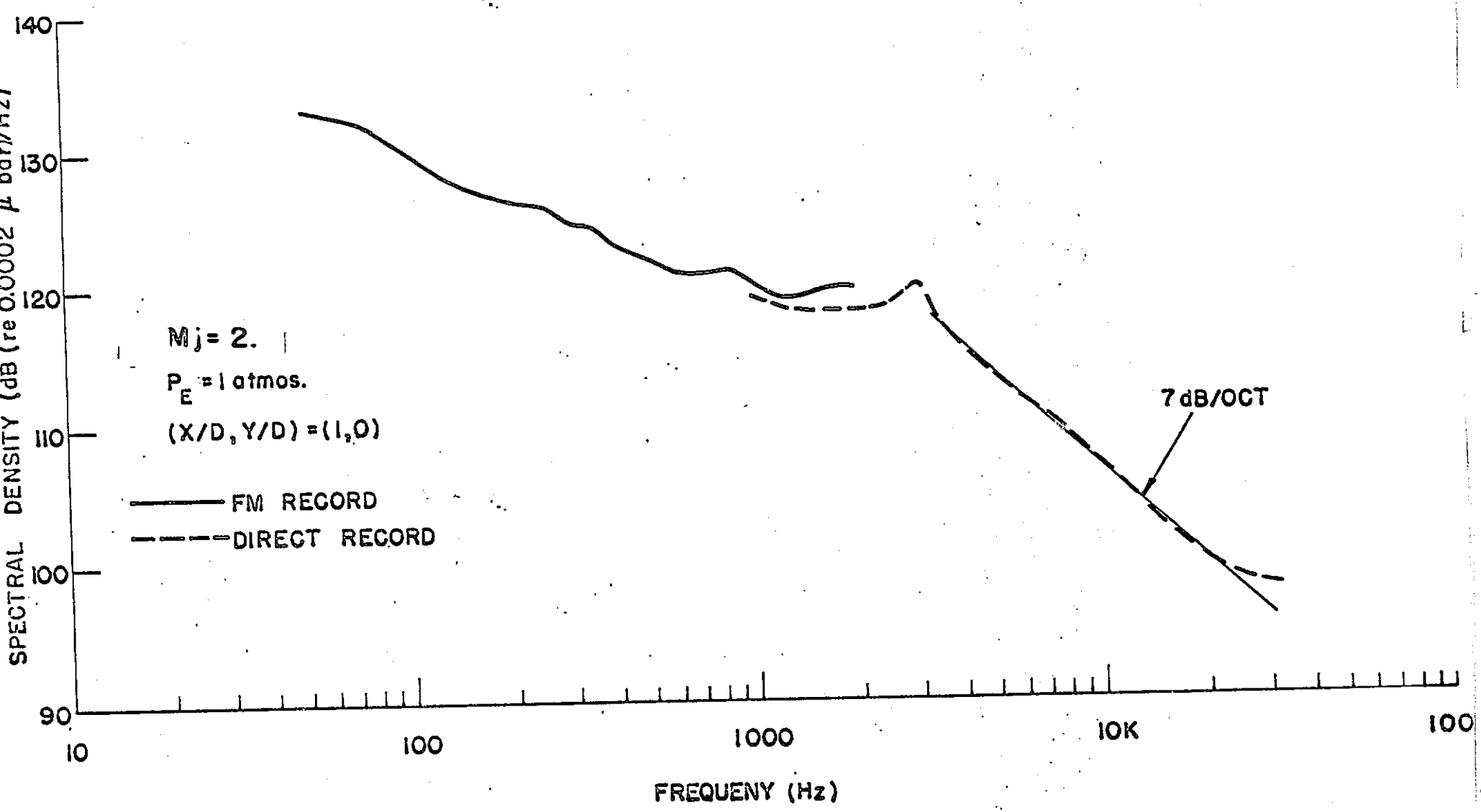

Fig. 33 Spectral distribution of the static pressure fluctuations at x/D = 1 along centerline of balanced jet

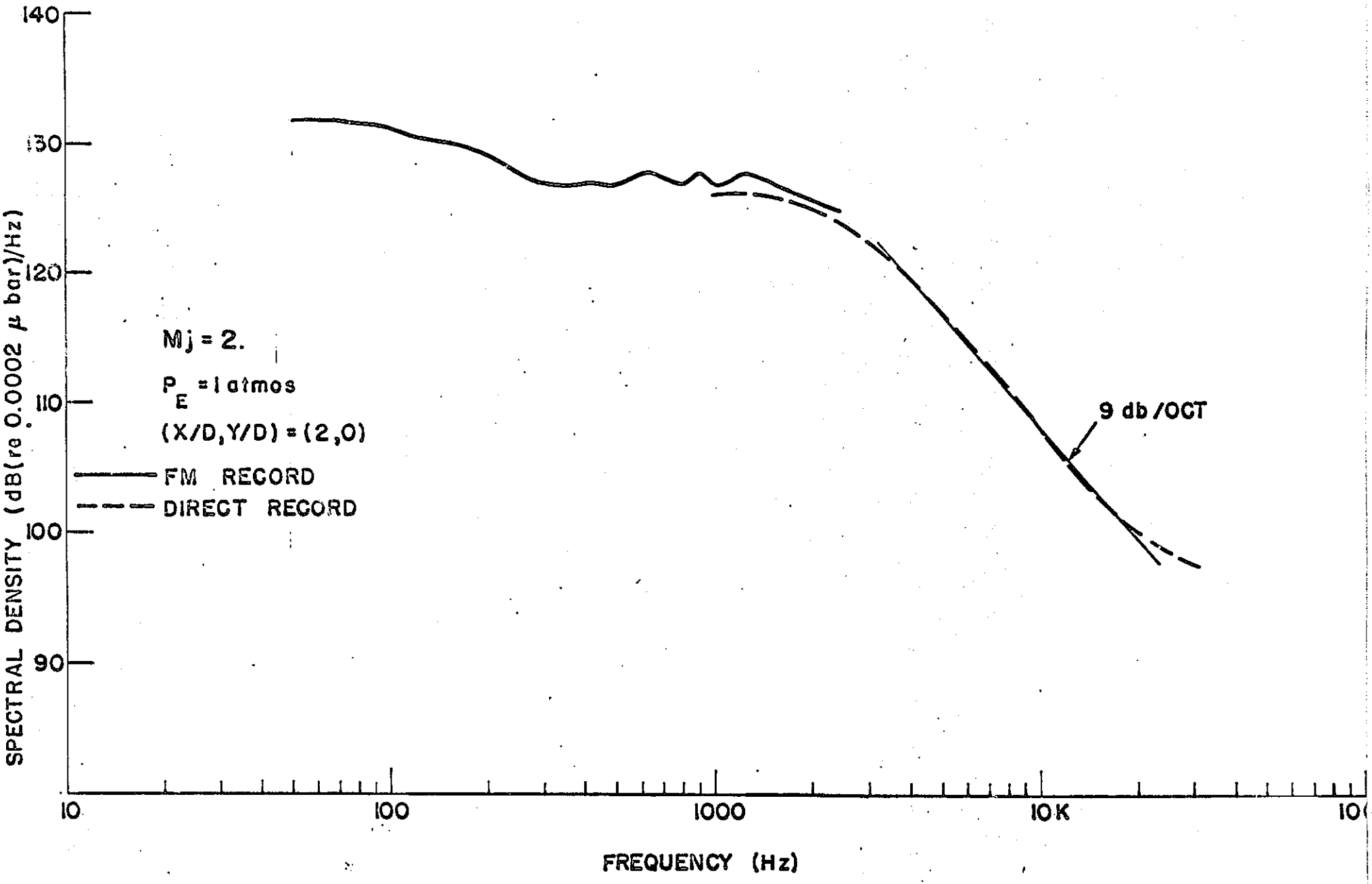

Fig. 34 Spectral distribution of the static pressure fluctuations at x/D = 2 along centerline of balanced jet

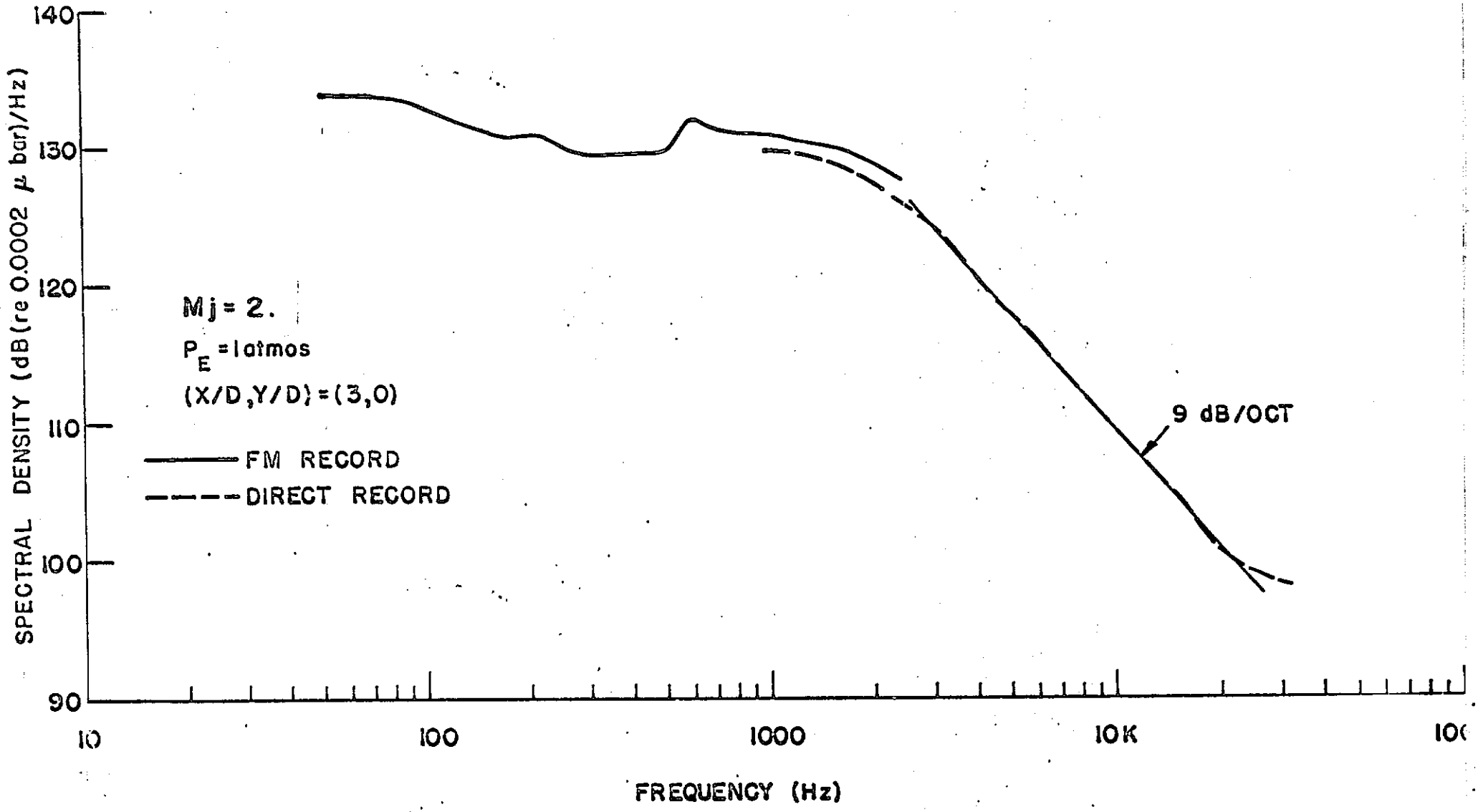

Fig. 35 Spectral distribution of the static pressure fluctuations at x/D = 3 along centerline of balanced jet

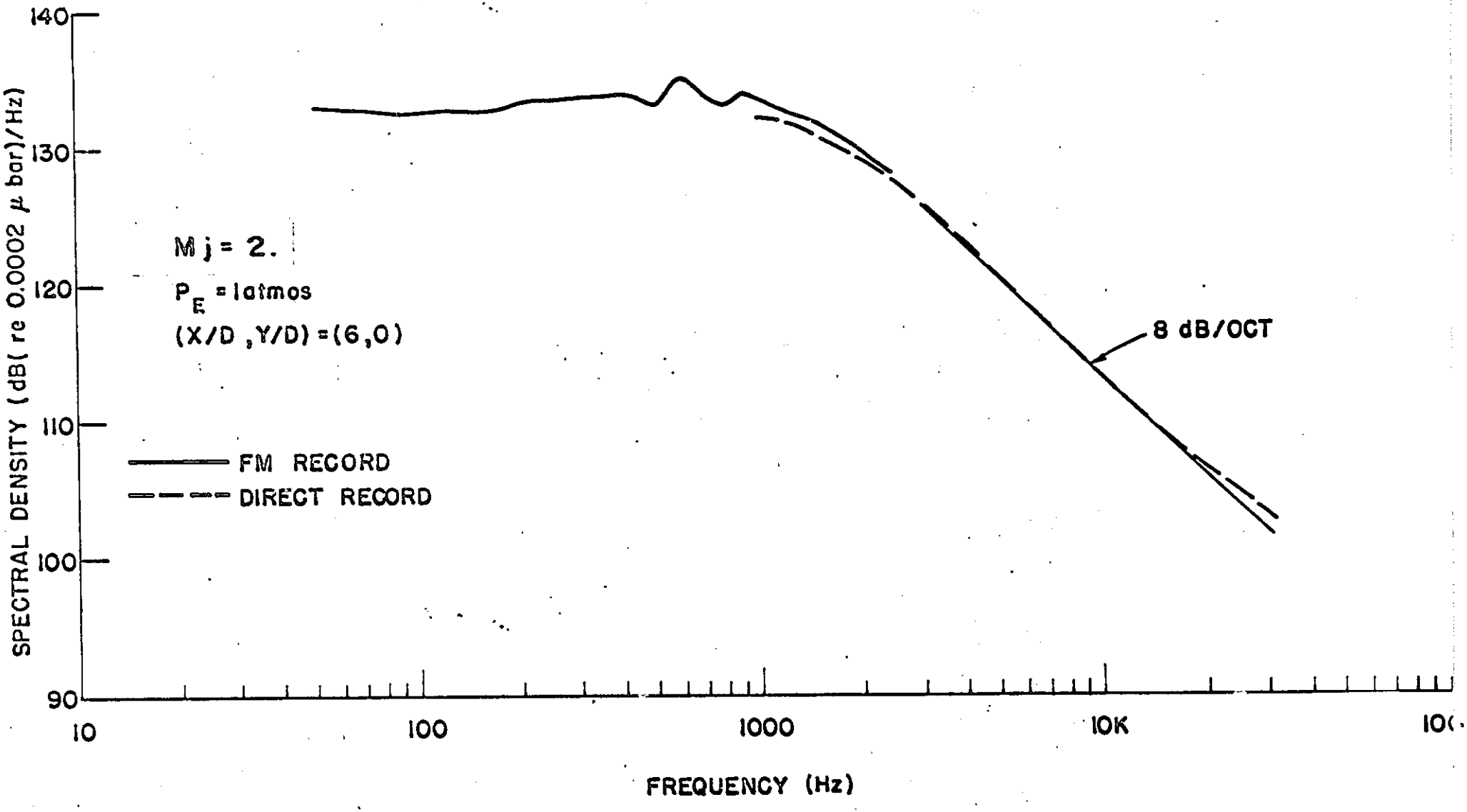

Fig. 36 Spectral distribution of the static pressure fluctuations at x/D = 6 along centerline of balanced jet

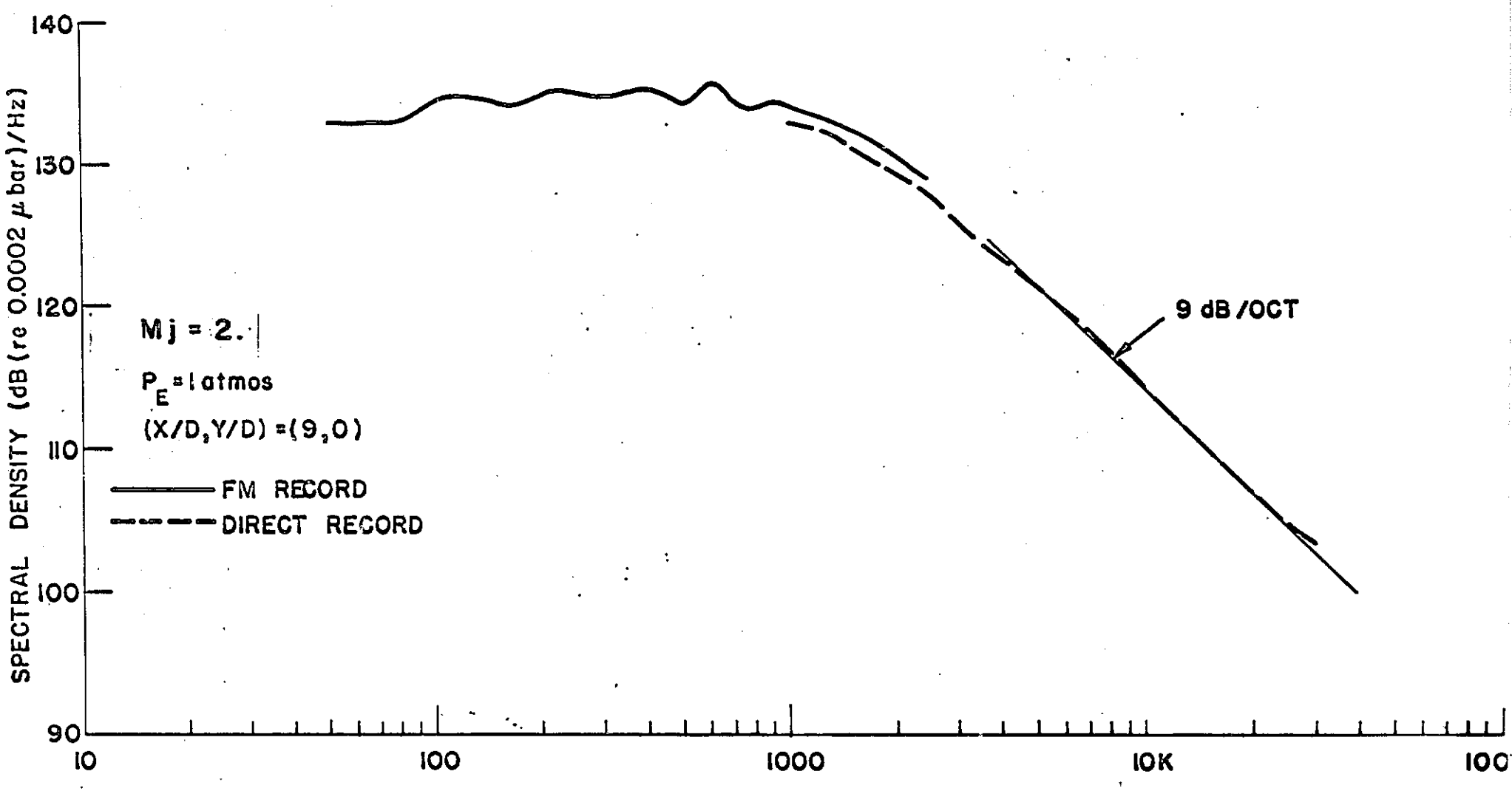

Fig 37 Spectral distribution of the static pressure fluctuations at x/D = 9 along centerline of balanced jet

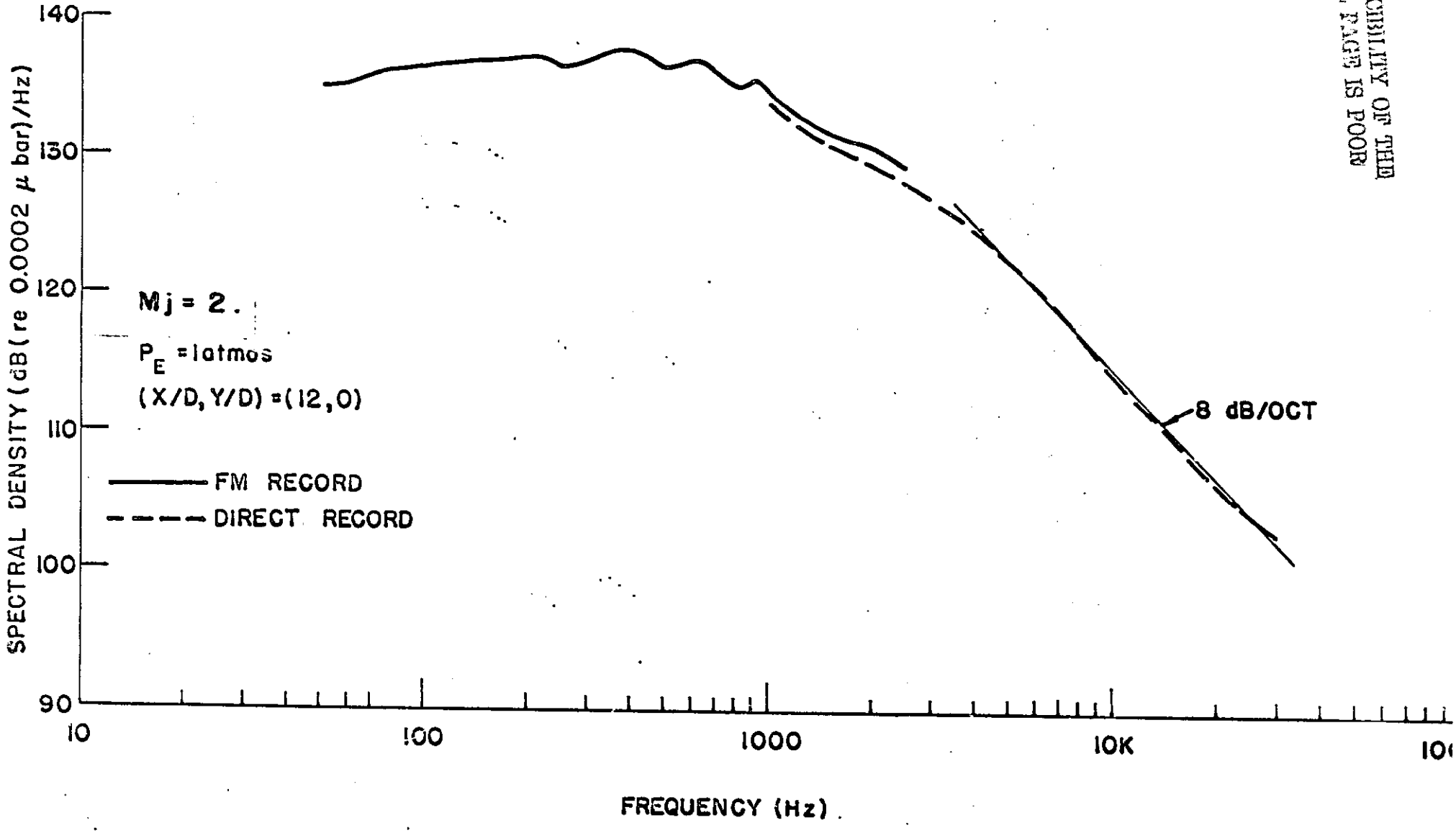

Fig. 38 Spectral distribution of the static pressure fluctuations at x/D = 12 along centerline of balanced jet

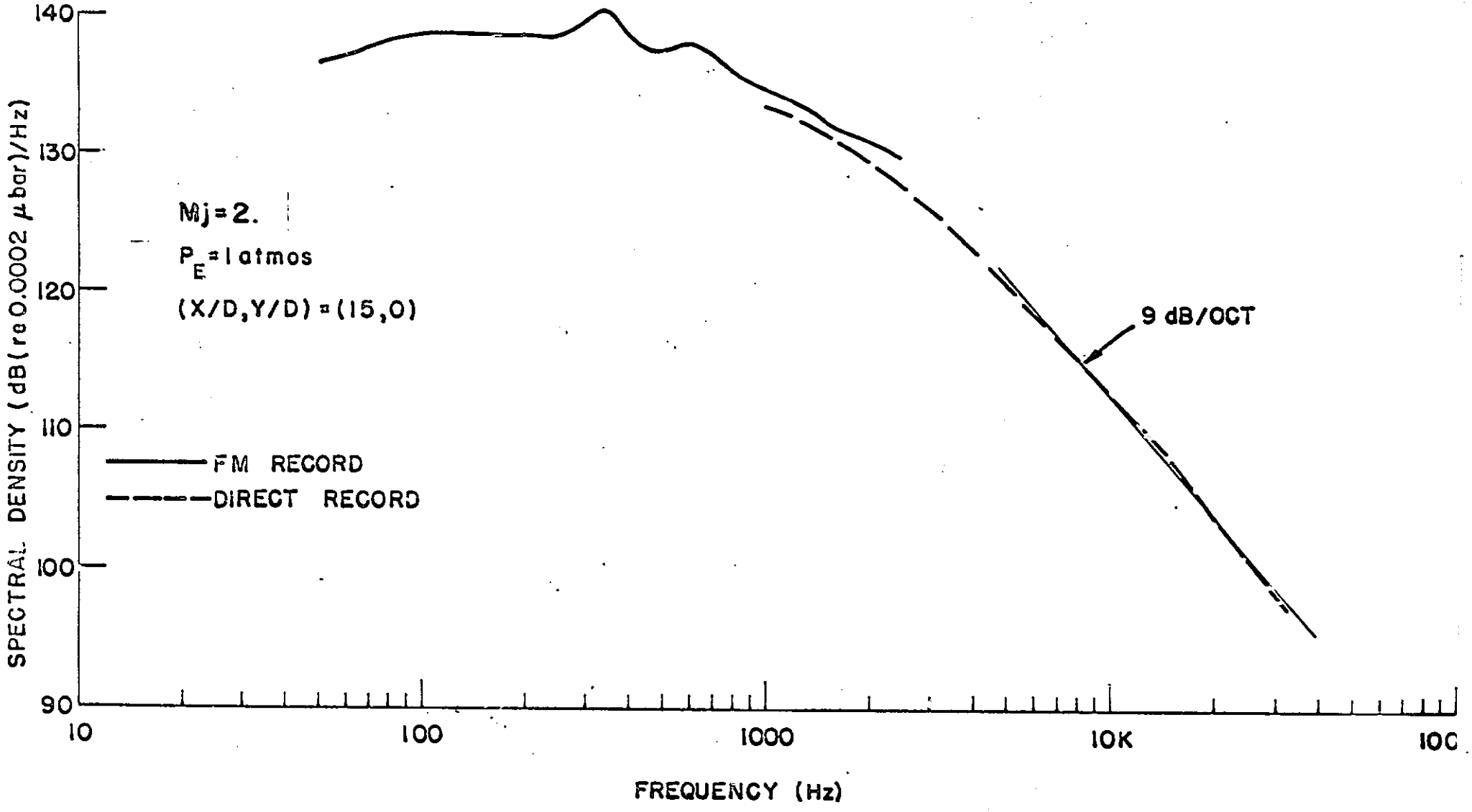

Fig. 39 Spectral distribution of the static pressure fluctuations at x/D = 15 along centerline of balanced jet

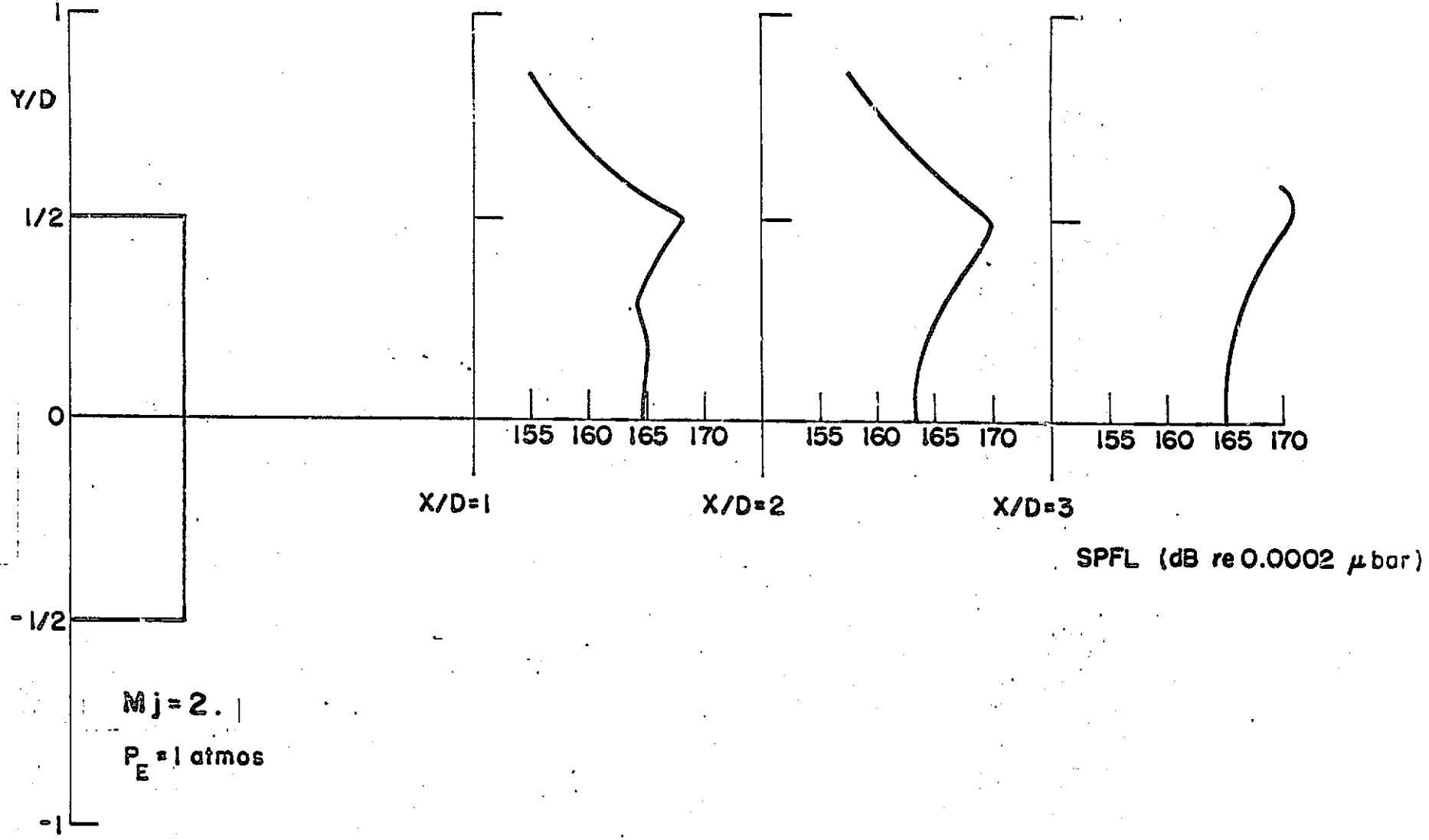

Fig. 40a Variation of static pressure fluctuation level with radial distance from centerline of balanced jet

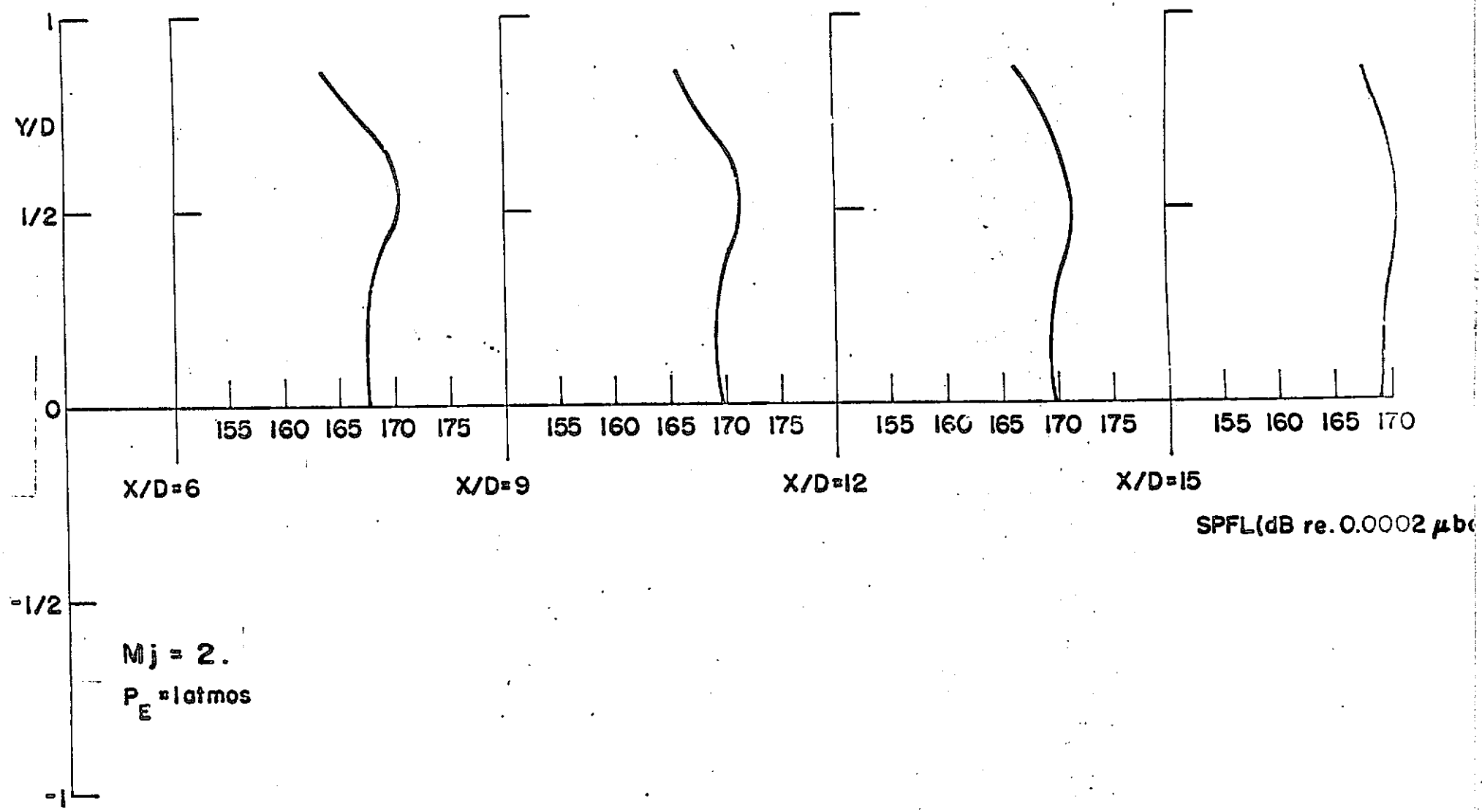

Fig. 40b Variation of static pressure fluctuation level with radial distance from centerline of balanced jet

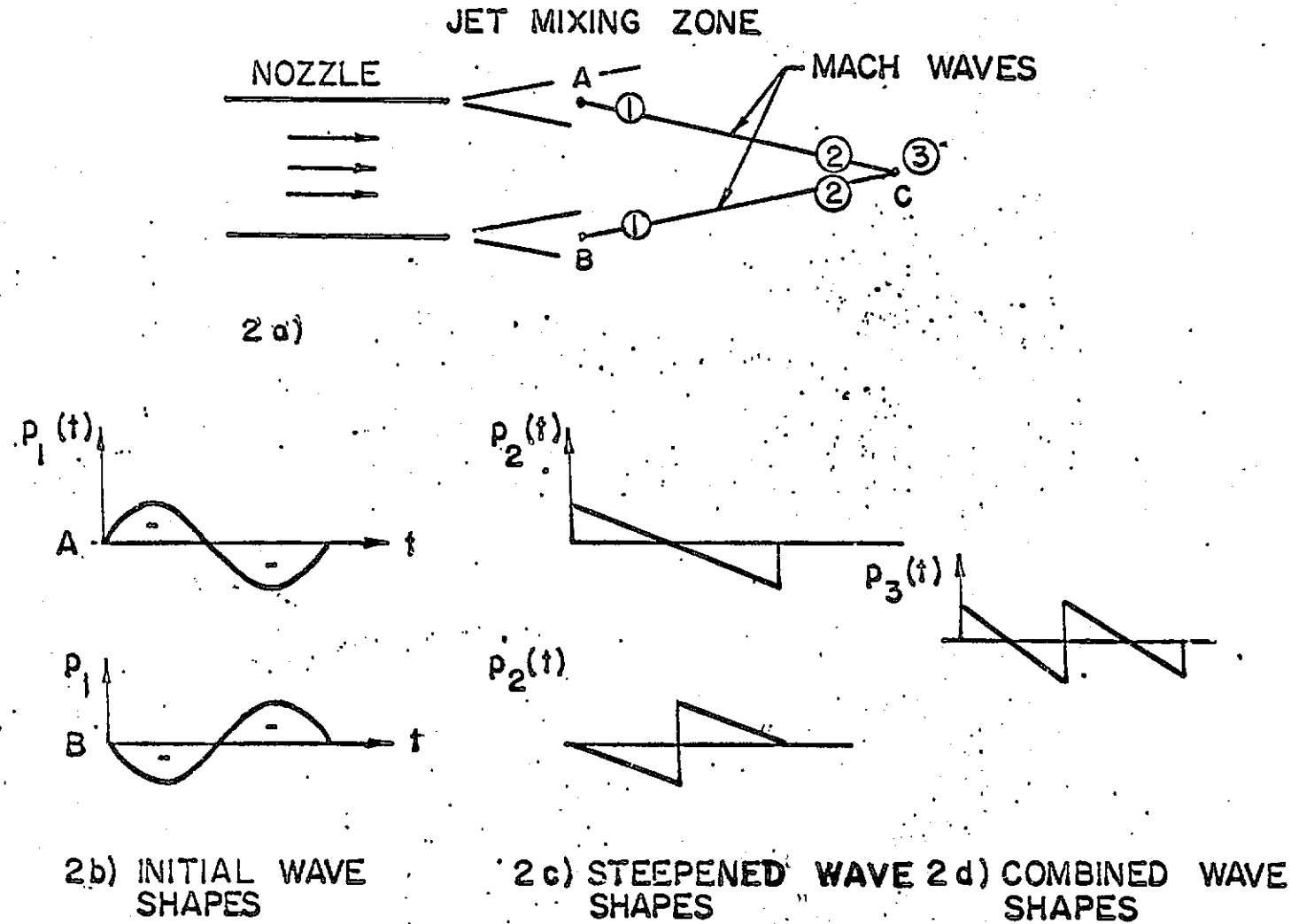

Fig. 41 Waves focussing at the jet axis

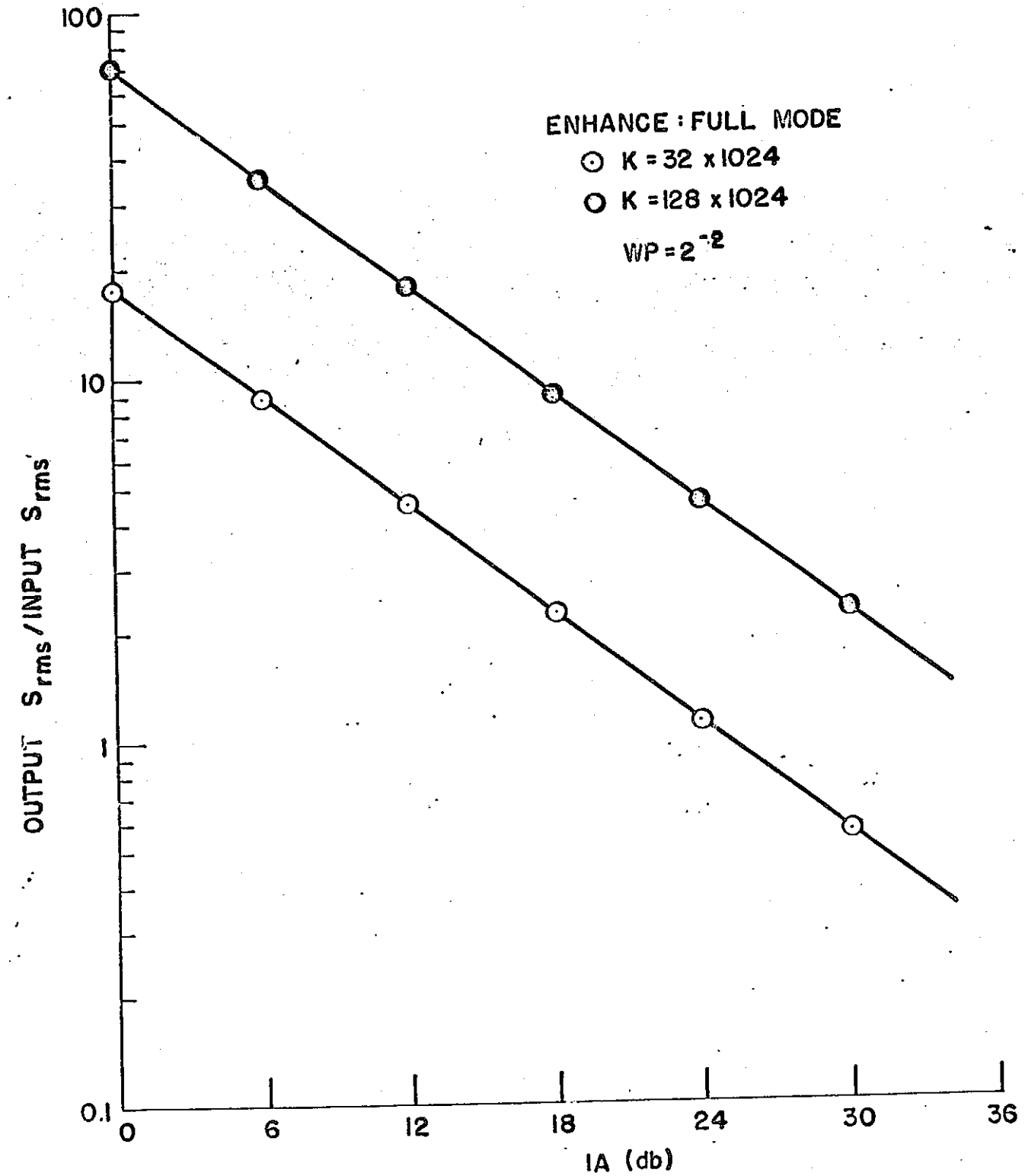

Fig. 42 Calibration of the full mode of ensemble averaging

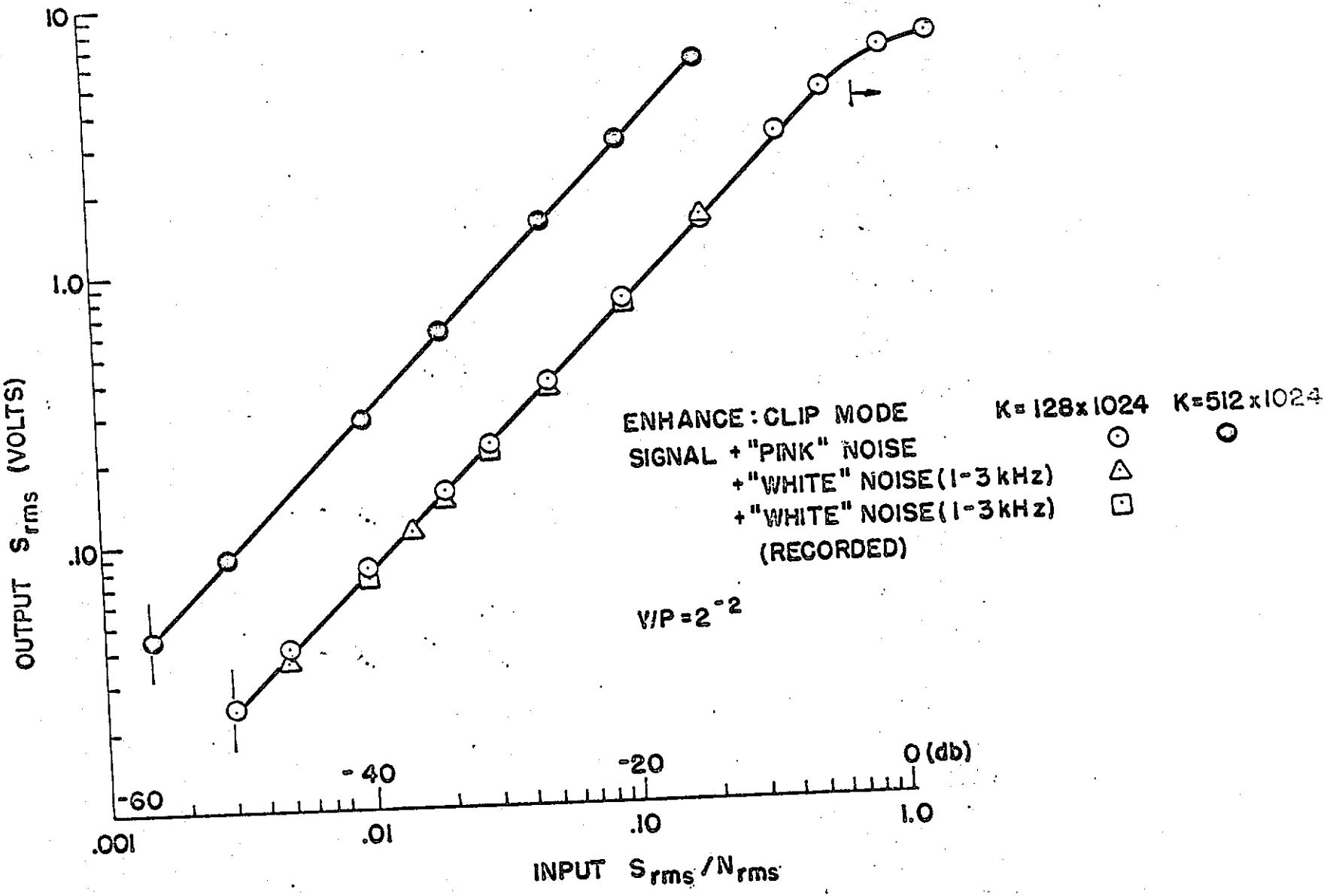

Fig. 43 Calibration of the clip mode of ensemble averaging

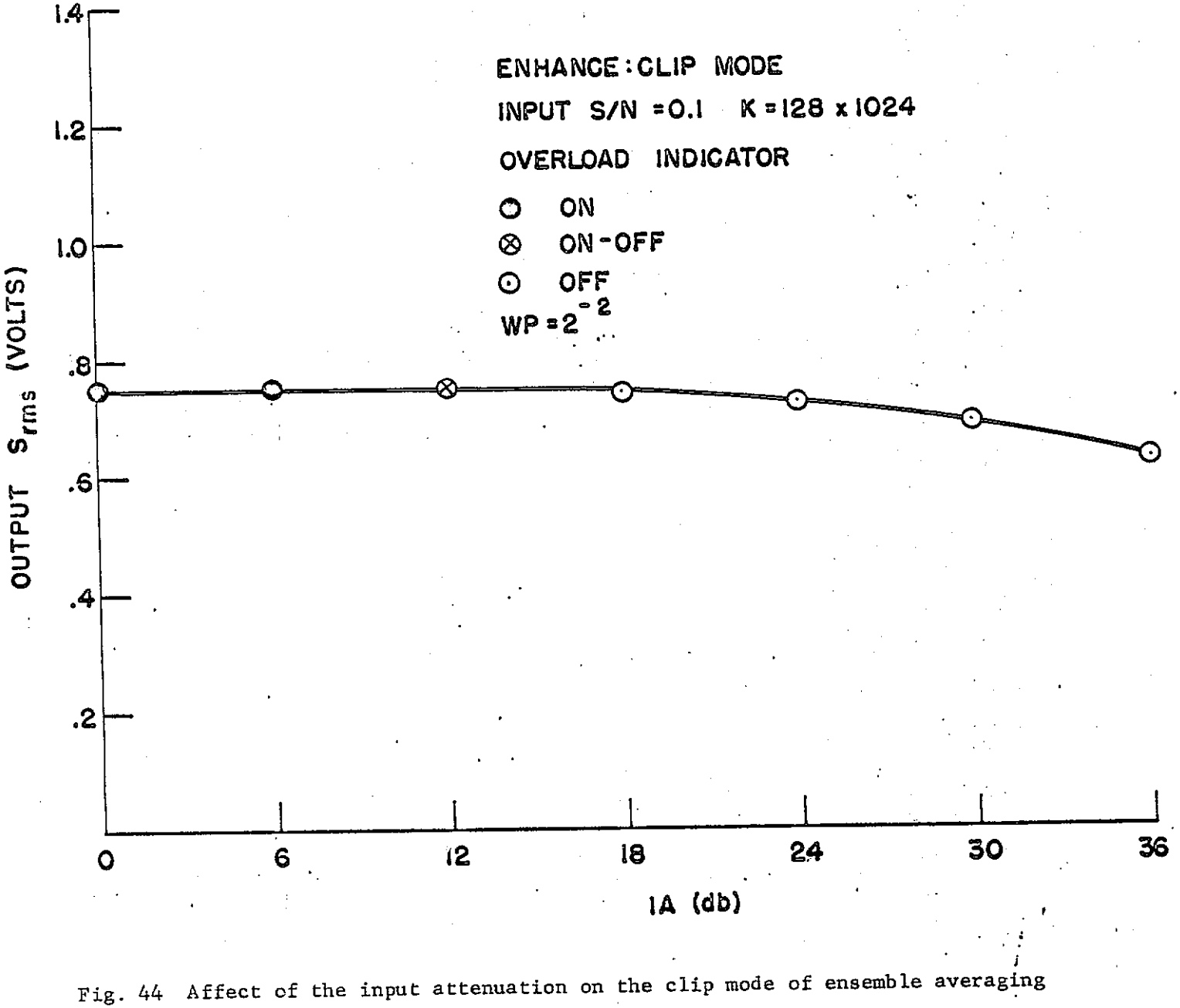

Fig. 44 Affect of the input attenuation on the clip mode of ensemble averaging

OUTPUT S_{rms} INPUT S_{rms}/N_{rms}

(VOLTS)

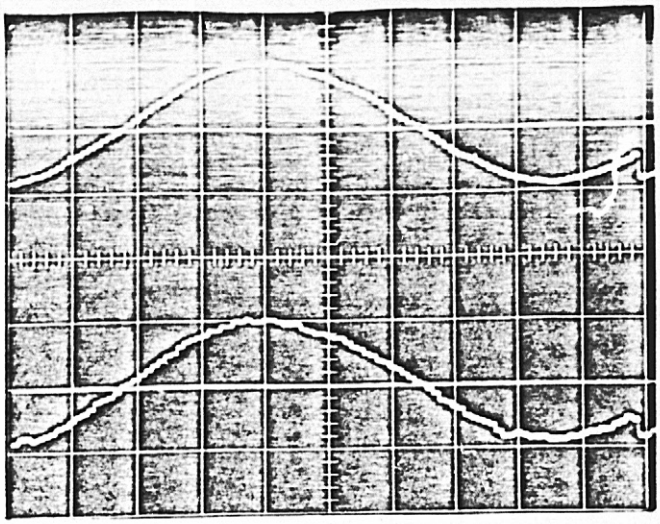

.74 -20 db

.37 -26 db

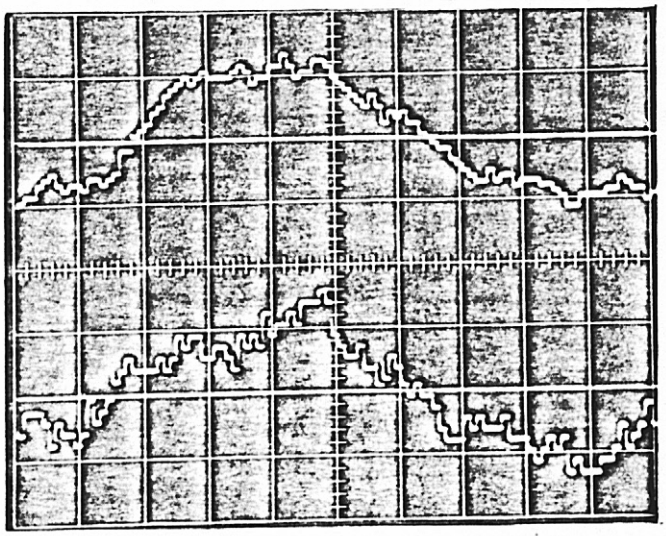

.079 -40 db

.039 -46 db

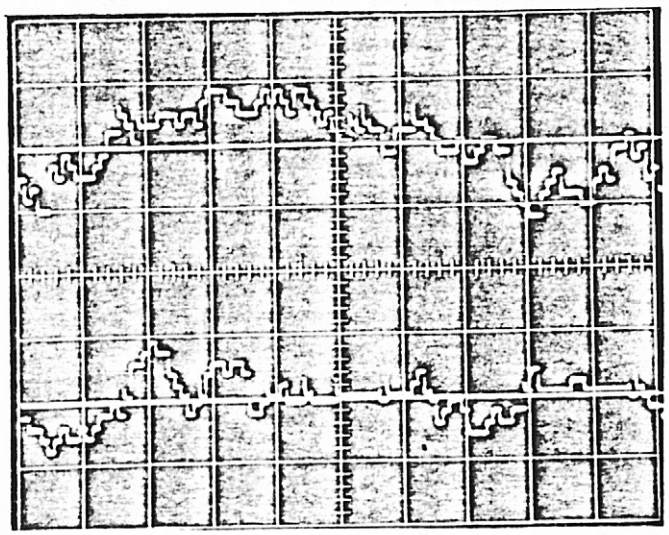

.024 -50 db

< .024 -56 db

ENHANCE: CLIP MODE

SIGNAL +"PINK NOISE" K = 128 x 1024 WP = 2^{-2}

Fig. 45 Typical signal traces obtained from the clip mode of ensemble averaging

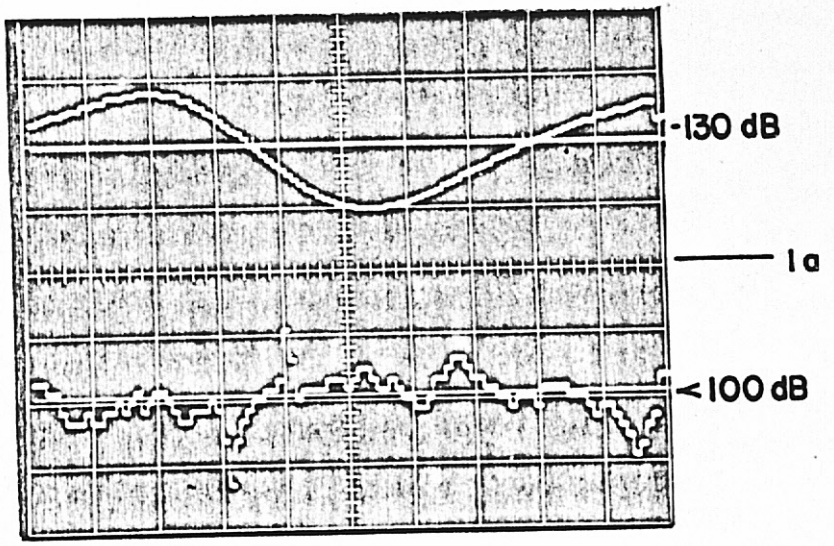

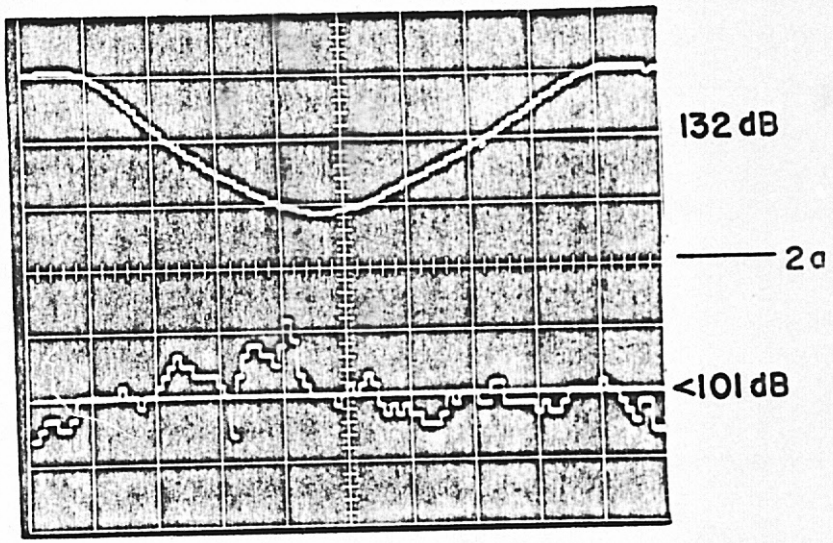

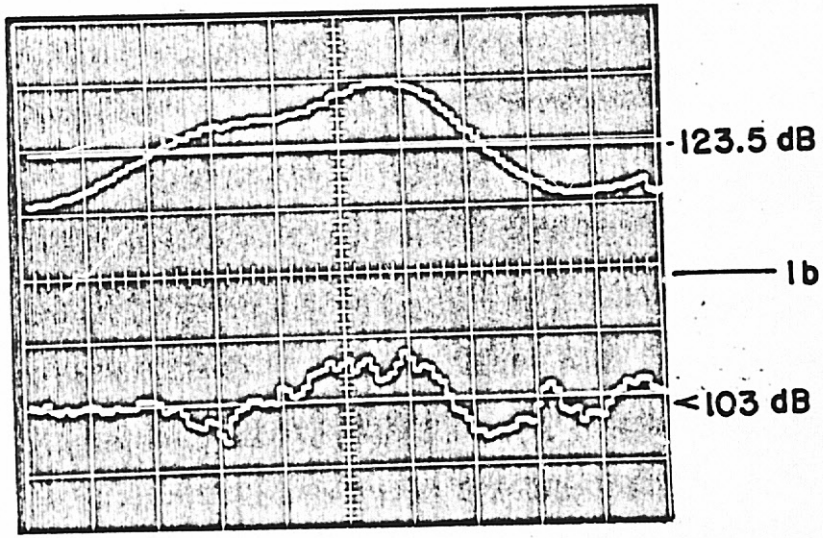

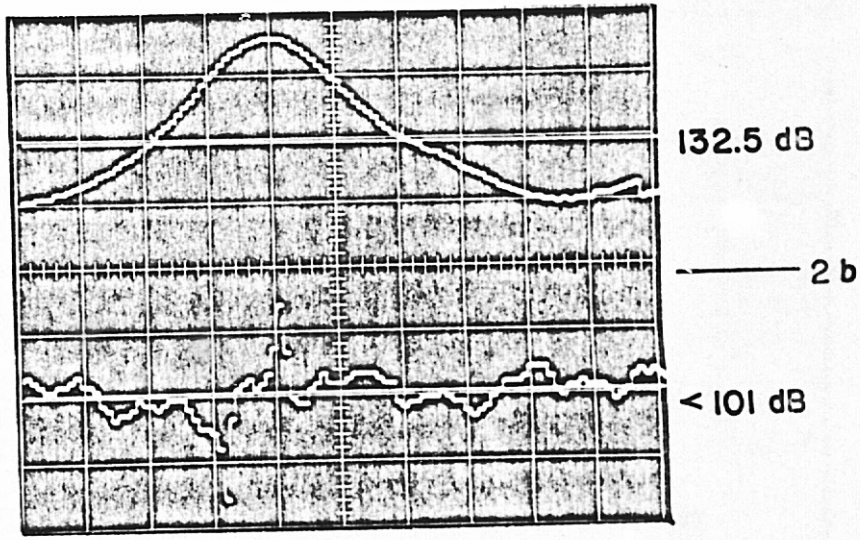

Fig. 46 Traces of the acoustic signal at the four positions in still air and in the balanced jet

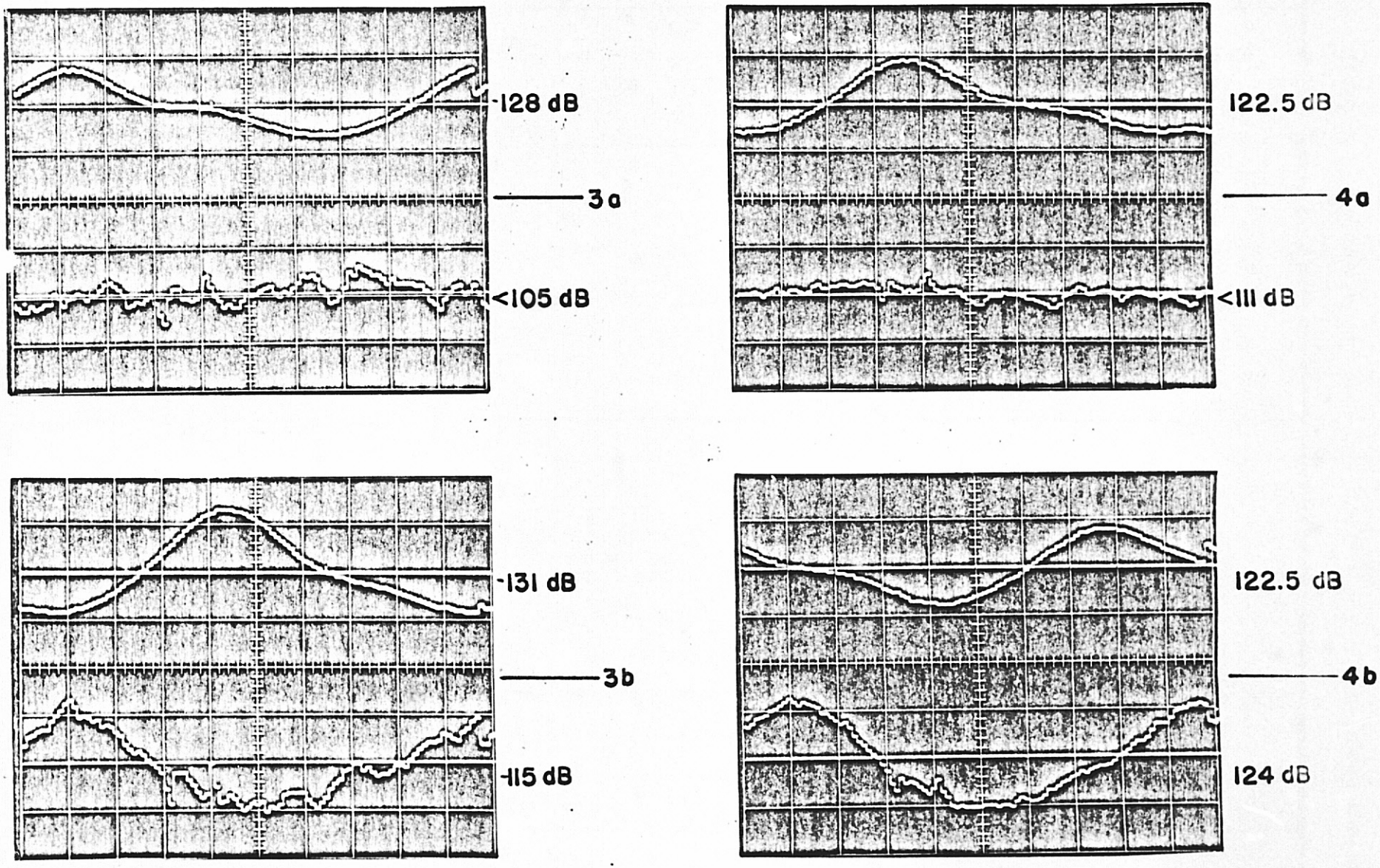

Fig. 47 Traces of the acoustic signal at four positions in still air and in the balanced jet

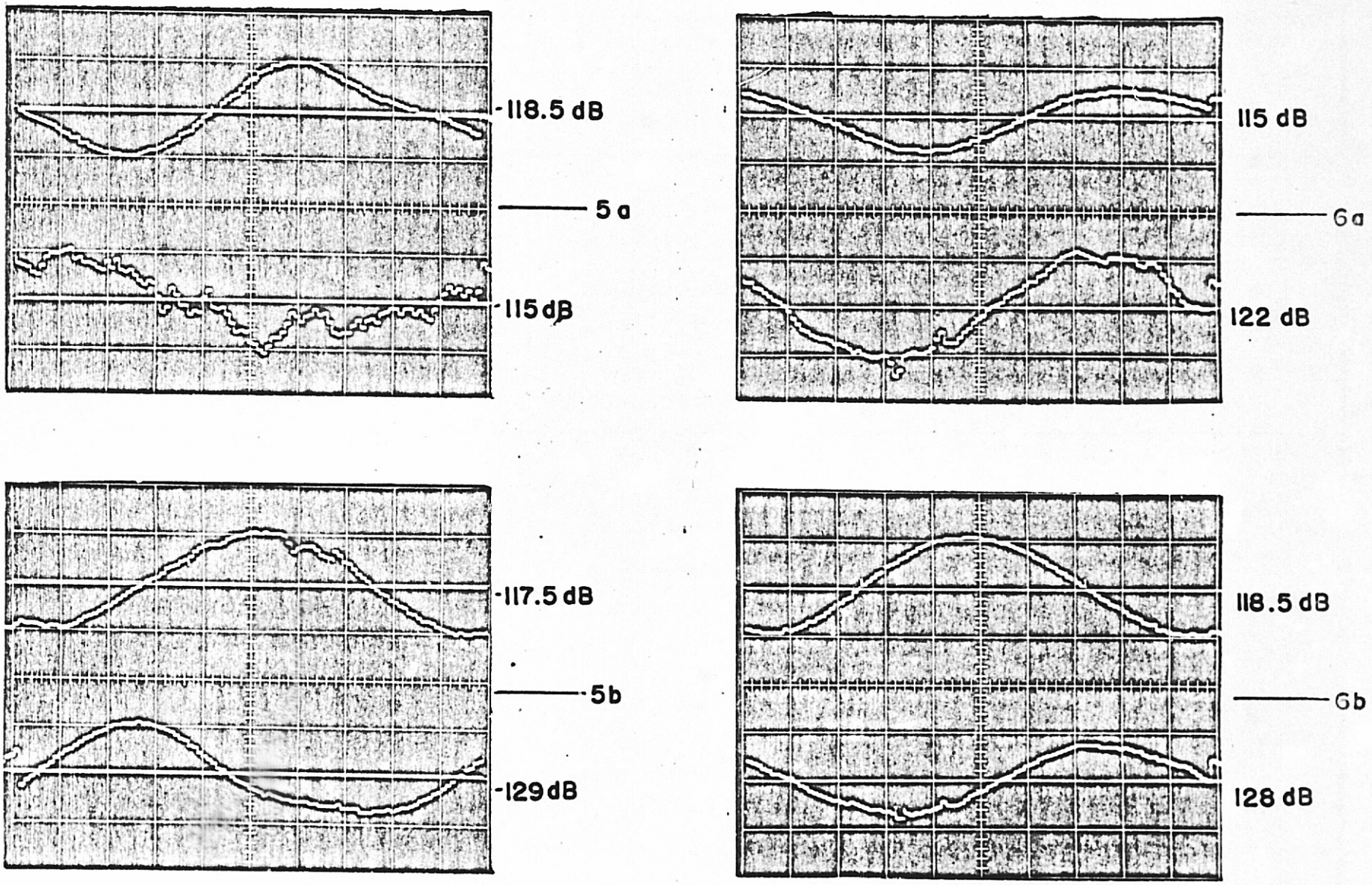

Fig. 48 Traces of the acoustic signal at four positions in still air and in the balanced jet

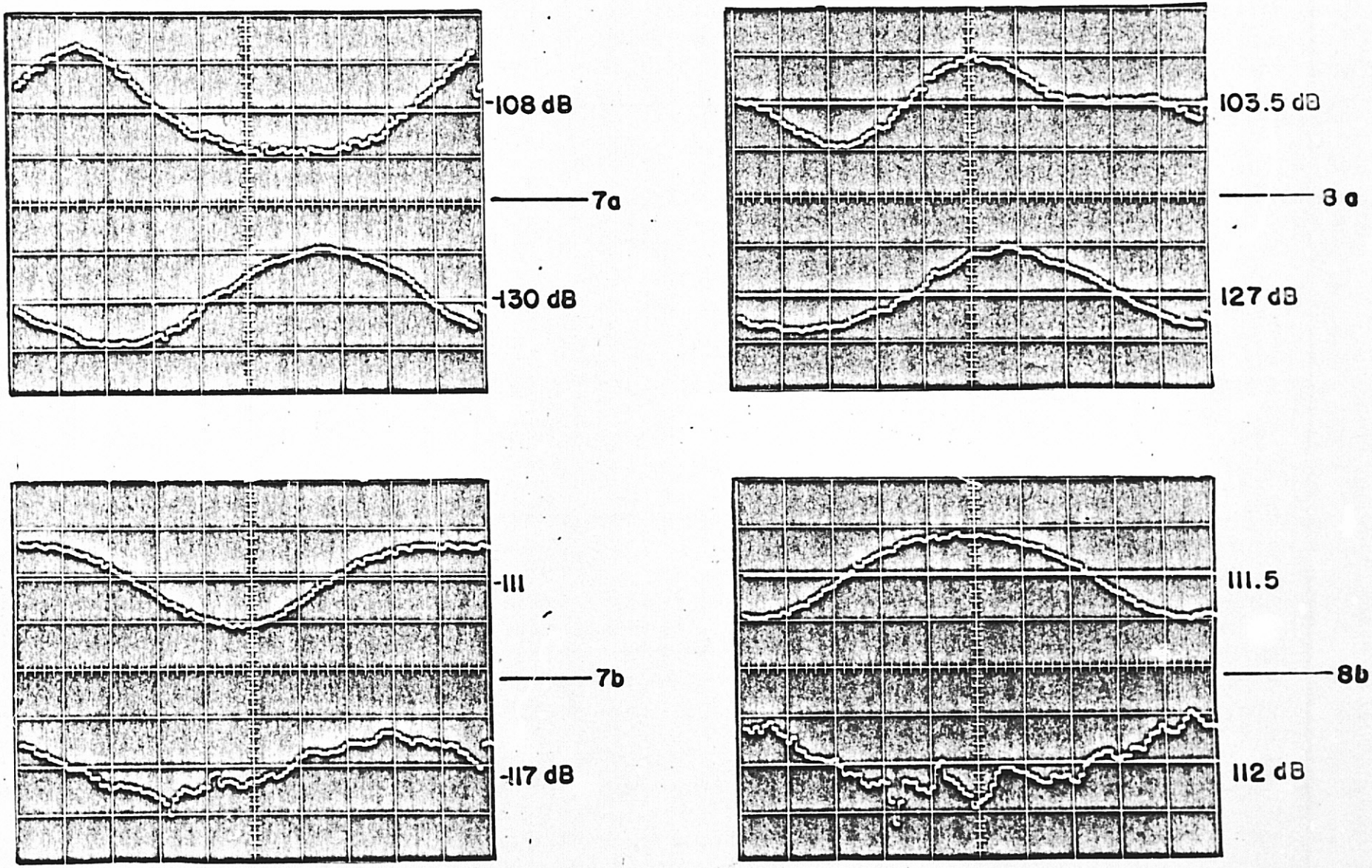

Fig. 49 Traces of the acoustic signal at four positions in still air and in the balanced jet

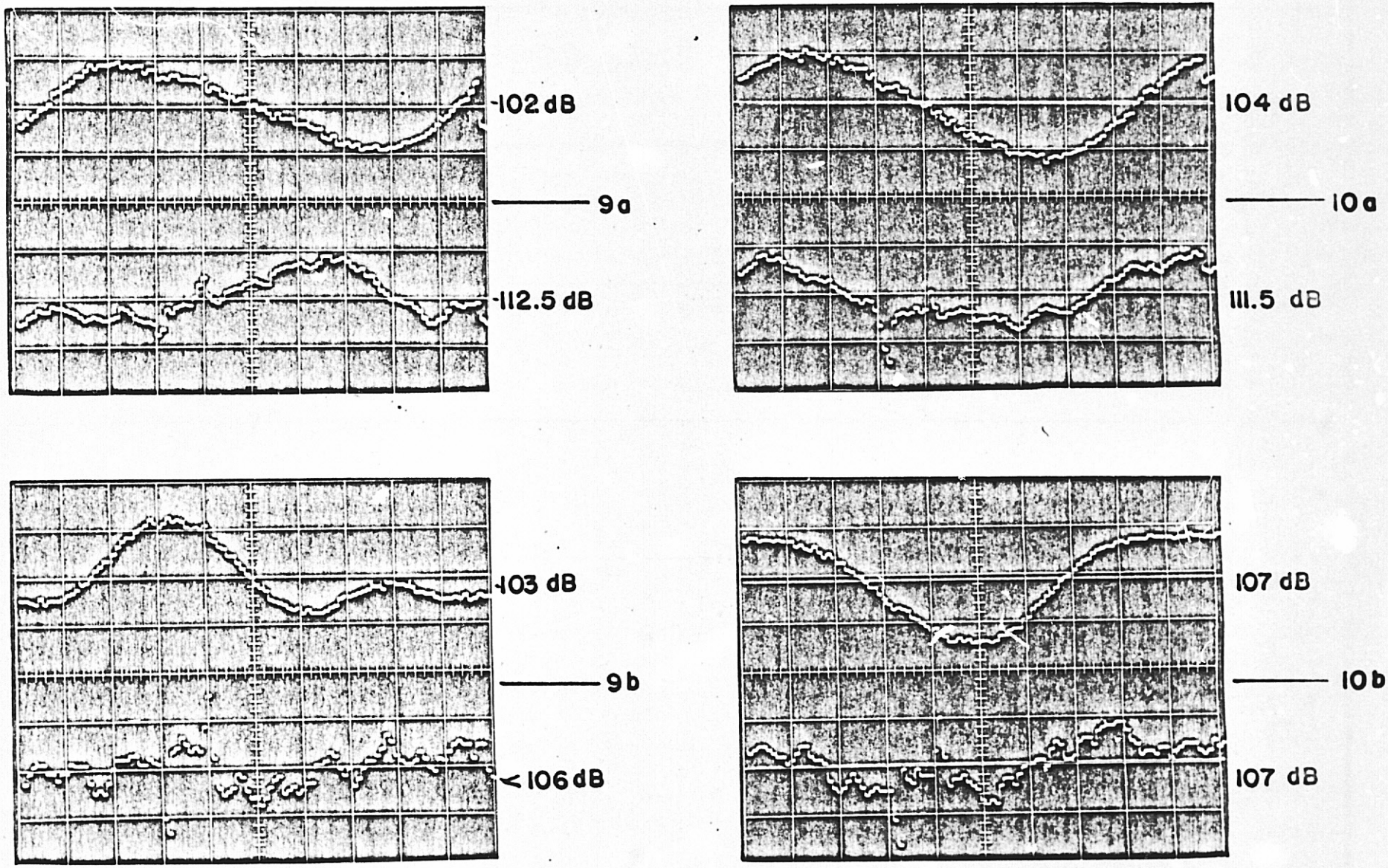

Fig. 50 Traces of the acoustic signal at four positions in still air and in the balanced jet

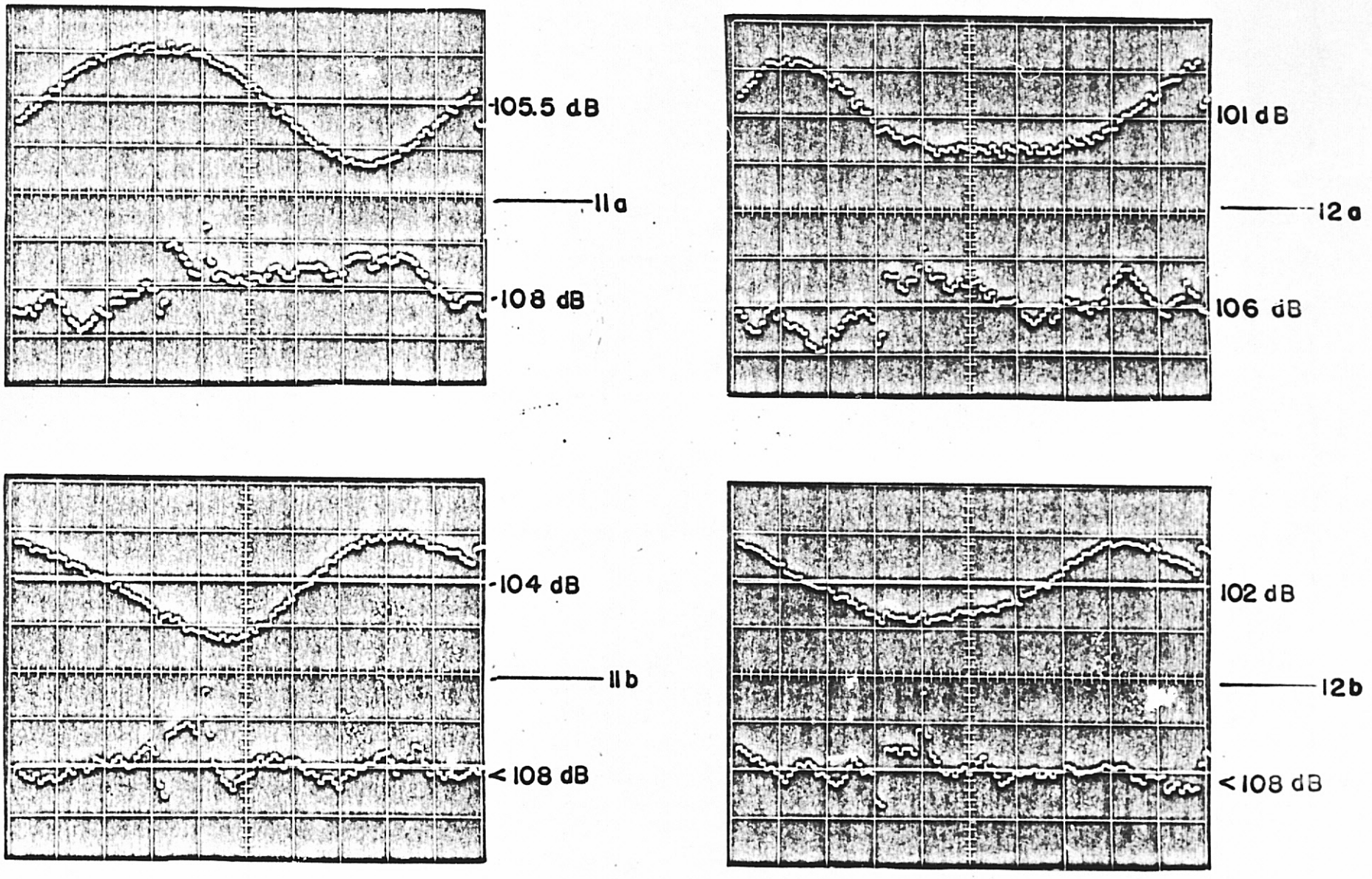

Fig. 51 Traces of the acoustic signal at four positions in still air and in the balanced jet

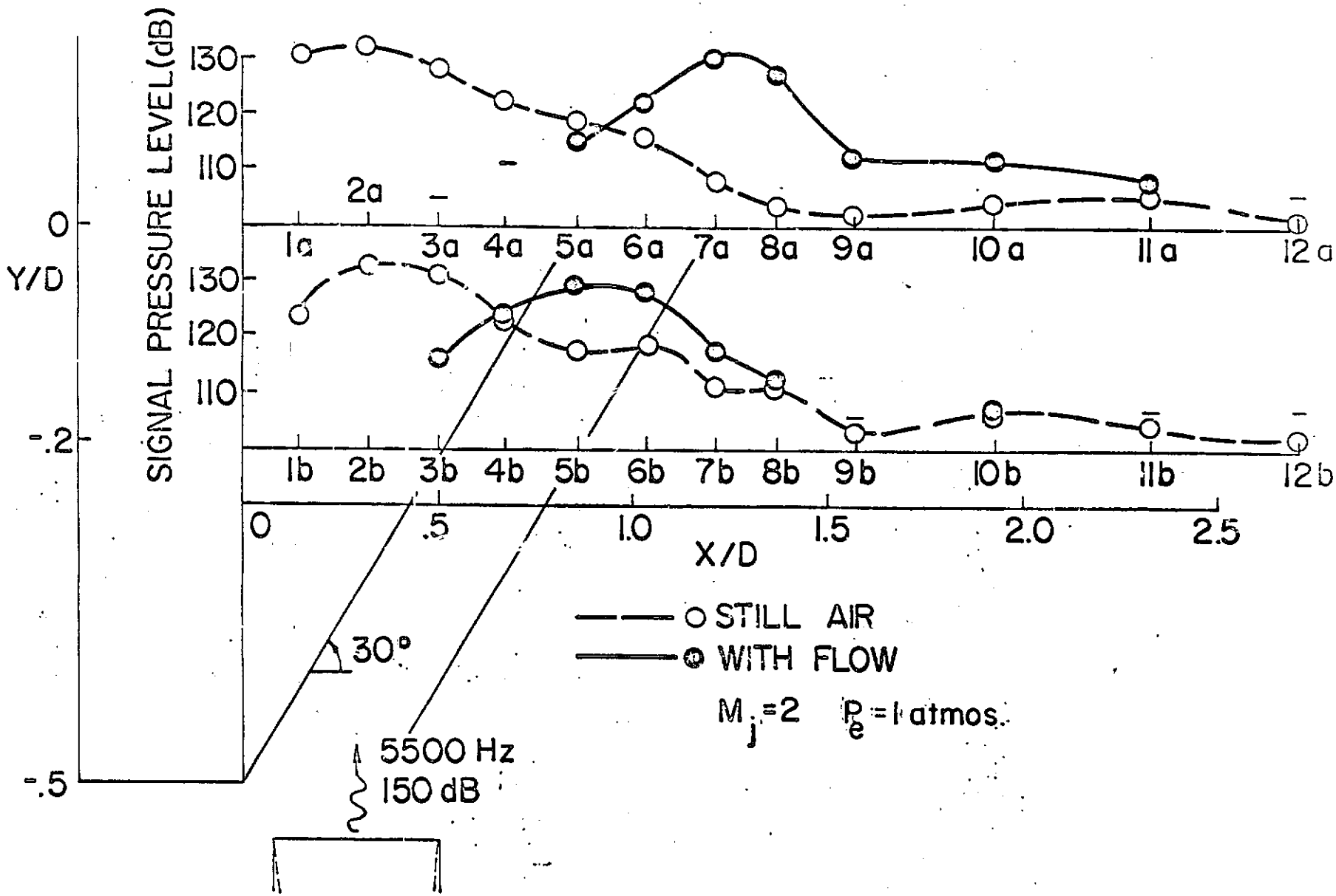

Fig. 52 Variation of the acoustic signal level in still air and in the balanced jet

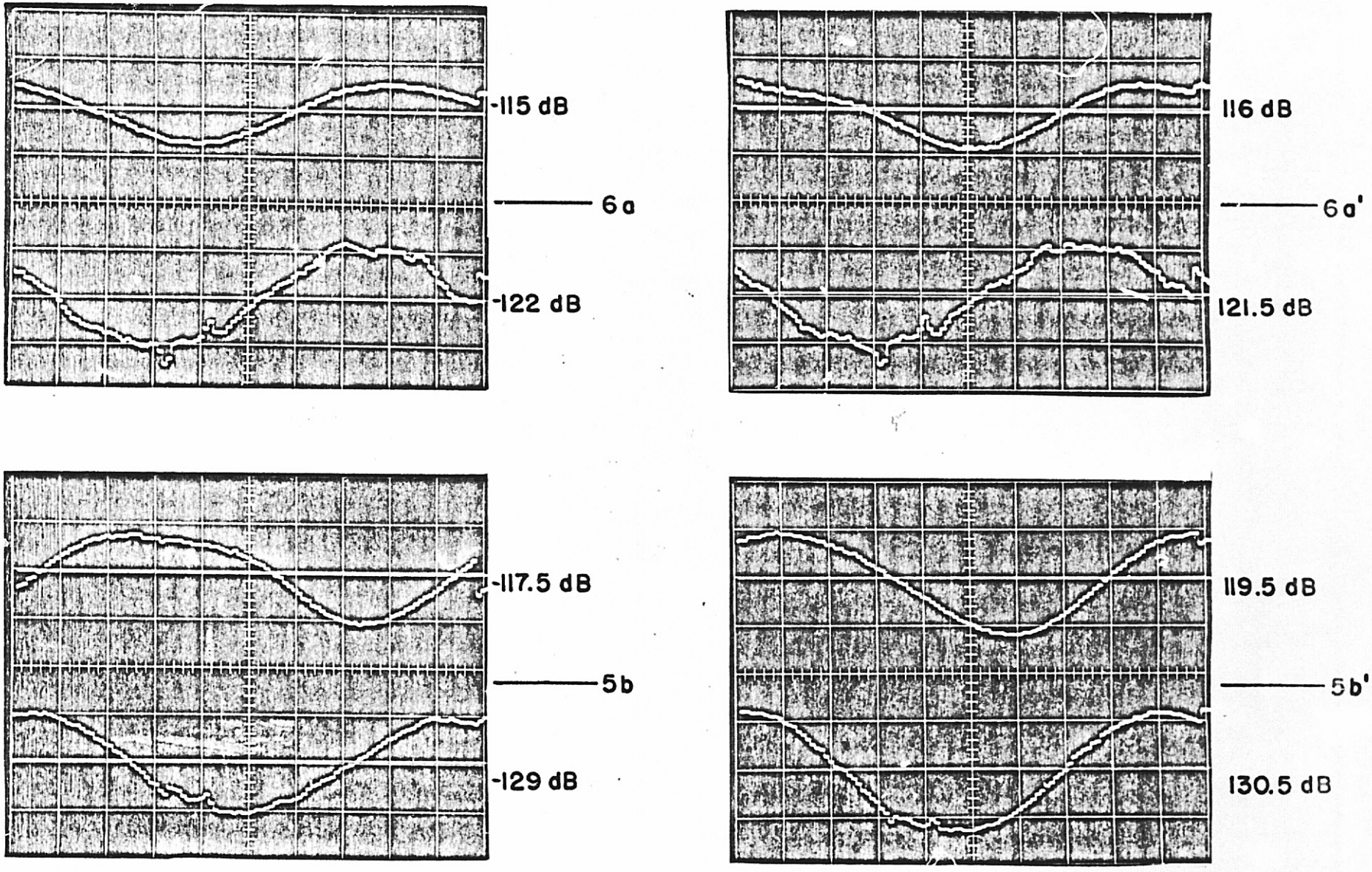

Fig. 53 Comparison of two repeated measurements

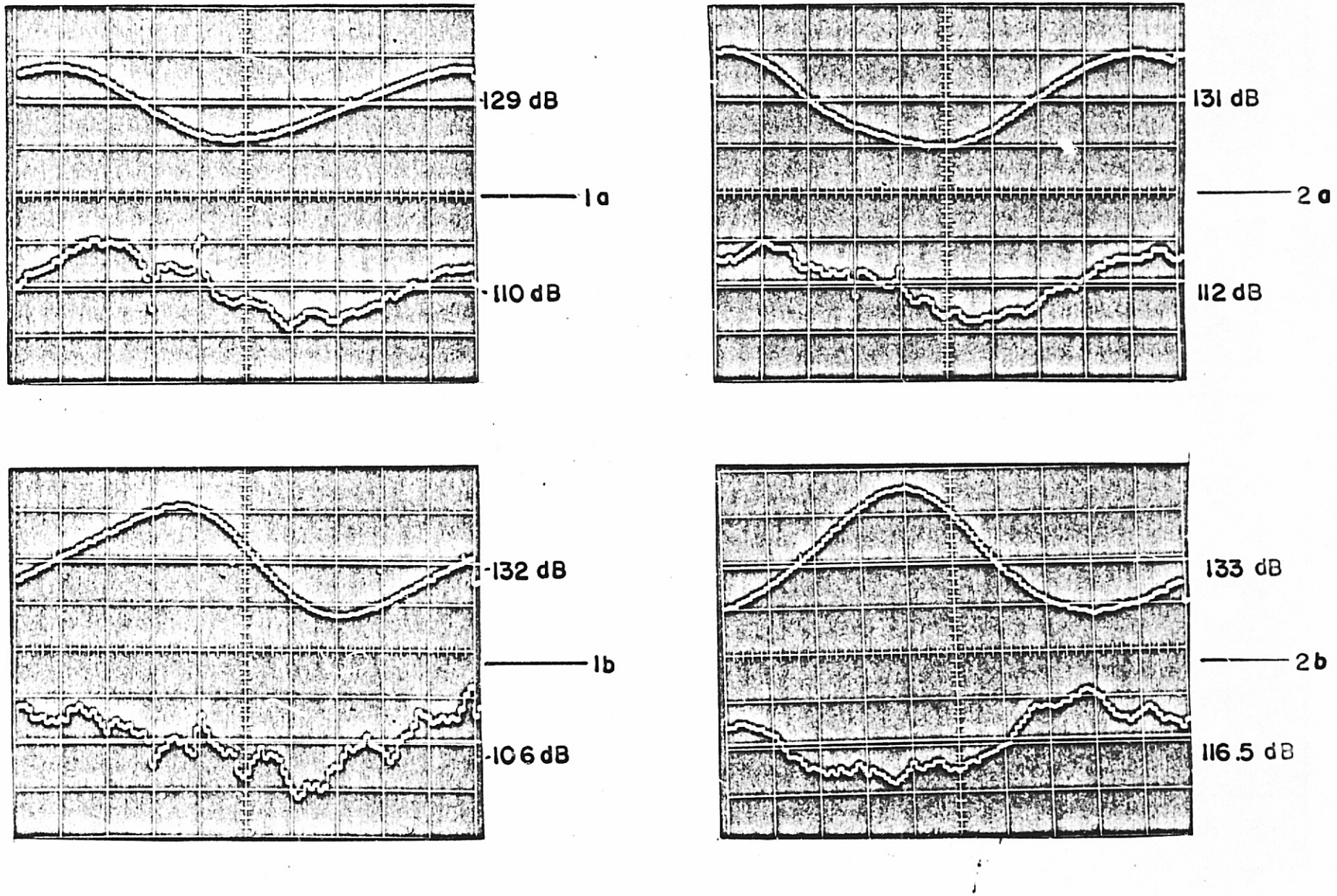

Fig. 54 Traces of the acoustic signal at four positions in still air and in the overexpanded jet

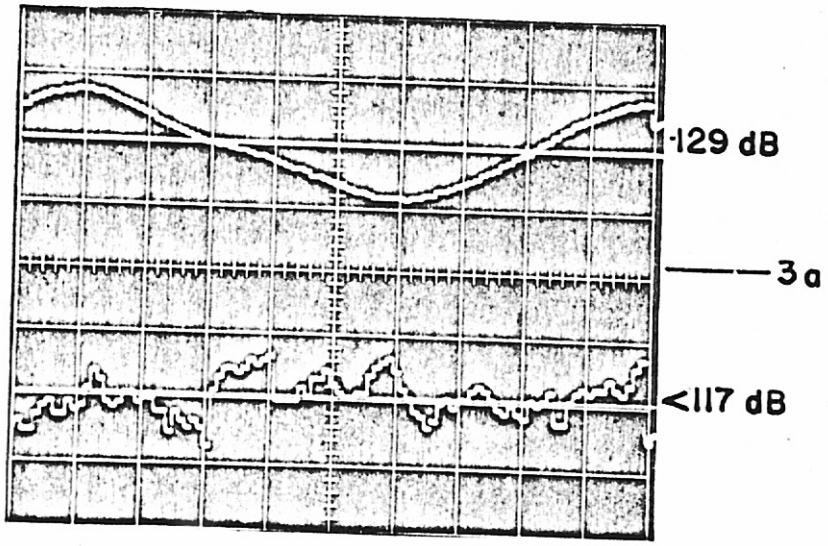

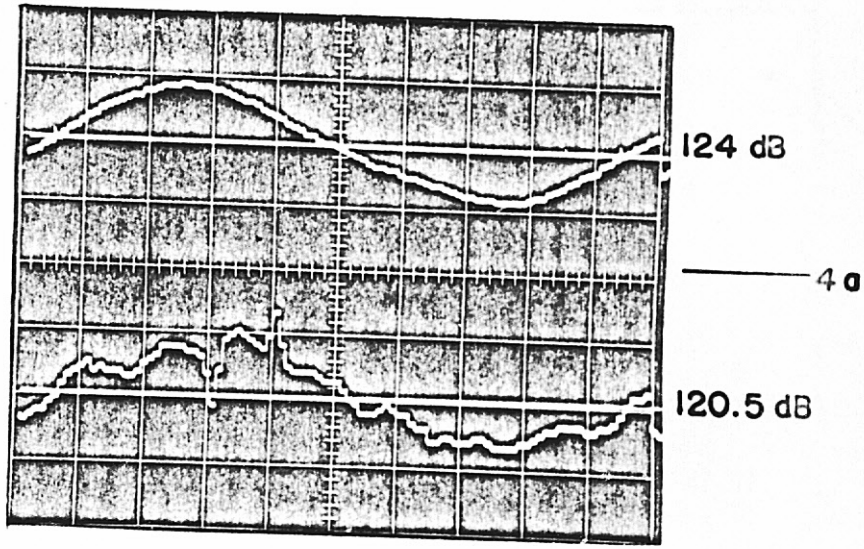

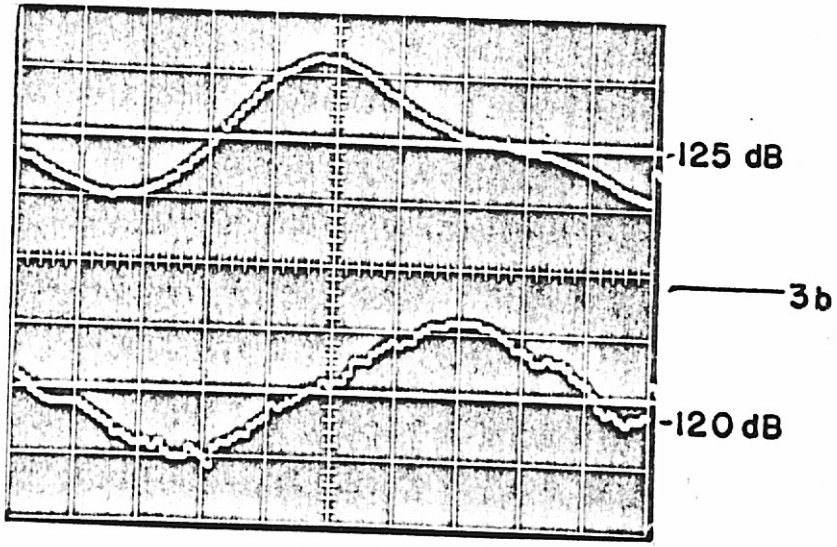

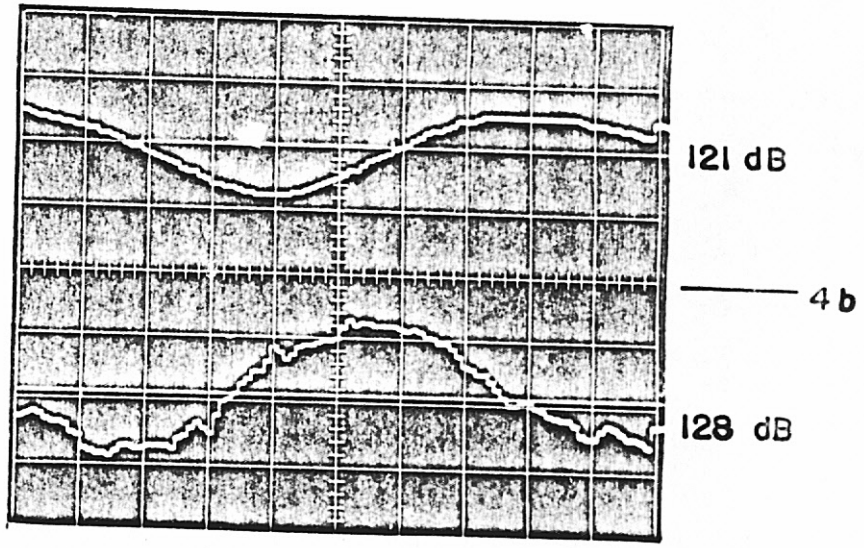

Fig. 55 Traces of the acoustic signal at four positions in still air and in the overexpanded jet

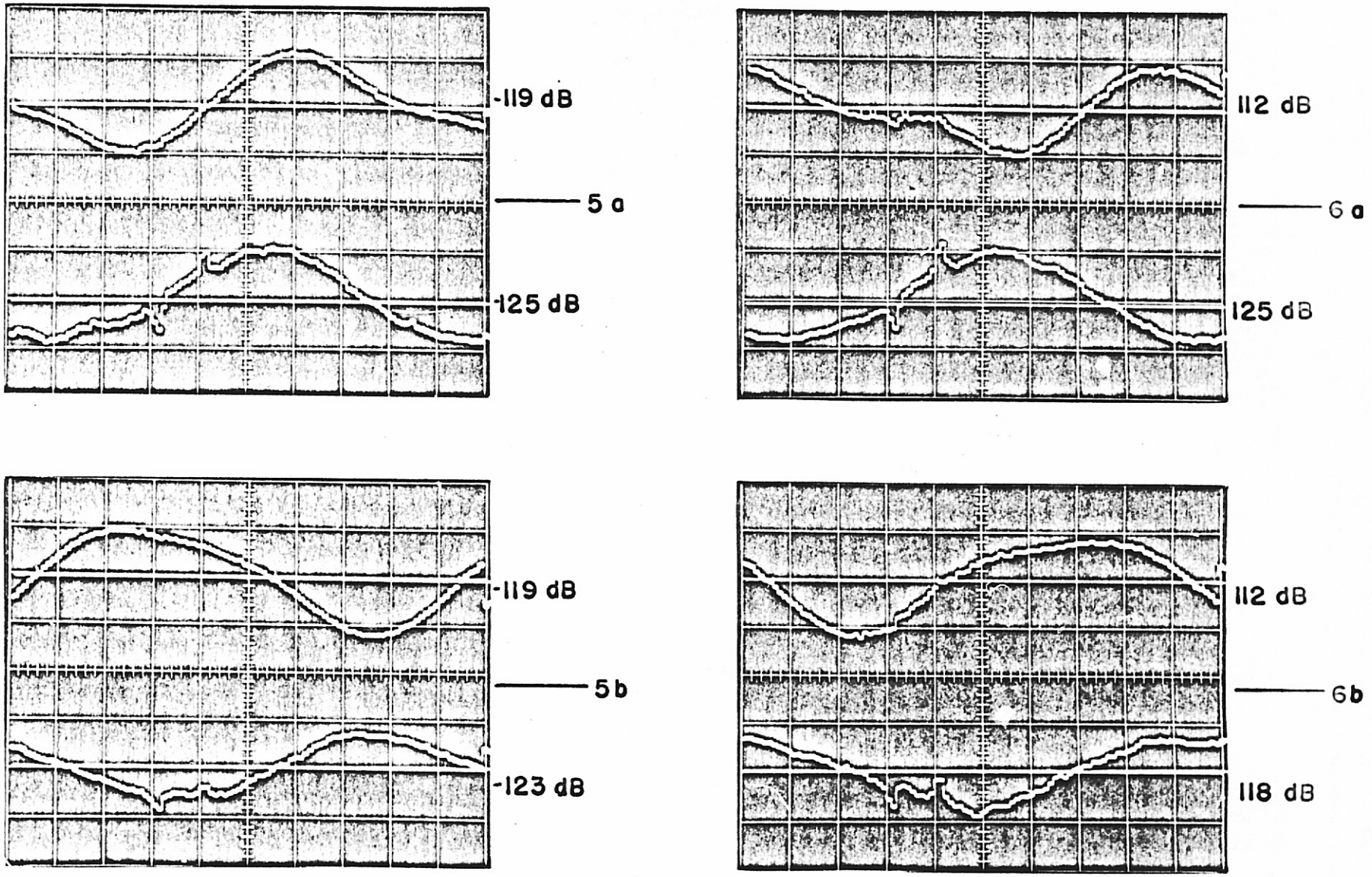

Fig. 56 Traces of the acoustic signal at four positions in still air and in the overexpanded jet

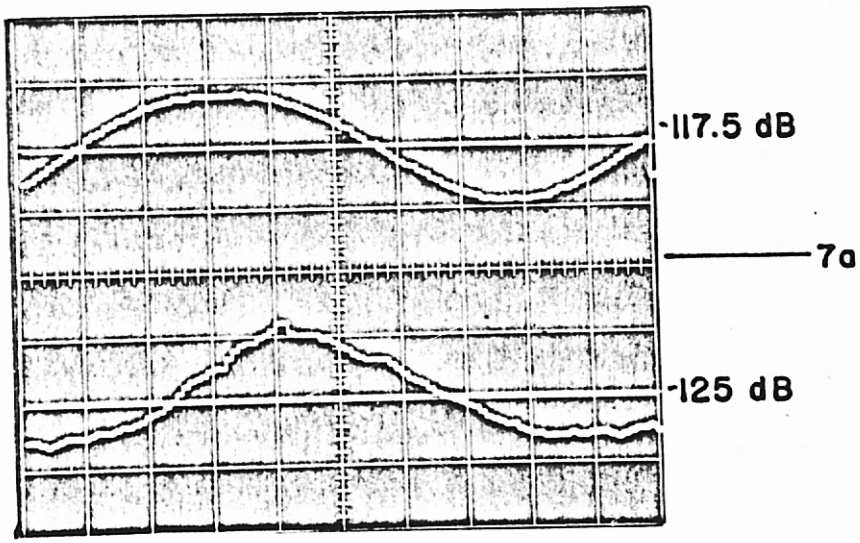

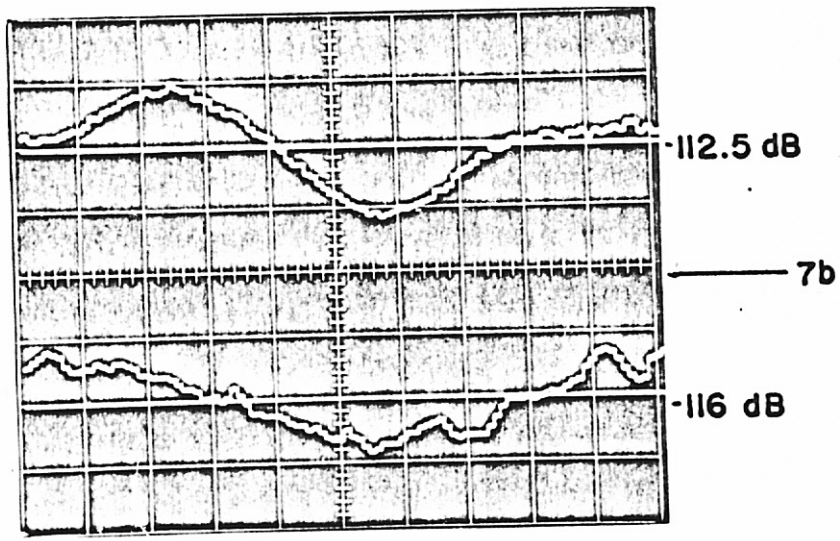

Fig. 57 Traces of the acoustic signal at two positions in still air and in the overexpanded jet

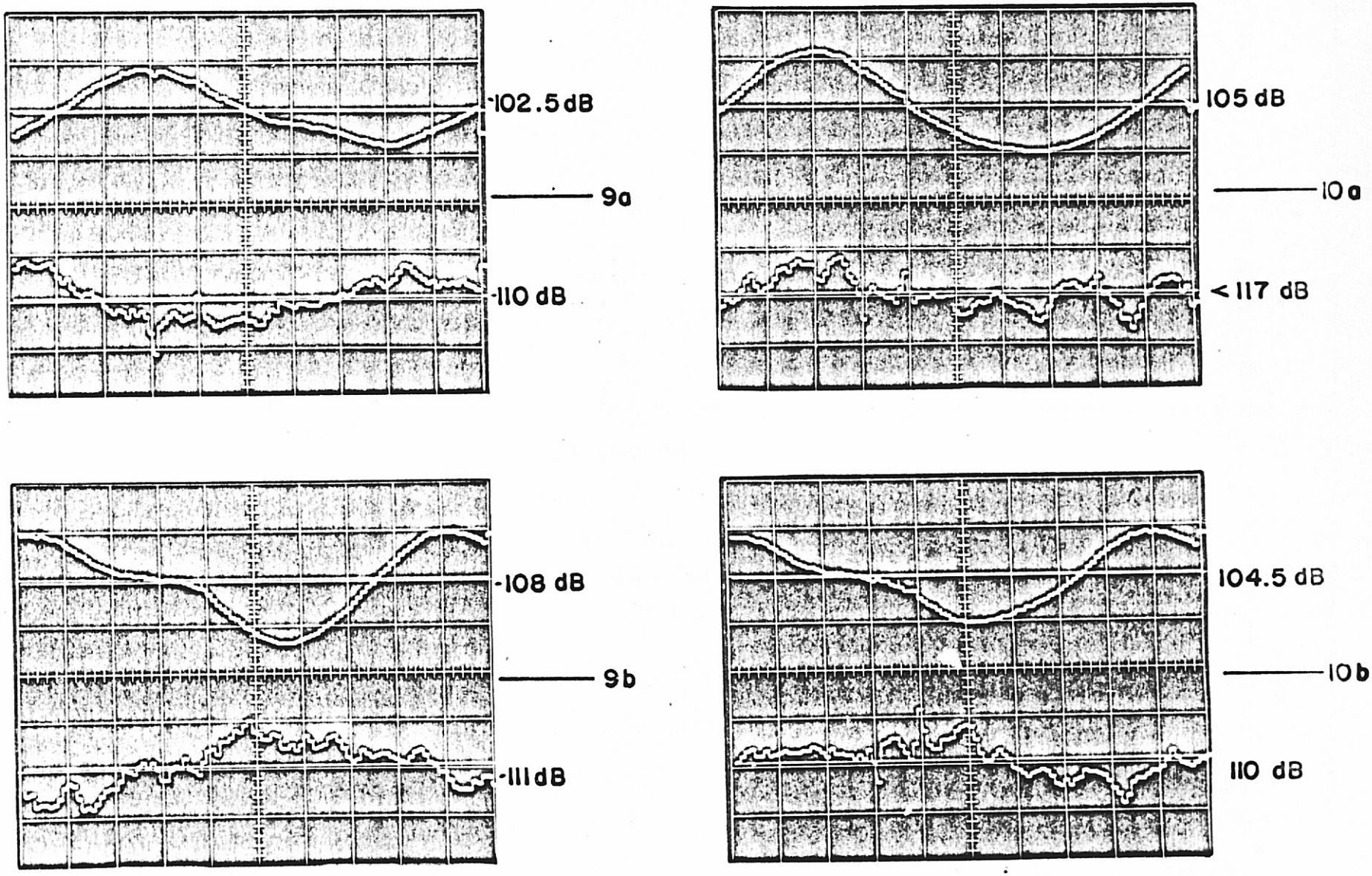

Fig. 58 Traces of the acoustic signal at four positions in still air and in the overexpanded jet

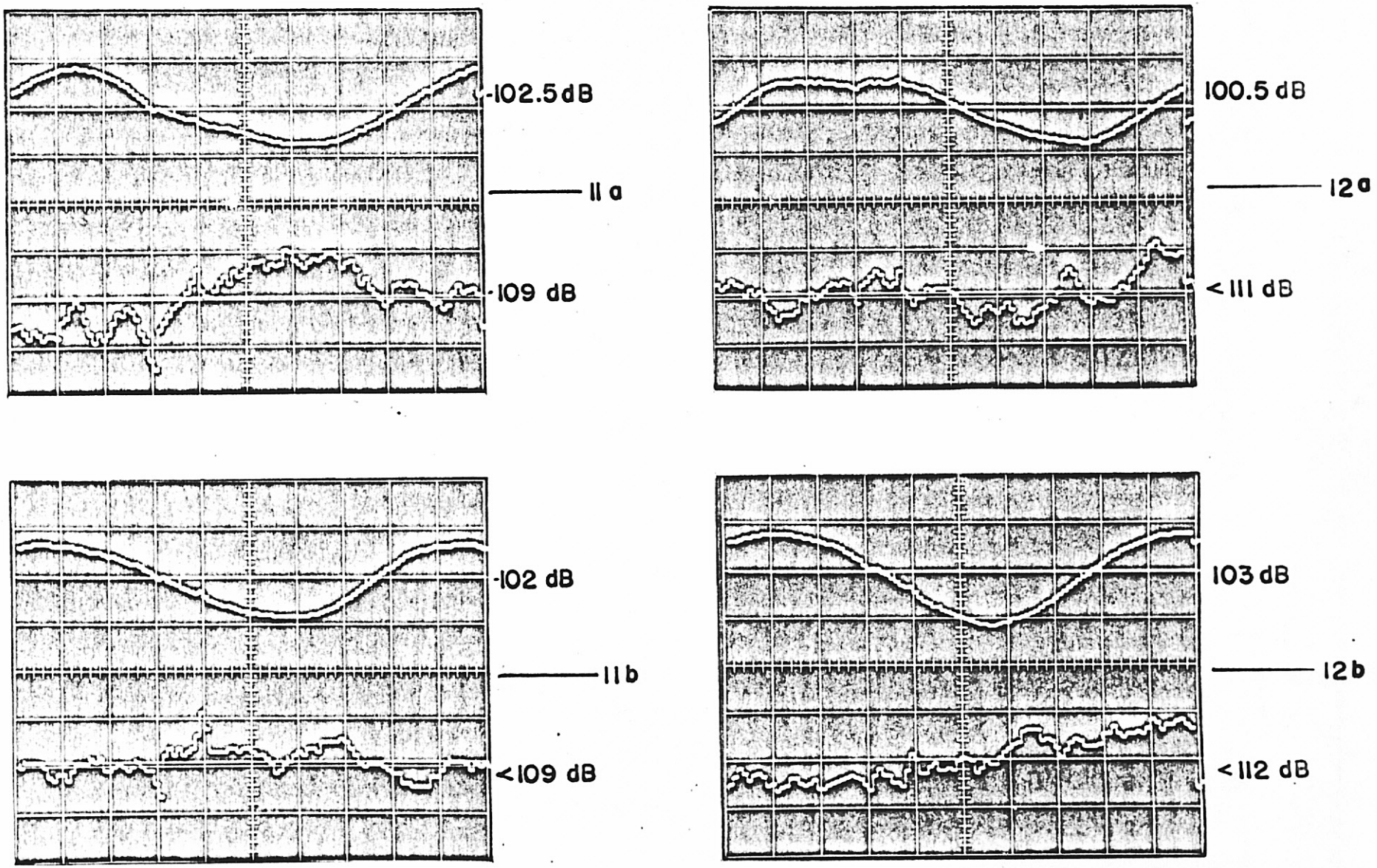

Fig. 59 Traces of the acoustic signal at four positions in still air and in the overexpanded jet

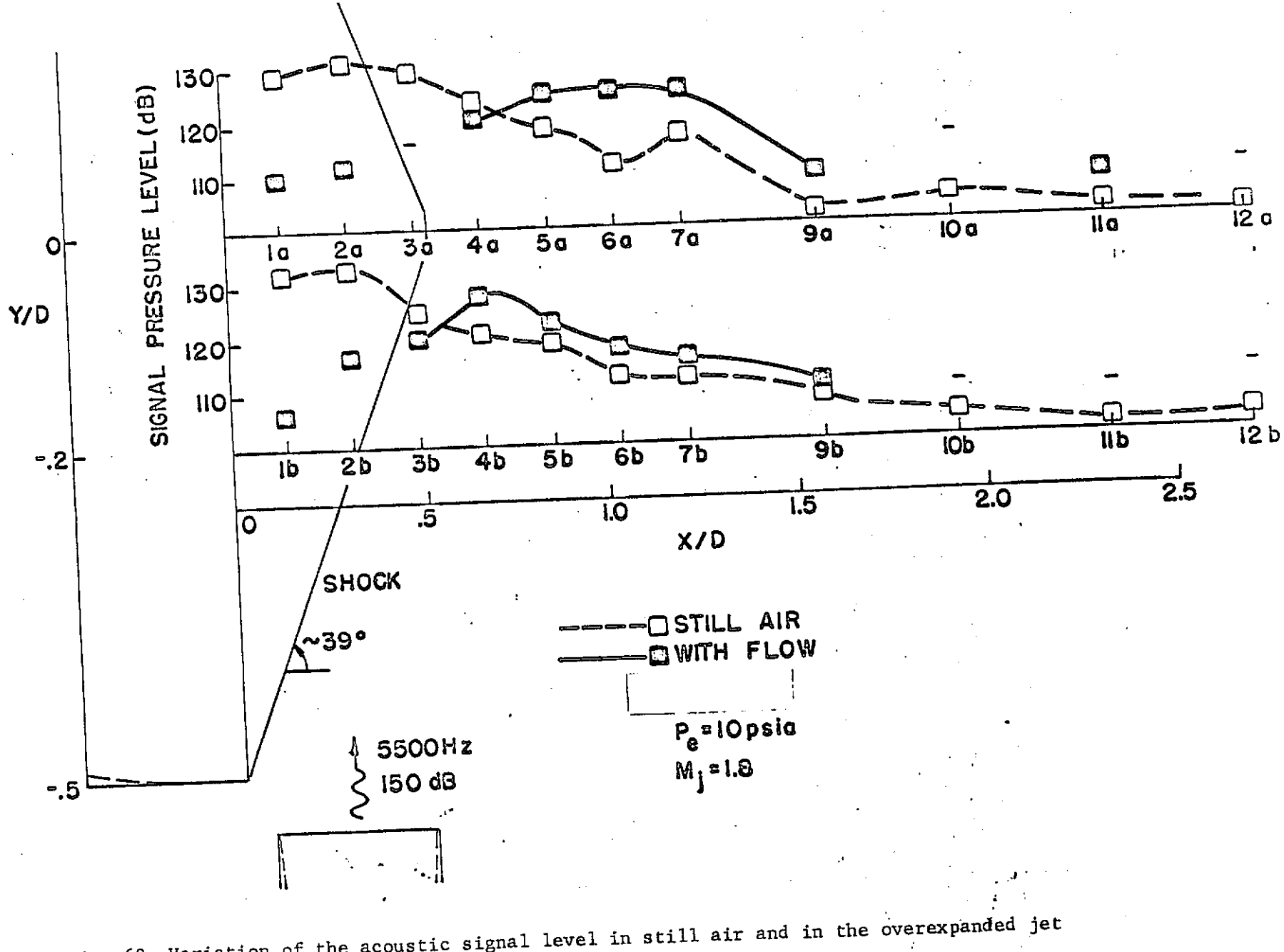

Fig. 60 Variation of the acoustic signal level in still air and in the overexpanded jet

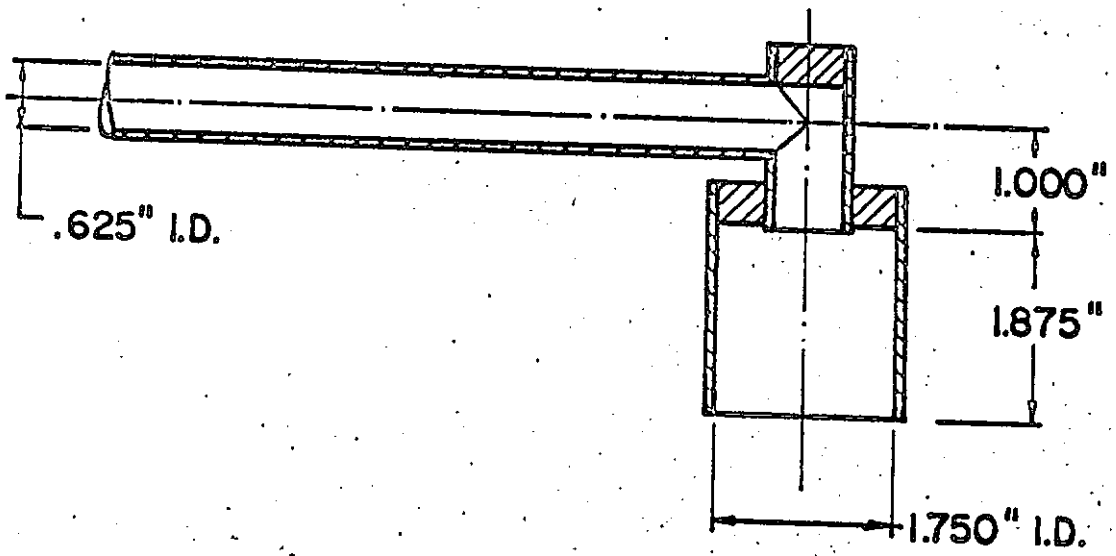

Fig. 61 Resonator used to regenerate sinusoidal signal

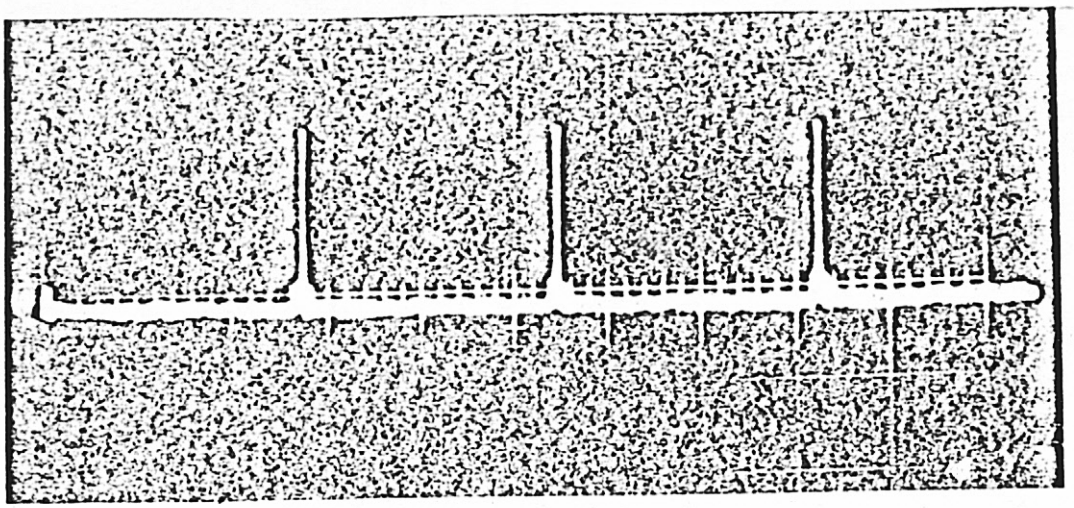

A) Pipe alone

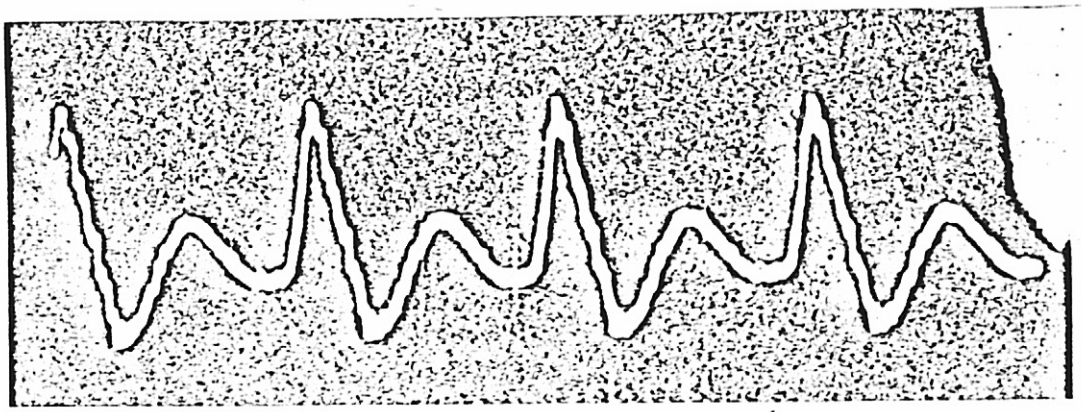

B) Pipe with resonator

Fig. 62 Signal measured 4" from outlet of 10' length of pipe emanating from siren

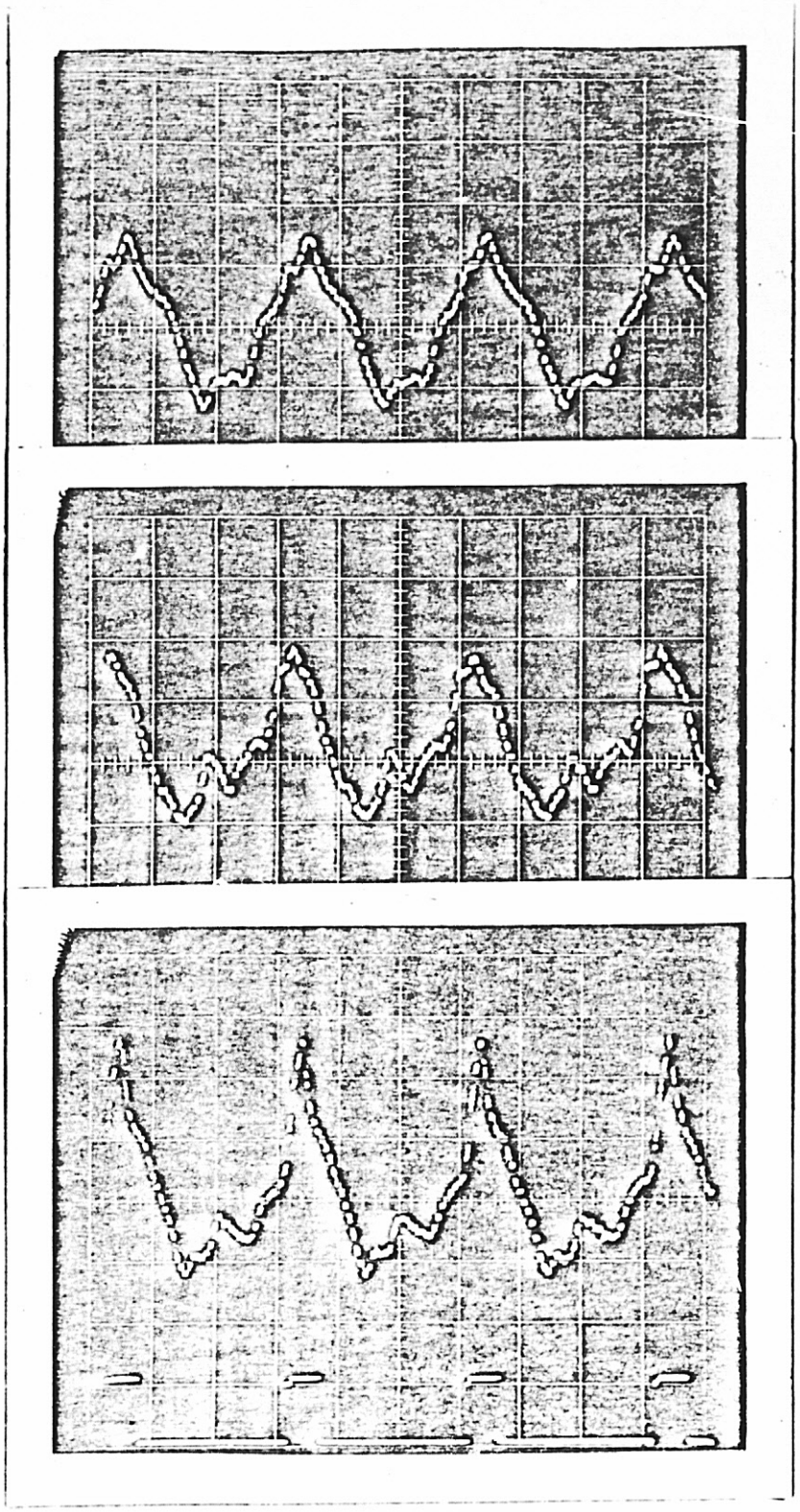

Fig. 63a Signals from multi-source pneumatic siren system
(f = 670 Hz, SPL $\tilde{=}$ 120 dB)

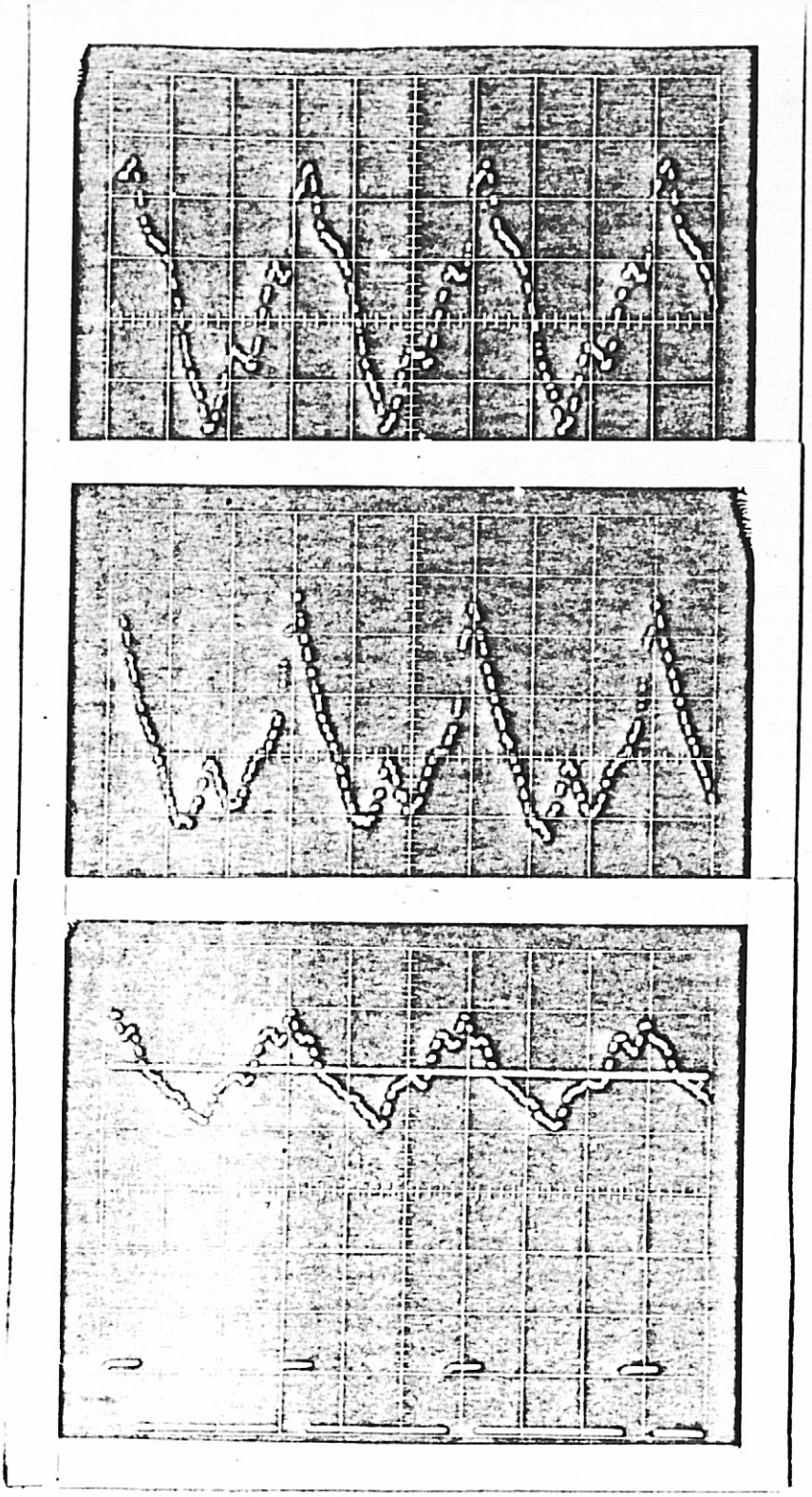

Fig. 63b Signals from multi-source pneumatic siren system
(f = 670 Hz, SPL $\cong$ 120 dB)

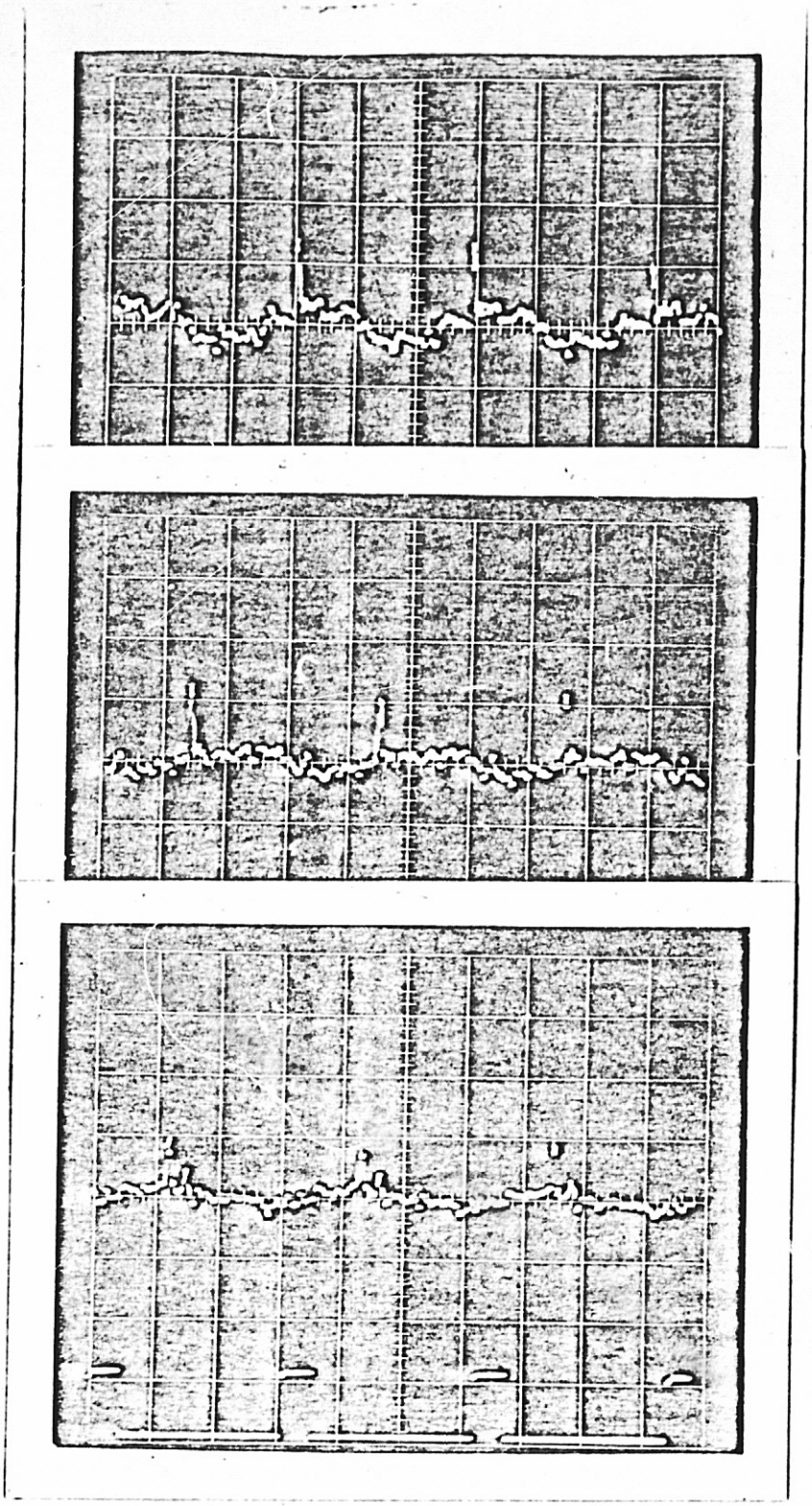

Fig. 64a High-pressure signals from multi-source pneumatic siren system (f = 670 Hz, SPL $\tilde{=}$ 137 dB)

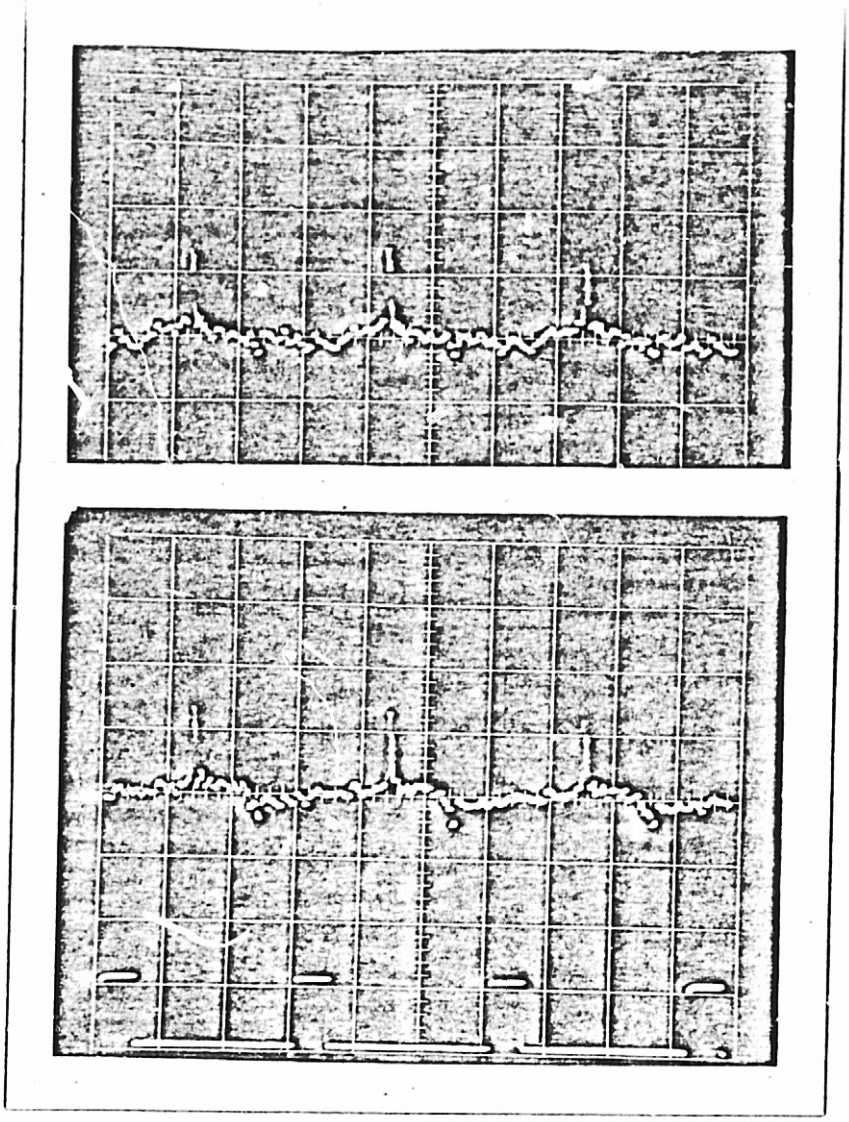

Source 4

Source 5

Fig. 64b High-pressure signals from multi-source pneumatic siren system (f = 670 Hz, SPL $\cong$ 137 dB)

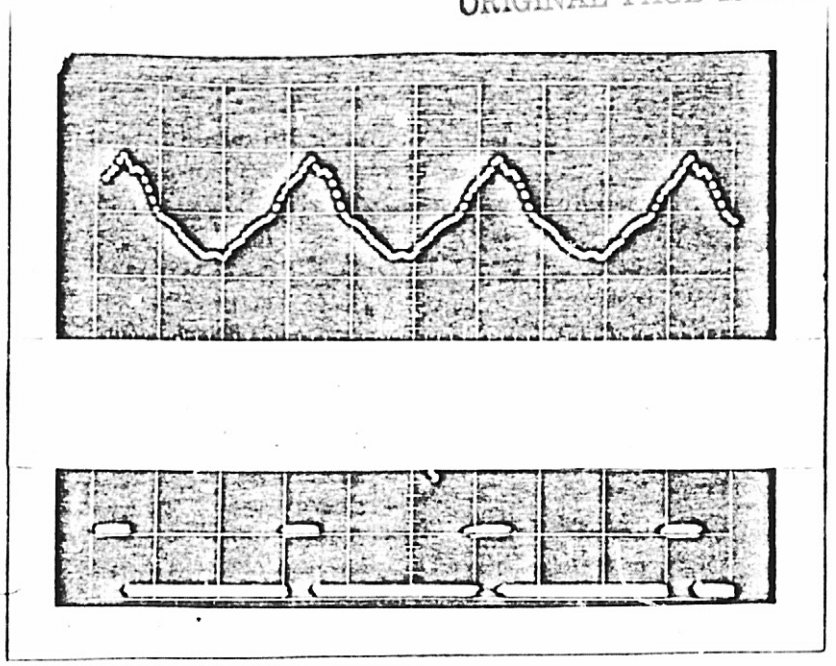

A) Sources 1-6

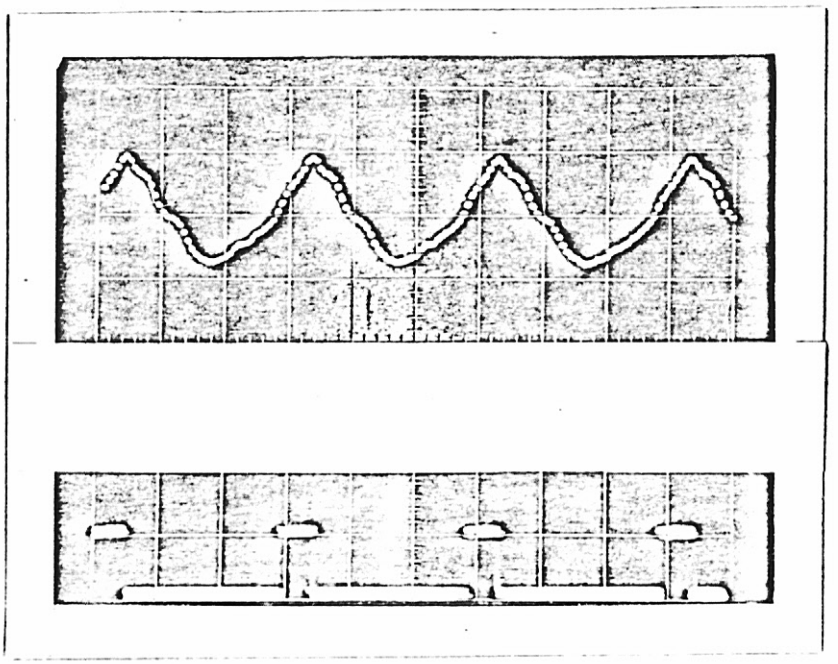

B) Sources 1-6
(Repeated)

Fig. 65 Combined signal from six sources of pneumatic siren system
(f = 670 Hz, SPL $\simeq$ 135 dB)